SHIMADZU
Excellence in Science

Livre Blanc

Spectrophotométrie

Volume 2

SHIMADZU, UNE ENTREPRISE PÉRENNE

Shimadzu est le groupe japonais **leader mondial** spécialisé dans l'instrumentation analytique et physique, le diagnostic médical et l'aéronautique. Son histoire débute en **1875 au Japon** avec son fondateur Genzo Shimadzu Sr., fabricant d'instruments de physique et de chimie. Aujourd'hui coté à la bourse de Tokyo, Shimadzu dégage un **chiffre d'affaires annuel** de **plus de 3 miliards de dollars.**

DES COLLABORATEURS EXPERTS ET PASSIONNÉS

Shimadzu a toujours misé sur le talent de ses collaborateurs passionés pour transformer l'industrie, à l'image de **Genzo Shimadzu Jr.,** récompensé comme l'**un des dix plus grands inventeurs japonais de tous les temps** ou encore de **Koichi Tanaka**, lauréat du **prix Nobel de Chimie en 2002** pour ses travaux de recherche sur la spectrométrie de masse et les macromolécules.

UN PIONNIER DANS L'INNOVATION

Tout au long de son histoire, Shimadzu n'a jamais cessé d'innover et a été à l'origine de **nombreuses découvertes et premières mondiales.** Aujourd'hui, notre groupe est présent à l'international dans **plus de 100 pays** avec des centres de Recherche & Développement ou de production en Europe, au Japon, en Chine, en Australie et aux Etats-Unis. **Plus de 10 000 collaborateurs** Shimadzu se mobilisent chaque jour autour d'un seul but : contribuer à l'amélioration de la société à travers la Science et la Technologie.

DES SOLUTIONS ADAPTÉES À VOS BESOINS

Notre effort en Recherche & Développement est constant, nos nouvelles technologies sont le fruit d'une **collaboration avec différentes institutions universitaires et centres de recherche.** Cette synergie nous permet de mettre au point **des solutions fiables et adaptées aux différentes problématiques industrielles.** Nous disposons de plusieurs laboratoires de démonstration ainsi que de centres de formation pour chaque gamme. Avec une **présence régionale complète**, nous proposons des solutions suivies pour chacun de nos clients à travers tout le pays.

RESPECTUEUX DES STANDARDS

Shimadzu fabrique mondialement selon les différentes normes de qualité reconnues et permet à ses clients de travailler **en accord avec les GLP, GMP, FDA** et les **méthodes standards décrites dans diverses pharmacopées.**

UN ACTEUR MONDIAL EN SPECTROPHOTOMÉTRIE...

Depuis **plus de 60 ans**, Shimadzu développe des instruments en spectroscopie moléculaire. Aujourd'hui, une gamme complète de spectrophotomètres UV-Visible et infrarouge (FTIR) dotés de logiciels adaptés aux différents besoins sont ainsi proposés. Afin de répondre aux réglementations strictes du secteur pharmaceutique, les spectrophotomètres Shimadzu permettent une **compatibilité avec les guides GMP's/GLP's, BPF/BPL, les Pharmacopées Européennes, USP** et **les exigences de la FDA et du 21 CFR Part 11.**

SOMMAIRE

SOMMAIRE

IRTracer-100 & AIM-9000

FTIR & EDX

3. Spectrofluorimétrie

RF-6000

![SHIMADZU — Excellence in Science]

1. Spectrophotométrie UV-Visible proche IR

SHIMADZU
Excellence in Science

Application News

No.A503

Spectrophotometric Analysis

Quality Analysis of Environmental Water
- Using a Water Analysis Program Designed for the UV-1280 -

In the environmental sector, regulations are in place and monitoring is performed on the quantities of specific substances present in industrial wastewater and river water. An increase in the concentration of phosphorus and nitrogen in river water can cause abnormal growth of algae and phytoplankton.[1] Japan uses river water among other sources for its tap water, which is treated to make it potable.[2] There are 51 "water quality criteria" and 26 "water control targets" prescribed for tap water in Japan.[3] These criteria and targets include prescriptions for parameters such as residual chlorine and hardness, which are items of relatively common concern.

We developed a water analysis program designed for use with the UV-1280 UV-VIS spectrophotometer, which provides easy analysis of 22 substances and 39 items (including phosphoric acid and residual chlorine) by mainly using the "PACKTEST" water quality testing kits from Kyoritsu Chemical-Check Lab., Corp.

We describe using this UV-1280 water analysis program to analyze day-to-day changes in phosphate-phosphorus levels in river water and residual chlorine, iron, and total hardness levels in tap water.

■ **Analysis of Phosphate Phosphorus in River Water**

The UV-1280 and a Kyoritsu Chemical-Check Lab., Corp. PACKTEST are shown in Fig. 1. The water analysis program displays the measurement procedure on-screen. An example procedure is shown in Fig. 2. The program also has built-in calibration curves created with standard samples, so concentration measurements can be made simply by following the on-screen instructions. New measurement items can also be added using a User-Defined Items function, and a trend graphing function can be used to show day-to-day changes in a single view.

River water (hereinafter river water A) was taken from a local river alongside weather recordings between February 15 and 26, 2016, and phosphate phosphorus measurements were made using the measurement conditions shown in Table 1.

The trend graph shown in Fig. 3 allows the user to understand day-to-day changes in the phosphate phosphorus concentration in river water A at a single glance. The phosphate phosphorus concentration was below the lower limit of detection (0.04 mg/L) on most days, while a maximum concentration of 0.398 mg/L was detected on February 16. Rainfall was observed close to the river water collection point on February 14 and 20, which probably caused the low levels of phosphate phosphorus detected on February 15, 16, and 22.

A photograph of the river water collection point is shown in Fig. 4. The photograph shows the water was clean and the riverbed was fully visible on sunny days.

Fig. 1 UV-1280 and PACKTEST
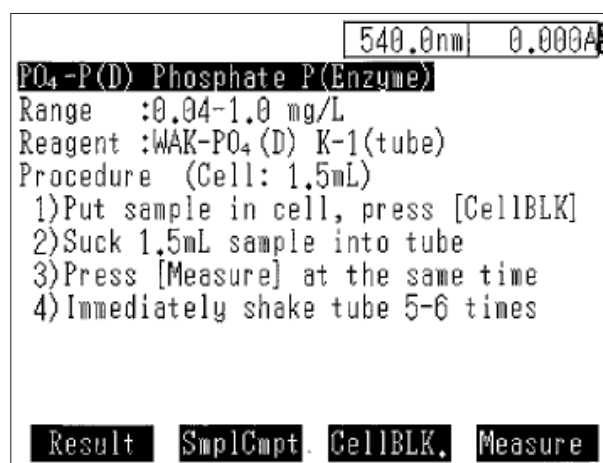
Fig. 2 Phosphate Phosphorus Measurement Procedure (Enzymatic Method)

Table 1 Measurement Conditions

Instruments used	: UV-1280 Water analysis program PACKTEST Phosphate-Phosphorus (Low Range)
Items measured	: Phosphate phosphorus (enzymatic method)
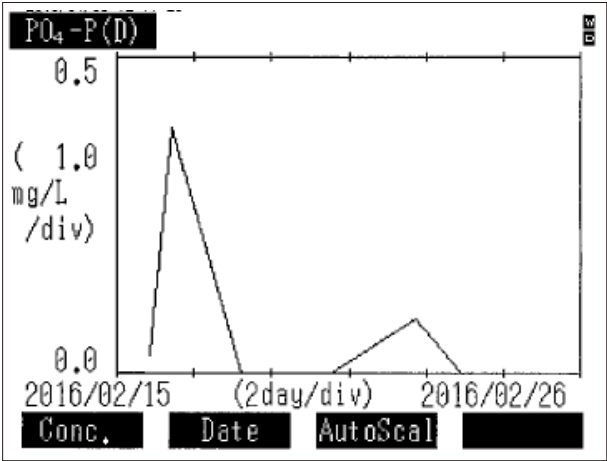
Fig. 3 Phosphate Phosphorus over Time (Trend Graph)

Fig. 4 River at Collection Point

■ Quality Analysis of Tap Water

Tap water contains substances such as residual chlorine, mineral content in the form of calcium and magnesium that is represented as total hardness, and iron. The prescribed water quality criteria levels for these items are ≥ 0.1 mg/L for residual chlorine, ≤ 300 mg/L for total hardness, and ≤ 0.3 mg/L for iron in Japan.

We collected tap water from a normal tap, a tap with water purifier attached, and a tap that is rarely used, and measured the above three items under the measurement conditions shown in Table 2.

The water samples before and after testing are shown in Fig. 5, and the test results are shown in Table 3. A small amount of residual chlorine was found in tap water that passed through a water purifier, but no residual chlorine was detected in tap water taken from the tap that was rarely used. We suspected some degradation of the water purifier. Probable reasons that residual chlorine was not detected in water taken from the tap that is rarely used are stagnation of water in the pipes and aging of the pipes themselves. Total hardness concentrations were within the water quality criteria levels and within the target levels (10 to 100 mg/L) in water taken from all three taps. Iron was only detected at 0.165 mg/L in water taken from the tap that was rarely used. Water taken from the tap that was rarely used appeared colored compared to other tap waters, and we inferred the iron present in the water originated from the pipes.

Table 2 Measurement Conditions

Instruments used	: UV-1280 Water analysis program PACKTEST Residual Chlorine (free), Total Hardness, Iron (low range)
Items measured	: Residual chlorine (free), total hardness, iron (low range)

Fig. 5 Left: Normal Tap Water, Middle: Tap Water with Water Purifier, Right: Rarely Used Tap Water

Table 3 Measurement Results

	Normal	With water purifier	Rarely used tap water
Residual chlorine (free)	0.18 mg/L	0.07 mg/L	< 0.05 mg/L
Total hardness	40 mg/L	48 mg/L	34 mg/L
Iron (low range)	< 0.05 mg/L	< 0.05 mg/L	0.17 mg/L

■ Conclusion

We easily performed water quality analysis of environmental water and tap water using the water analysis program designed for the UV-1280 and the PACKTEST series of products from Kyoritsu Chemical-Check Lab., Corp. We also used the trend graphing function to observe day-to-day changes in a single view.

[References]
1) Kyoritsu Chemical-Check Lab., Corp. PACKTEST water analysis kit
2) Kyoto City Waterworks and Sewerage Bureau website
3) Japan's Ministry of Health, Labour and Welfare website

Example of Reflectance Measurement Using Integrating Sphere -Difference Between Diffuse Reflectance and Diffuse + Specular Reflectance Measurements-

Reflectance measurements using UV spectrophotometers are utilized in a wide variety of fields. The integrating sphere is a spectrophotometer accessory that is particularly effective for analyzing samples that do not have shiny surfaces. Integrating spheres are generally used to measure diffuse reflectance.

In addition, it can be also applied to measure diffuse plus specular reflectance by changing the angle of the light irradiated to the sample. This Application News introduces examples of measuring samples with different surface conditions, using diffuse reflectance, and diffuse + specular reflectance.

■ Out line of Integrating Sphere

Fig. 1 and 2 show the appearance and structure of integrating sphere.

Integrating sphere is a spectrophotometer accessory effective for analyzing samples whose surfaces are not shiny. All interior surfaces are coated with barium sulfate so that all of the scattered light is focused toward the detector. By changing the angle of incidence, it is possible to switch between diffuse reflectance measurement (incident angle of 0 degrees) and diffuse + specular reflectance measurement (incident angle of 8 degrees). When the angle of incidence is set to 8 degrees, specular reflectance also remains inside the integrating sphere, allowing diffuse + specular reflectance measurement.

Fig.1 Appearance of Integrating Sphere
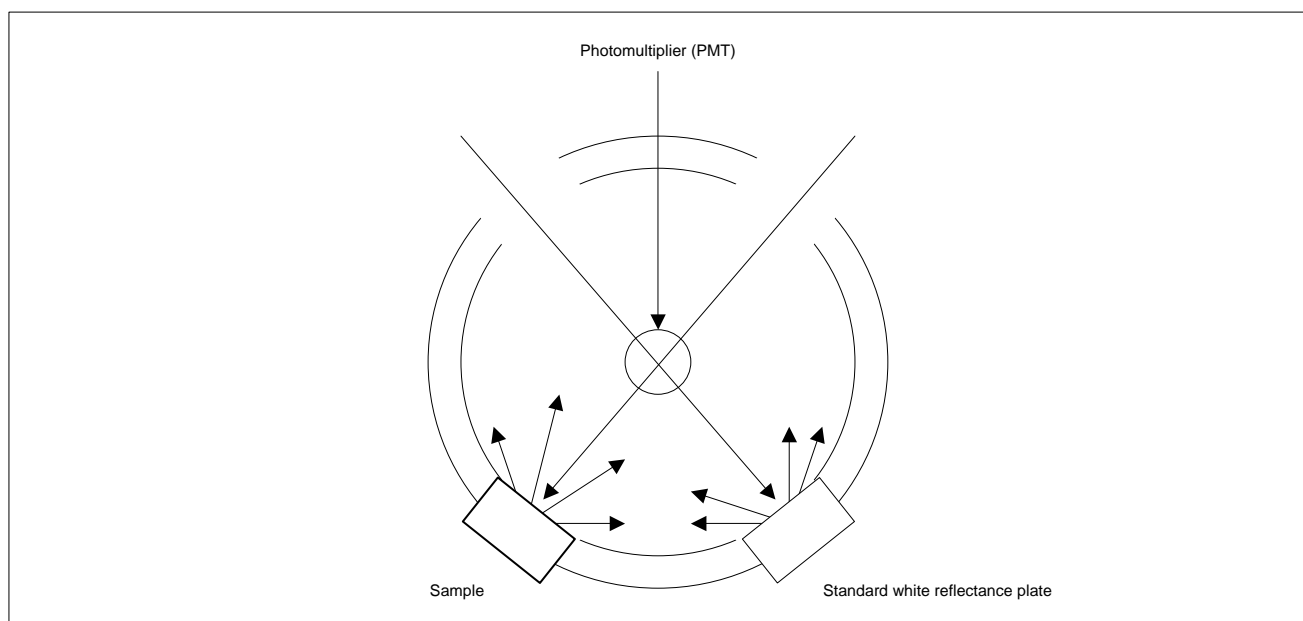
Fig.2 Schematic diagram of integrating sphere

■ Analysis of Plastic Surface

Fig. 3 shows the reflectance spectrum of a plastic surface, obtained with an incident angle of 0degrees (diffuse reflectance). In Fig. 4, the diffuse reflectance spectrum (red line) is overlaid with the spectrum obtained with an incident angle of 8degrees (diffuse + specular reflectance) (blue line).

The results clearly show that the reflectivity differs between the two measurement methods. This is caused by the condition on the plastic surface, where both diffuse and specular reflectance occurs. With the incident angle of 0degrees, only diffuse reflectance is detected. However, by changing the incident angle to 8degrees, both diffuse and specular reflectance is detected simultaneously.
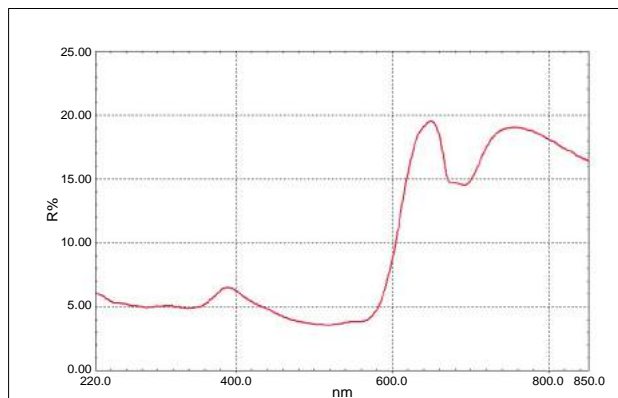
Fig.3 Reflection Spectrum of Plastic Surface (Diffuse Reflectance)
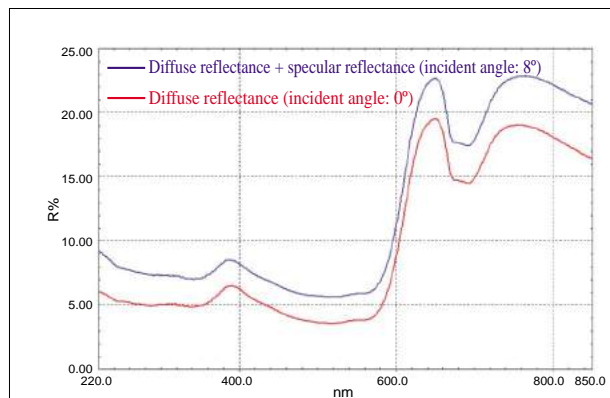
Fig.4 Reflection Spectra of Plastic Surface (Comparison of diffuse reflectance and diffuse + specular reflectance)

■ Analysis of Tissue Paper

Fig. 5 shows an example of measuring tissue paper. The pink line indicates diffuse + specular reflectance and the green line diffuse reflectance. There is no significant difference between these two spectra. This indicates that suface of tissue paper is rough and almost no specular reflectance occurs.

As shown above, by using the integrating sphere and adjusting the incident angle, reflectance spectrum measurements become possible for samples both with and without surface luster.
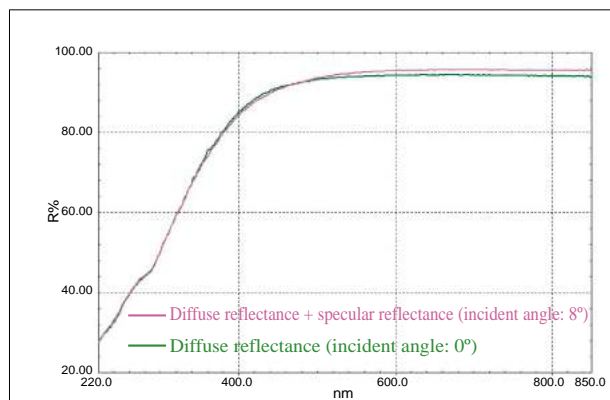
Fig.5 reflection spectra of tissue paper

SHIMADZU
Excellence in Science

Application News

No.A450A

Measurement of the Ultra Violet Protection Factor assigned to Ultraviolet Protection Clothes

■ Introduction

Sunlight that reaches the earth is composed of various wavelengths designated as visible light (VIS), which can be seen by humans, ultraviolet light (UV), and infrared light (IR). The visible region of the spectrum lies between the shorter wavelength ultraviolet light and the longer wavelength infrared light. The ultraviolet radiation (UV) with shorter wavelengths has stronger energy associated with it and substances exposed to UV radiation for long periods of time can undergo deterioration and decomposition.

For humans, long exposure to UV radiation can cause skin blemishes such as freckles and in the worst case, cancers. Given the current concern for UV exposure, there are many UV protected textile fabrics on the market. In this application, we use UV-Visible spectrophotometry to measure the UV protection value for these items to verify how well they protect the wearer from harmful UV radiation. The Ultraviolet Protection Factor (UPF) value is a regulated Standard in Europe, America, and Oceania. Here we examine common UPF values for UV protected clothing.

■ Analytical Conditions for UPF

The UPF value is a number representing the ultraviolet protection factor, and is an indication of how well the item protects the user from sun burn. The UV wavelength of interest is specified to be between 280-400 nm (in some cases it is specified as 290-400 nm). In this wavelength range further categorization can include the UVA at 315-400 nm, and the UV-B at 280-315 nm (in some case 290-315 nm). Various regulations currently use different measuring conditions and formulas to calculate UPF values. Table1 shows the different measuring conditions that are specified by the Germany / British, America, and Australia / New Zealand regulations.

Table1 Test methods of Germany / British, America, and Australian / New Zealand

|	Germany / British DIN EN13758-1 BS EN135758-1	America AATCC 183	Australian / New Zealand AS/NZS 4399
Wavelength	290 - 400 nm	280 - 400 nm	290 - 400 nm
Sampling Pitch	1 nm	2 nm	5 nm
Value	UPF (290 - 400 nm)	UPF (280 - 400 nm)	UPF (290 - 400 nm)
	UVA (315 - 400 nm)	UVA (315 - 400 nm)	UVA (315 - 400 nm)
	UVB (290 - 315 nm)	UVB (280 - 315 nm)	UVB (290 - 315 nm)

Table2 Calculation Formula for UVA, UVB and UPF

	Germany / British DIN EN13758-1 BS EN135758-1	America AATCC 183	Australian / New Zealand AS/NZS 4399
UVA	$\dfrac{1}{86}\sum\limits_{\lambda=315}^{\lambda=400} T_i(\lambda)$	$\dfrac{\sum\limits_{315\,nm}^{400\,nm} T_\lambda \times \triangle\lambda}{\sum\limits_{315\,nm}^{400\,nm} \triangle\lambda}$	$\dfrac{T_{315}+T_{320}+T_{325}+\cdots+T_{395}+T_{400}}{18}$
UVB	$\dfrac{1}{26}\sum\limits_{\lambda=290}^{\lambda=315} T_i(\lambda)$	$\dfrac{\sum\limits_{280\,nm}^{315\,nm} T_\lambda \times \triangle\lambda}{\sum\limits_{280\,nm}^{315\,nm} \triangle\lambda}$	$\dfrac{T_{290}+T_{295}+T_{300}+T_{305}+T_{310}+T_{315}}{6}$
UPF	$\dfrac{\sum\limits_{\lambda=290}^{\lambda=400} E(\lambda)\varepsilon(\lambda)\triangle\lambda}{\sum\limits_{\lambda=290}^{\lambda=400} E(\lambda)T(\lambda)\varepsilon(\lambda)\triangle\lambda}$	$\dfrac{\sum\limits_{280\,nm}^{400\,nm} E_\lambda \times S_\lambda \times \triangle\lambda}{\sum\limits_{280\,nm}^{400\,nm} E_\lambda \times S_\lambda \times T_\lambda \times \triangle\lambda}$	$\dfrac{E_{eff}}{E'} = \dfrac{\sum\limits_{290}^{400} E_\lambda \times S_\lambda \times \triangle\lambda}{\sum\limits_{290}^{400} E_\lambda \times S_\lambda \times T_\lambda \times \triangle\lambda}$

■ Calculation Formula for UPF

Table 2 shows the formulas used by each country for the calculation of UVA, UVB, and UPF. UVA is calculated in the wavelength range of 315-400 nm, and UVB is calculated in the wavelength of 280-315 nm (some case 290-315 nm).

Where:

E_λ : relative erythemal spectral effectiveness (see each regulation)

S_λ and $\varepsilon(\lambda)$: solar spectral irradiance (see each regulation)

T_λ : average spectral transmittance of the specimen(measured)

$\triangle\lambda$: measured wavelength interval(nm)

■ Measurement of Ultraviolet Protection values for Clothes and Umbrellas

Fig. 1 shows the UV Protection provided by clothes (both light and dark areas) and the UV protection provided by an umbrella. The samples were analyzed by a SHIMADZU UV-2600 UV-Vis Spectrophotometer and an ISR-2600 Plus integrating sphere accessory. Table 3 shows the measurement analytical conditions, and Fig. 2 shows transmittance spectra. The transmittance spectrum of the umbrella (green) shows that very little UV radiation transmits through the umbrella. In regards to the clothing, the black areas block more UV radiation than do the white areas. Table 4 shows each calculated UPF value as defined by each regulation. The table shows that the same clothing area can have differing UPF values depending upon the regulation used to calculate the value. When a sample is measured to have a UPF value that is greater than 50, then only "50+" or "UPF>50" need be reported, as specified in each regulation. In table4 the calculated UPF values are displayed as specified by each regulation for comparison purposes.

Fig. 1 Photograph of clothing and an umbrella that can be used for Ultraviolet Protection and used in this application news

Table 3 Analytical Conditions

Apparatus	: SHIMADZU UV-2600 Integrating Sphere ISR-2600Plus
Wavelength	: 280-400 nm
Scan Speed	: Medium
Sampling Pitch	: 1.0 nm
Measurement Mode	: Transmittance
Slit	: 5 nm
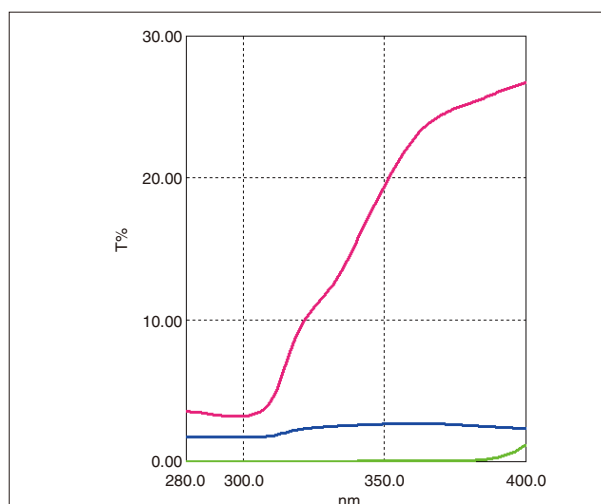
Fig. 2 Transmittance Spectra of Ultraviolet Protection Clothes (light areas red and dark areas blue) and Umbrella (green)

■ Conclusion

Each piece of clothing tested had the same catch phrase "UV cut-off", but as the spectral measurements demonstrate exhibit different spectral transmittance. In addition, the same spectrum may give different UPF values depending upon a specific Country's formulation for UPF calculation.

Because of this it is necessary to refer to each governing regulation when analyzing UV protection materials.

[References]
• DIN EN13758-1
  Textile Solar UV protective properties-
  Part1: Method of test for apparel fabric(includes Amendment A1: 2006)
  English version of DIN EN 13758-1: 2007-03
• BS EN 13758-1
  BRITISH STANDARD
  Textiles-Solar UV protective properties-
  Part1: Method of test for apparel fabrics
• AATCC Test Method 183-2010
  Transmittance or Blocking of Erythemally Weighted Ultraviolet Radiation through Fabrics
• Australian / New Zealand Standard
  Sun Protective clothing-Evaluation and classification

Table 4 UPF for ultraviolet protection Clothes and Umbrella

	Germany / British DIN EN13758-1 BS EN135758-1	America AATCC 183	Australian / New Zealand AS/NZS 4399
White part of UVprotected clothes	16.2	16.2	19.0
Black part of UVprotected clothes	UPF>50 (51.7)	50+ (51.7)	50+ (53.2)
UVprotected Umbrella	UPF>50 (3640)	50+ (3740)	50+ (4060)

SHIMADZU

Shimadzu Corporation

www.shimadzu.com/an/

SHIMADZU
Excellence in Science

Application News

No.A524

Differentiating Olive Oils Using UV-VIS Spectrophotometer and Spectrofluorophotometer

■ Introduction

There is growing interest in food safety and organic foods, with an increasing number of shops specializing in a variety of food products and increasing circulation of high price import goods. One of these foods is olive oil, which is supposed to have both health and aesthetic benefits. The most expensive form of olive oil is extra virgin olive oil, which is regulated by the International Olive Council. Only olive oil that is chemically unprocessed, produced by squeezing and filtering olive fruit, and with an acidity of no more than 0.8 % qualifies as extra virgin olive oil. Another olive oil called pure olive oil is created by purification and high-temperature treatment. Differentiating between extra virgin olive oil and pure olive oil based on appearance alone is difficult. This article describes an attempt to differentiate between these two olive oil types by spectrum measurement using Shimadzu UV-2700 UV-VIS spectrophotometer and RF-6000 spectrofluorophotometer, then performing multivariate analysis.

Fig. 1 UV-2700 UV-VIS Spectrophotometer

■ Absorbance Measurement of Olive Oils

Fig. 1 shows Shimadzu UV-2700 that was used to measure absorbance. Fig. 2 shows some of the olive oils tested. They each differ in terms of color, odor, and place of origin. Ten different extra virgin olive oils were prepared from a total of 6 producers. Samples were named in the format "○ ✕ E", where "○" was replaced by letters A through F to refer to each producer, and "✕" was replaced by each producer's consecutive numbers in order of increasing olive oil price. Pure olive oil was also prepared from producers A and B. These samples were named in the format "○ ✕ P". Each olive oil was placed in a quartz cell, then its absorption spectrum was measured. Measurement conditions are shown in Table 1, and three spectra representative of the spectra obtained are shown in Fig. 3. Absorption peak wavelengths are almost identical between spectra, though with obvious differences in their degree of absorption. Results confirmed the extra virgin olive oils tended to exhibit higher absorbance than the pure olive oils.

Fig. 2 Various Olive Oils

Table 1 UV-2700 Measurement Conditions

Spectrum Type	: Absorption spectrum
Measurement Wavelength Range	: 330 nm to 800 nm
Scanning Speed	: Intermediate
Sampling Pitch	: 0.5 nm
Light Source Switching Wavelength	: 323 nm

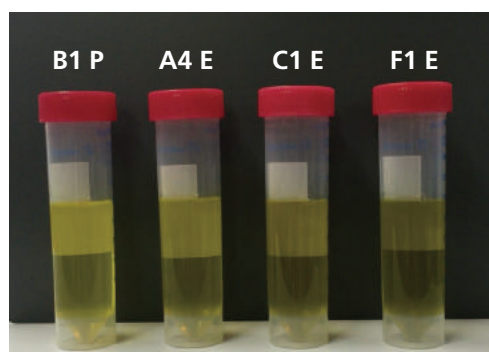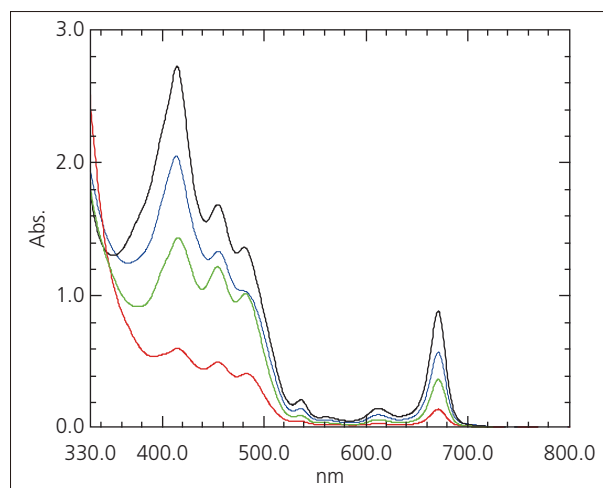**Fig. 3 Olive Oil Absorption Spectra**
Red: B1 P, Green: A4 E, Blue: C1 E, Black: F1 E

■ Multivariate Analysis Using Absorption Spectra

We attempted to differentiate between pure olive oil and extra virgin olive oil by performing a multivariate analysis of the results obtained by absorbance measurement. The Unscrambler®X[1] multivariate analysis software was used to perform difference analysis on absorbance at 7 peak wavelengths.

Principal component analysis (PCA) and cluster analysis were used to differentiate between olive oil types. With PCA, scores are calculated to allow visual differentiation by the analyst (score plot). A loading plot is also used to determine characteristic factors in each grouping that have a strong influence on the score plot. Cluster analysis differentiates samples based on a tree diagram. The shorter the horizontal line that connects each sample, the more similar those samples.

The score plot obtained by PCA is shown in Fig. 4. Pure olive oils are clustered in the negative direction along the dominant PC-1 axis, while extra virgin olive oils are clustered in the positive direction along the dominant PC-1 axis. This shows successful differentiation between olive oil types. The loading plot in Fig. 5 shows a characteristic of the extra virgin olive oils tested is strong signals at short wavelengths, such as 415 nm and 454.5 nm.
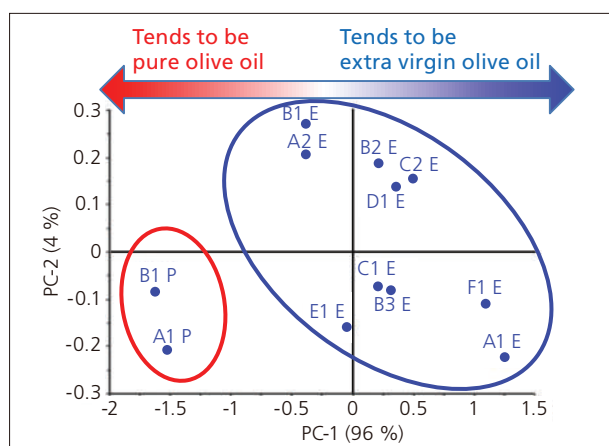
Fig. 4 Score Plot Based on Olive Oil Absorbance
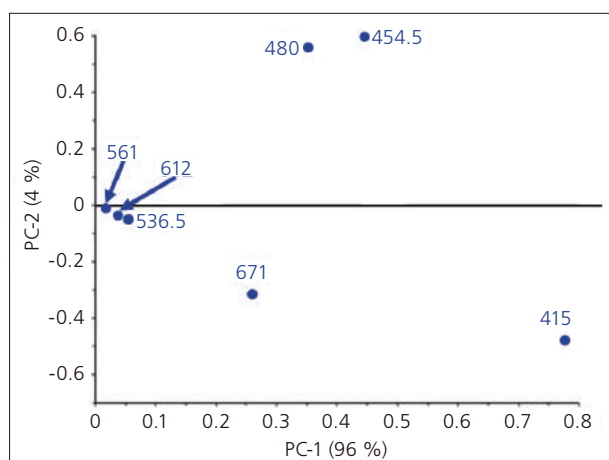
Fig. 5 Loading Plot Based on Olive Oil Absorbance

Cluster analysis results are shown in Fig. 6. At a glance, the tree diagram shows the olive oils separated into 2 groups and the degree of similarity between the samples. This result shows we successfully differentiated between pure olive oils and extra virgin olive oils.
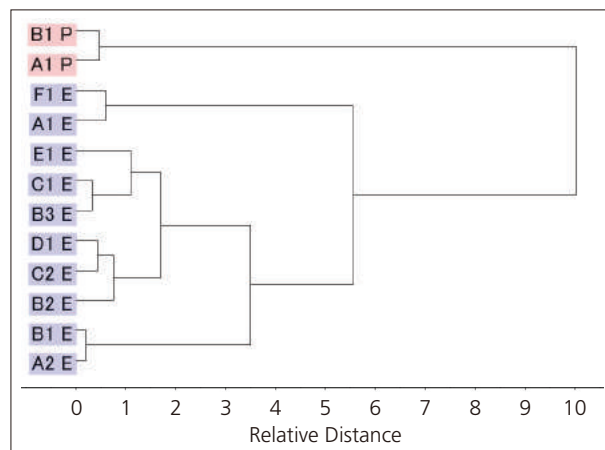
Fig. 6 Cluster Analysis Result Based on Olive Oil Absorbance

■ Three-Dimensional Spectra Measurements of Olive Oils

The three-dimensional emission spectra of olive oils were measured using Shimadzu RF-6000 spectrofluorophotometer. Fig. 7 shows the instrument used. Due to the high absorbance exhibited by the samples, a solid sample holder (Fig. 8) was used to compensate for self-absorption effects. Self-absorption is the phenomenon of light emitted by the sample being absorbed by the sample itself. When the absorption spectrum of a highly absorbing sample is measured in a normal cell holder, the amount of emission light that enters the detector can be reduced due to emission light being absorbed by the sample itself. A solid sample holder was used to direct excitation light towards the corner of the quartz cell as shown in Fig. 9. This reduces the amount of sample through which emission light travels, and so reduces the effects of self-absorption.
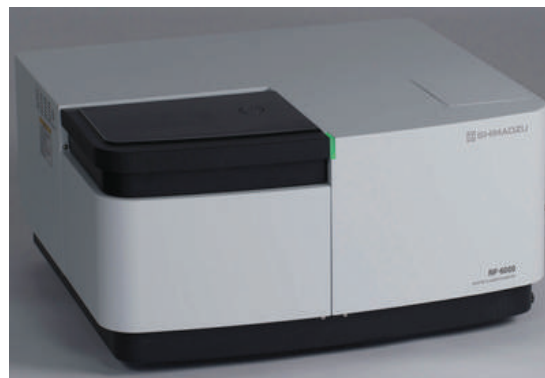
Fig. 7 RF-6000 Spectrofluorophotometer
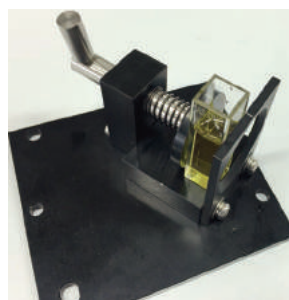
Fig. 8 Solid Sample Holder   **Fig. 9 Measurement Method**
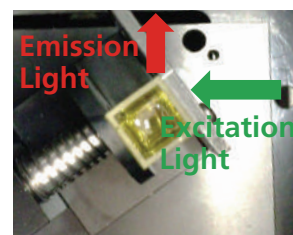
Table 2 shows the measurement conditions used. A filter (IHU310) that blocks light below 310 nm was placed in the path of emission light to prevent high-order excitation light reaching the detector. Fig. 10 shows two of the three-dimensional spectral diagrams obtained. Emission light predicted to be derived from chlorophyll was confirmed at Em 680 nm in both samples. Emission light at this wavelength was detected more strongly from extra virgin olive oil samples compared to pure olive oil samples. Also, strong emission light in the vicinity of Em 400 nm was mainly detected from pure olive oil samples. This 400 nm emission light is predicted to be derived from vitamins. Fig. 11 compares a pure olive oil and an extra virgin olive oil showing emission spectra obtained at an excitation wavelength of 300 nm. The excitation light region shown in Fig. 11 is indicated by the white dotted lines in Fig. 10. The emission spectra show different peak strengths and peak tail shapes between 300 nm and 500 nm.

Table 2 RF-6000 Measurement Conditions

Optional Accessory	: Solid sample holder, IHU310
Spectrum Type	: 3D spectrum
Measurement Wavelength Range	: Ex 200 nm to 800 nm
	Em 250 nm to 800 nm
Scanning Speed	: 6000 nm/min
Wavelength Interval	: Ex 5.0 nm, Em 1.0 nm
Bandwidth	: Ex 5.0 nm, Em 5.0 nm
Sensitivity	: Low
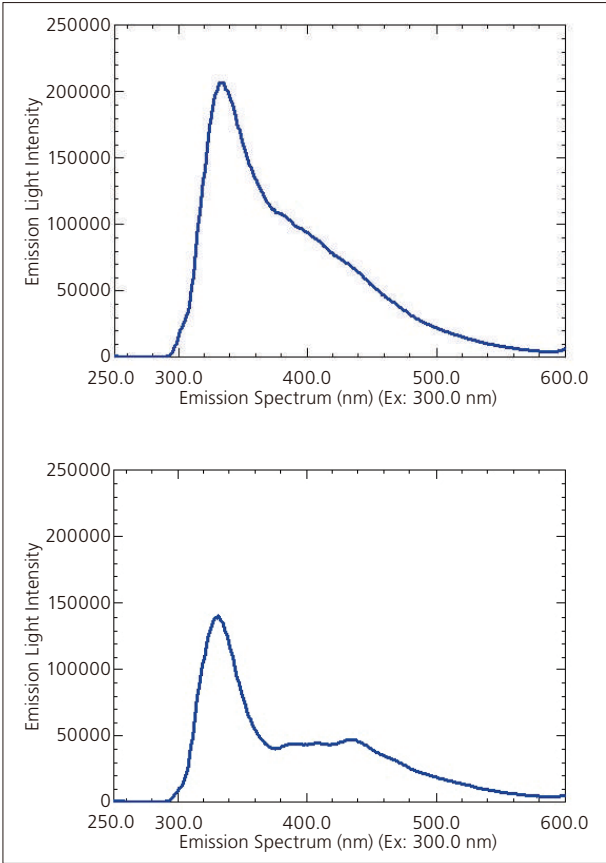
Fig. 11 Emission Spectrum of Olive Oils Excited at 300 nm
Top: A1 P, Bottom: F1 E

Fig. 10 Three-Dimensional Spectra of Olive Oils
Top: A1 P, Bottom: F1 E

■ **Multivariate Analysis Based on Three-Dimensional Spectra**

Similar to absorbance analysis, a multivariate analysis was performed on the three-dimensional spectra to differentiate between pure olive oils and extra virgin olive oils. Emission light intensity at the 10 points shown in Fig. 12 (A through J) was used for this analysis.

Fig. 12 Analysis Points for Multivariate Analysis

The score plot obtained by PCA is shown in Fig. 13. Pure olive oils are clustered in the positive direction along the dominant PC-1 axis and extra virgin olive oils are clustered in the negative direction along the dominant PC-1 axis. This shows the olive oil types have been separated.

Compared to the score plot created based on absorbance, the A2 E and B1 E samples are positioned closer to the pure olive oil samples. While A2 E and B1 E are both extra virgin olive oils, we can predict they are similar to pure olive oils. The loading plot is shown in Fig. 14. It shows a characteristic of the pure olive oils is for strong signals at emission light analysis points A through D, which are points predicted to be derived from vitamins.

Results of the cluster analysis are shown in Fig. 15. Compared to the results obtained based on absorbance, the A2 E and B1 E samples are included in the pure olive oil group. This result also shows that while these samples are extra virgin olive oils, they tend to be closer to pure olive oils. Using emission light spectra, we could predict which extra virgin olive oils are likely to contain more vitamins.

Fig. 13 Score Plot Based on Olive Oil Absorbance
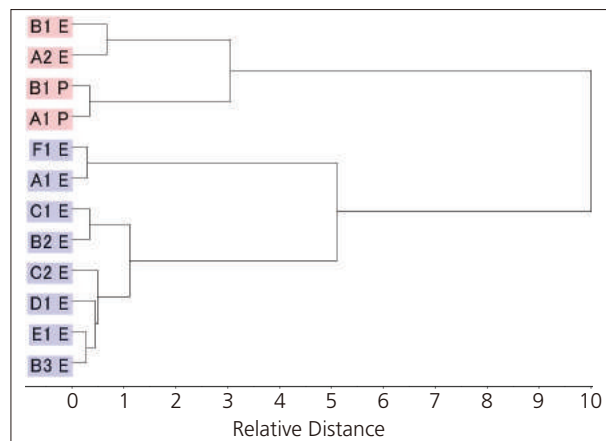
Fig. 15 Cluster Analysis Result Based on Olive Oil Absorbance

■ Conclusion

Shimadzu UV-2700 UV-VIS spectrophotometer was used to measure absorption spectra. Results showed the extra virgin olive oils have a higher absorbance than the pure olive oils. Next, the three-dimensional emission spectra of olive oils were measured using Shimadzu RF-6000 spectrofluorophotometer. Differences in emission light intensity and peak width were confirmed in the three-dimensional emission spectra results. Multivariate analysis was then performed based on each spectrum. This allowed successful differentiation between the extra virgin olive oils and pure olive oils, while results obtained from the RF-6000 allowed identification of extra virgin olive oils particularly similar to pure olive oils.

1) The Unscrambler®X is a trademark or registered trademark of CAMO Software.

Fig. 14 Loading Plot Based on Olive Oil Absorbance

SHIMADZU

Shimadzu Corporation

www.shimadzu.com/an/

Application News

No. SCA-100-017

Wine bottle measurement with UV-2600 and MPC-2600 Quality control of color

The packaging of food is of mayor interest since the modern world is using modern materials as factor of design for food. Should it be new style in carton (since 1977) or classical in glass (since 17th century)? In case of wine it seems that the classical glass wine bottle is still the most favorite packaging.

Fig. 1: Red wine Bottles from the Shimadzu Wine Edition I at left and Edition II at right side.

The glass appears transparent and emphasize a feeling of being clean, and the wine should be less influenced by additives which can be result from the carton. The glass color can be blue, green, brown or white for liquids. It seems that glass which is not clear green or direct brown can be result of mixture caused by melting green and brown glass fraction in one or the adequate mixture of inorganic oxides causing such final color during the glass melting process. It is written in the literature that green glass can pick up to 15% of other colors. And brown glass add up to 8%. For the human eye it is still in the category green and brown glass.

Fig. 2: Typical colors of wine bottles, the green glass is easy to identify, at the right side the color is subjective more brown green

It is difficult to judge for the human eye if the right bottle from figure 1 is a dark green, brown, or? To overcome such handicap the UV-VIS spectroscopy can be a neutral instrument to characterize the color of the glasses. The application shown in this experiment is a measurement through wine bottles.

■ Experiment

The wine bottle in its appearance was completely set into the sample compartment of the MPC-2600. It was positioned so that the light energy could pass through the two wine bottle walls, without touching the paper prints on the glass bottle wall. The UV-VIS spectra were recorded for the two bottles. By the presence of two thick bottle walls the ground absorbance of the glass spectrum

resulted in a high baseline and high signal values. The measurement in this way was destroying free.
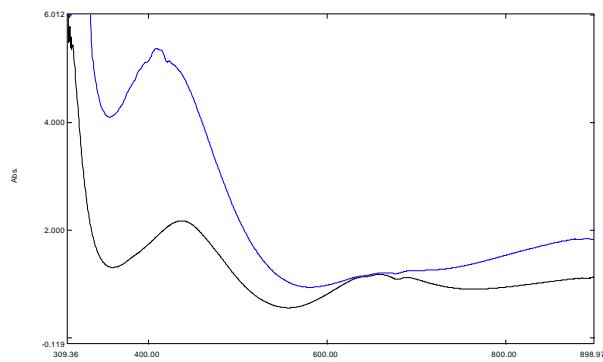
Fig. 3: blue line shows the UV-VIS spectrum from the brown-green glass and the black line is the spectrum from the green glass.

In figure 3 are shown two spectra from each sample. The range of interest is 310 to 890 nm. The green glass spectrum has two maxima ranges at around 650 and 440nm (black line). The blue lined spectrum has its maxima with a weak at 650nm and a very high at 410nm and a higher absorbance at >800nm. In detail it is at 650nm minimum a triplet signal or even a multiple which is saturated. With the help of the 2nd derivative spectroscopy it is possible to make this situation visible. The position of the maxima can be given as: 686.4, 669.9, 654.2, and 636 nm (Fig. 4). These absorbance maxima are typical signals belonging to Chromium 3^{+} in form as Chromium oxide Cr_2O_3 (1). This oxide is used to generate green color in glass ware. The same profile but less in height is visible in the green-brown glass spectrum, but the mayor signal in the range of 400 is shifted from 440 to 410. A broad signal with an internal maximum at 410nm. Brown color is result from the investigation of Manganese oxide (2). This is more present in the second sample because of less contents on Chromium oxide. A screening by Shimadzu EDX-7000 showed a factor of 3 lower

contents of chromium in the brown-green sample.
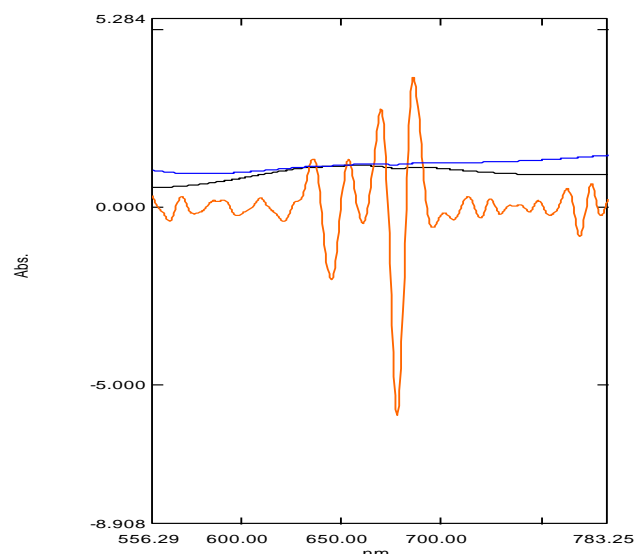
Fig. 4: 2nd derivative spectrum from the green glass spectrum (red), up to four signals can be separated at 650nm as characteristic for Cr_2O_3.

The manganese has influence on the redox process regards changes in the iron oxides under heat of melting. Absorption of yellow color falls into the visible spectrum. The presence of manganese oxide is also responsible for the more intense iron oxide signals at 380 to 430nm. The 2nd derivative spectrum extracts signals at. 420, 412, 400, 390, 385 nm.

■ **Instrumentation**

UV-2600
MPC-2600 and Plane stage for a wine bottle

■ **Literature:**

(1) The effect of chromium oxide on optical spectroscopy of sodium silicate glasses, Bahman _Mirhadi, Behzad Mehdikhani, Journal of Optoelectronics and Advanced Materials, Vol. 13, No. 9, September 2011, p. 1067 -1070

(2) Effect on Manganese oxide on redox iron in sodium silicate glasses, Bahman _Mirhadi, Behzad Mehdikhani, Journal of Optoelectronics and Advanced Materials, Vol. 13, No. 10, October2011, p. 1309-1312

SHIMADZU

Shimadzu Europa GmbH

www.shimadzu.eu

![Shimadzu - Excellence in Science]

Application News

No. UV-022

Thin Film Coating Comparison between the UV-2600 and SolisSpec-3700 UV-Vis-NIR Spectrophotometers

CM Talbott, Ph.D.

■ Introduction

Many times the instrumentation between an R&D department and the production or QA/QC departments is different. Typically, R&D instrumentation has more features that provide more detail and variety in their ability to investigate samples, whereas typical QA/QC instrumentation may be more focused on their tasks. Often, the question of how spectra from one bench will compare to spectra of another bench is posed. To demonstrate the uniformity of the Shimadzu line of instrumentation, samples with thin film coatings were examined by reflection and transmission on the research-type SolidSpec-3700 and the QA/QC style UV-2600 UV-Vis-NIR spectrophotometers.

■ Experimental

Samples were analyzed for 5-degree reflectance, and transmittance at 0, 5, 15, and 30 degrees on both the UV-2600 and SolidSpec-3700 instruments. For each bench, the bandwidth was set to optimum for the measurements (5nm-UV-2600, 20nm-SS-3700) and the scan speeds were set to medium with a 2.0 nm sample pitch. On the UV-2600 spectrophotometer, the 5-degree specular reflectance accessory was used to acquire reflectance spectra and the Variable Incident Angle Film Holder was used to acquire transmission spectra. On the SolidSpec-3700, the Variable Angle Measurement Accessory (VAMA) was used to acquire both reflectance and transmittance spectra. Results for the two thin film-coated samples are shown below.
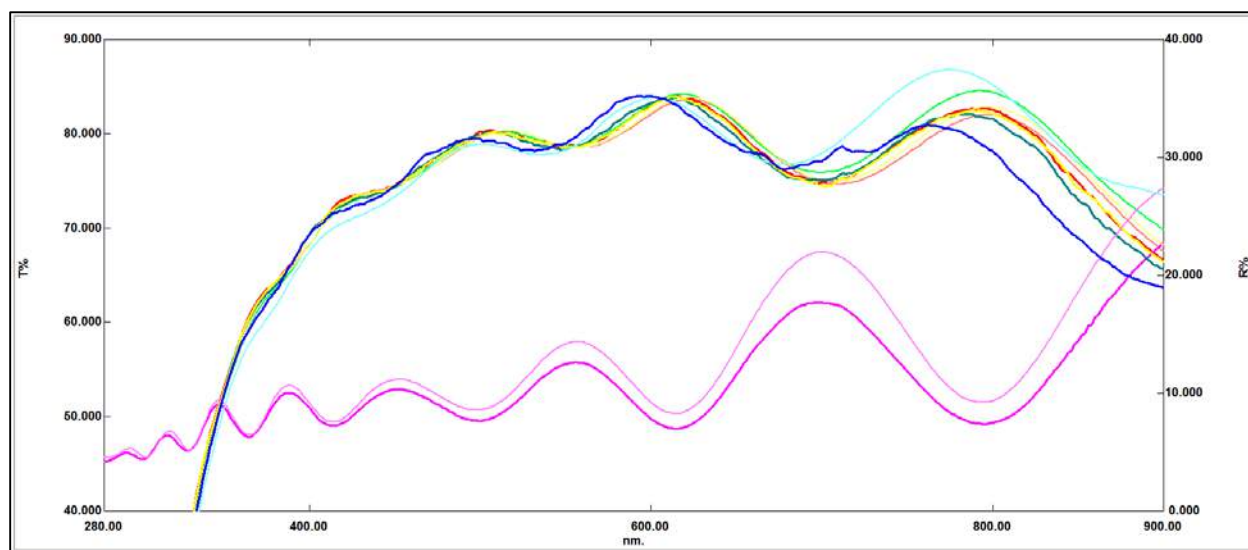
Sample 1; 5-deg reflectance (magenta), 0-deg trans (red), 5-deg trans (yellow), 15-deg trans (green), and 30 degree trans (blue), UV-2600 thin lines, SolidSpec-3700 thick lines.
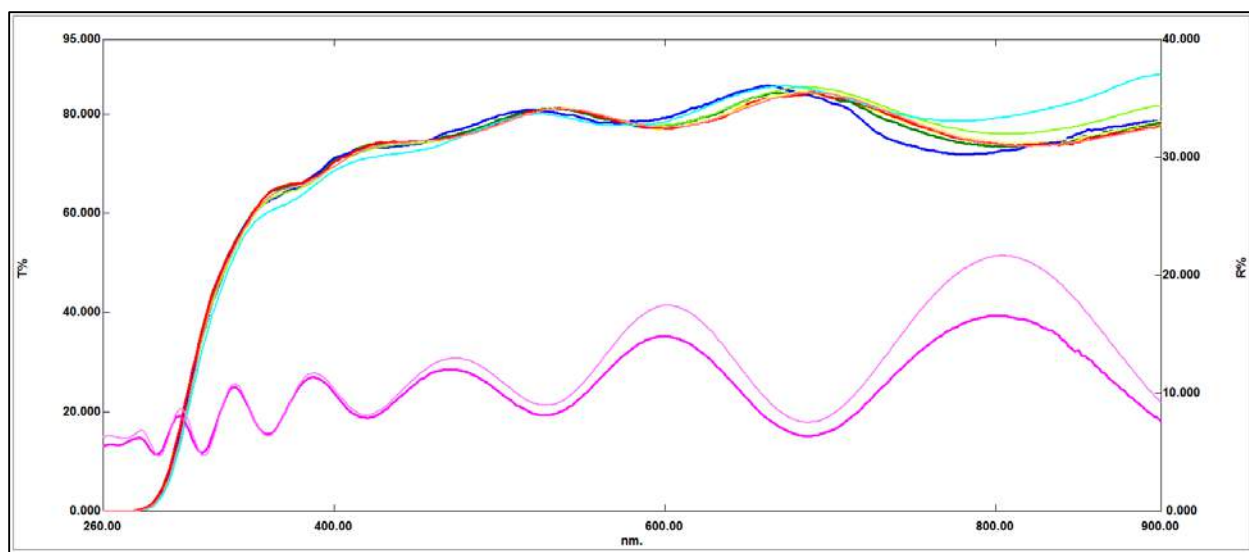
Sample 1; 5-deg reflectance (magenta), 0-deg trans (red), 5-deg trans (yellow), 15-deg trans (green), and 30 degree trans (blue), UV-2600 thin lines, SolidSpec-3700 thick lines.

■ Results

The reflectance spectra for both samples (magenta in the graphs above) match very well between the two spectrophotometers and reflectance accessories. The difference in intensity at the higher wavelengths of these reflectance spectra can be attributed to the VAMA accessory's ability to measure absolute spectral reflectance whereas the 5-degree accessory can measure relative reflectance only. The difference in reflection at the higher wavelengths then are due to the spectral absorption for the mirror used to acquire the background with the 5-degree accessory.

The variable angle transmission spectra do show slight changes in the interference fringes of the transmitted light as the angle of incidence is changed from 0 degree normal to 30 degrees normal, as would be expected. Furthermore, in the transmission spectra, good correlation exists between the spectra acquired on the UV-2600 (thin lines) and those acquired on the SS-3700 (thick lines).

The above spectra show that good correlation exists between transmitted and reflected spectra acquisitions on different spectrophotometer benches. If film thickness was the desired result of the measurements, no changes would be observed between thicknesses measured on one bench over the other. Similarly, if the relative reflectance was corrected to absolute by the use of a standard, no reflectance differences nor transmission differences would be observed between the benches as well.

■ Conclusion

Shimadzu offers a wide range of UV-Vis-NIR spectrophotometers to meet all customer needs and budgets. This study has demonstrated that confidence can be had that there are no differences in spectral quality when samples are run on different instrument.

Application News

Spectrophotometric Analysis

No. UV-008

Thin Film Analysis using the Shimadzu UV-2600 and 5 Degree Relative Specular Reflectance Accessory

Jeff Head, M.S., John Kinyanjui Ph.D., Mark Talbott, Ph.D.

■ Introduction

Thin films play a critical role in our everyday lives. They are used in electronics, solar cells, and are applied as coatings in eyeglasses in order to reduce glare as well as increase the amount of transmitted light through the lenses. For example, anti-reflection (AR) coatings are applied to lenses in order to reduce glare that would otherwise be present in uncoated lenses. This has become an attractive feature for many consumers and therefore measurement and control of the AR coating has become increasingly important. Figure 1 shows two reflectance spectra of industry ophthalmic lenses. The black spectrum is the reflectance spectrum of a lens that contains a hard coating as well as an AR coating, whereas the red spectrum is a lens that only has a hard coating.

(a)

(b)

Figure 1: (a) Ophthalmic lens with AR coating and hard coating; (b) Reflectance spectra of ophthalmic lenses. The black spectrum represents a lens that contains both a hard coating and AR coating, whereas the red spectrum represents a lens that contains only a hard coating.
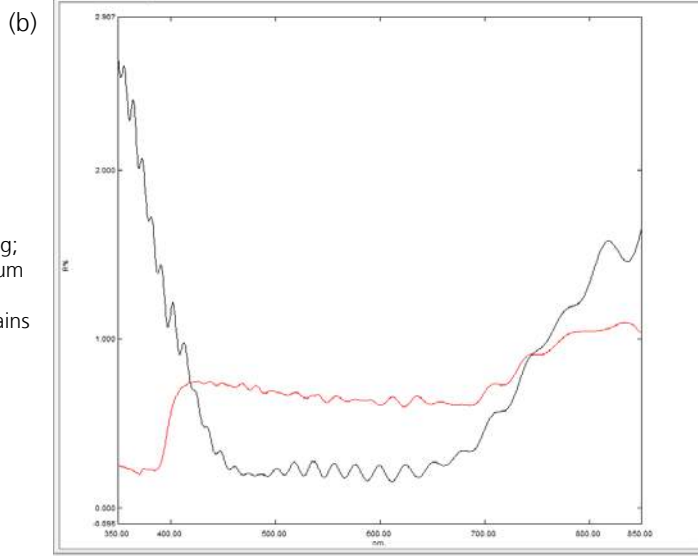
The industry of applying coatings as thin films relies heavily on the ability to determine the thickness of the coating for quality control purposes. In ophthalmics spectral reflectance is used to measure AR as well as hard coating thickness. The ophthalmic industry takes advantage of the capability to add multiple coatings in various combinations in order to provide the best consumer products. Shimadzu offers the ability to analyze a single film on a lens with the Film Thickness software, such as hard coatings on lenses. In figure 1, the area of interest for the hard coating is between 650 and 500 nm.

Film thickness, d, is determined from the wavelength between peaks and valleys in interference patterns. It is required that the refractive index of the coating and the incident angle are known prior to calculating film thickness, as given in equation 1, where n is the refractive index of the film, Θ is the angle of incidence, λ_1 and λ_2 are wavelengths of two noticeable peaks (or valleys), and Δm is the number of peaks between $\lambda 1$ and $\lambda 2$.[1]

$$d = \frac{\Delta m}{2\sqrt{n^2 - \sin^2 \theta}} \bullet \frac{1}{(\frac{1}{\lambda_2} - \frac{1}{\lambda_1})}$$

■ **Method**
Reflectance spectra of an acrylic lens with a single protective coating were acquired on the UV-2600

- Wavelength Range (nm): 350 to 850 nm
- Scan Speed: Fast
- Slit Width: 5.0
- Sampling Interval: 0.5
- Auto Sampling Interval: Enabled
- Scan Mode: Single

A background scan was obtained by mounting the mirror assemblies on the sample and reference stages with the mirrors face down and then acquiring a baseline scan. It should be noted that for measuring lenses and other acrylic materials on the 5 degree relative specular reflectance accessory the ideal background would be obtained by replacing

In ophthalmics, the area of interest lies in the ability to analyze multiple coatings that are comprised of hard coatings and AR coatings. The industry of applied coatings is broad and diverse. Whether multiple or single coatings are being applied to a substrate, it is of critical importance that the individual coatings by themselves have been analyzed for film thickness prior to making a finished product. This application news focuses on the ability to measure a single protective coating on an acrylic substrate using the Shimadzu UV-2600 with 5 degree relative specular reflectance accessory and film thickness software.

using the 5 degree relative specular reflectance accessory under the following scan conditions:

the sample-side reference mirror with a blank un-coated lens. However, for the purposes of this report an aluminum mirror was used as a sample mirror during the baseline scan in order to acquire a baseline scan. The sample mirror was then removed and replaced with the acrylic lens in order to acquire a reflectance spectrum as shown in figure 2.

(a)

(b)
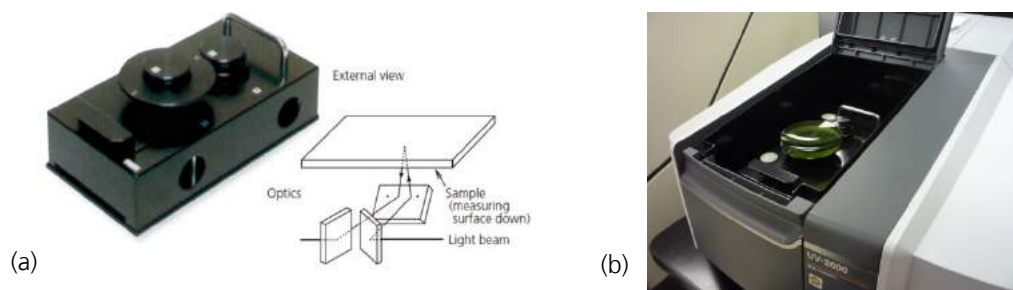
Figure 2: (a) 5 degree relative specular reflectance accessory and external view of light beam path with accessory in place; (b) 5 degree relative specular reflectance accessory sitting in UV-2600 sample compartment with acrylic lens in place.

The refractive index of the protective coating present on the acrylic lens was estimated by etching away a small layer of the coating and suspending it in solutions of various refractive indices and then using

the Becke line test to estimate the refractive index of the coating. In analyzing the coating using the Becke line test the refractive index was estimated to be between 1.393 and 1.440.

■ Results and Discussion

Reflectance spectra of the acrylic lens with protective coating are shown in figure 3.
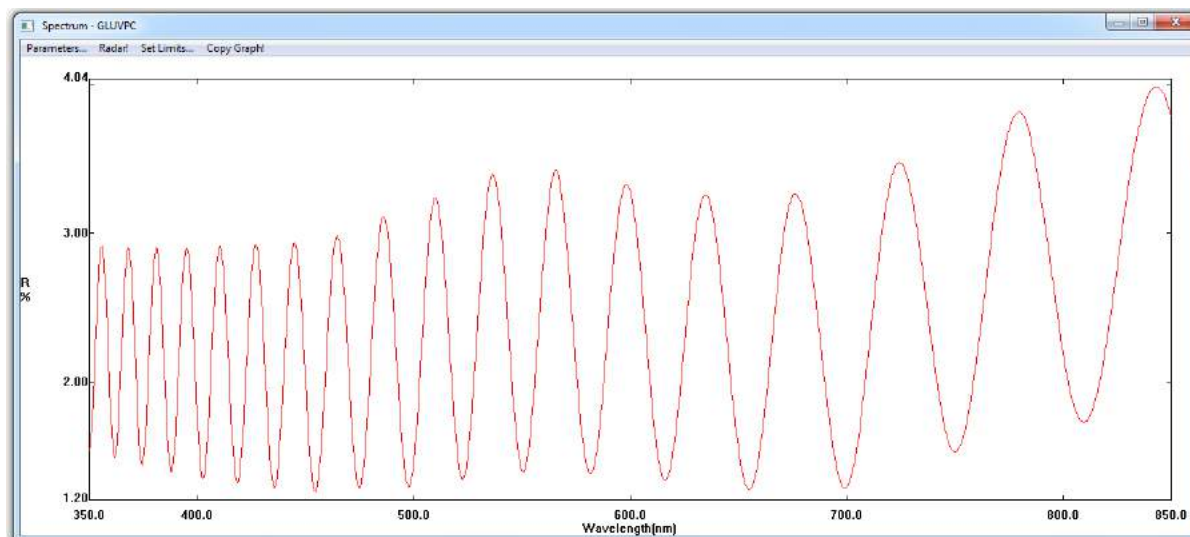
Figure 3: Reflectance spectra of acrylic lens with hardcoat layer.

The thickness of the protective coating can be determined using the Shimadzu Film Thickness software. It is required to know the refractive index of the coating as well as the incident angle of light.

Figure 4 shows the images acquired of the sample and estimating the refractive index using the Becke line test.
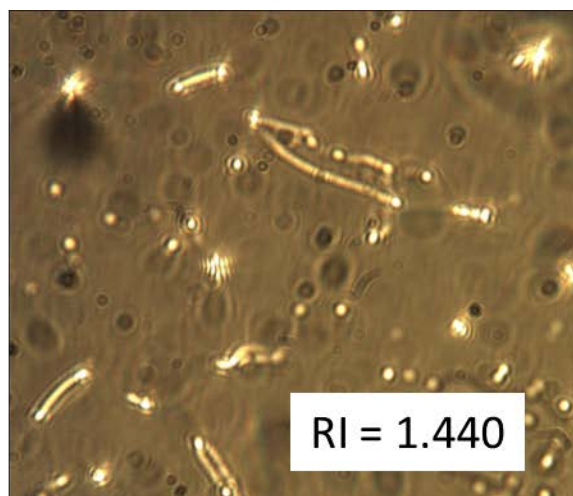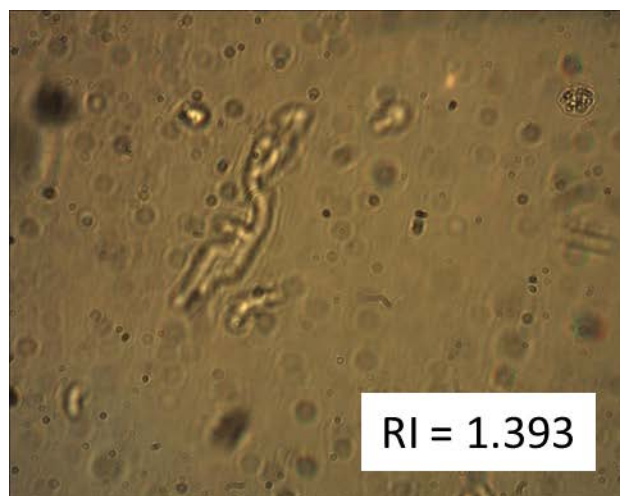
Figure 4: Becke line test of coating particles suspended in solutions with refractive indices of 1.393 and 1.440.

With an incident angle of 5 degrees, the thickness of the coating was calculated to be between 3.638 and 3.761 µm as summarized in figure 5.

```
Calculation Parameters

    Wavelength(nm)          Max    850.0    Min      350.0
    Refractive Index              1.393  (0.8-100)
    Incident Angle                  5.0  (0-90)
    Smoothing dWL           ⊙ Disable    ○ Enable
                            [ Interval X  ○ 10  ○ 20  ○ 40  ○ 80 ]
    Threshold of Peak          0.0010  (0-100)

    Repetition                  1   (1-99)
    Auto Plot Out          ⊙ Disable    ○ Enable

              OK                    Cancel
```

File   Edit   Configure   Spectrum   Presentation   Help

Seq. #	Sample ID	Thickness (um)	Peak SD	Refractive Index	Incident Angle	CalcWL(nm) MAX	MIN	File Name
1	1	3.638	3.71	1.440	5.0	850.0	350.0	GLUVPC
* 2	2	3.761	3.71	1.393	5.0	850.0	350.0	GLUVPC

Figure 5: Summary of film thickness calculations by the film thickness software.

■ **Conclusion**

In conclusion, this application note demonstrates the ability to measure the thickness of a single coating so long as the refractive index and the incident angle of light are known prior to using the Film Thickness software from Shimadzu. The software allows for a quick and easy way to calculate the film thickness of various coatings.

■ **References**

Instruction Manual. UVPC Optional Film Thickness Measurement Software (P/N 206-66877).

SHIMADZU

Application News

No. UV-012

Spectrophotometric Analysis

Maple Syrup Color Analysis using the Shimadzu UV-2600 UV-Vis Spectrophotometer

Jeff Head, M.S., John Kinyanjui Ph.D., Mark Talbott, Ph.D.; Robert Clifford, Ph.D.

■ Introduction

UV-Visible spectrophotometry is a valuable tool in the laboratory for measuring the properties of various liquids and solids. One of the most common applications for QA/QC environments is Color Analysis and being able to assign a color value to finished products. The color value of a material can be obtained by collecting a % transmittance or reflectance spectrum of the sample under consideration. The Shimadzu UV-2600 spectrophotometer is ideal for making accurate color measurements due to the large photometric range of 5 abs. units. Therefore, dilution is not required for highly absorbing samples such as maple syrup. Samples can be analyzed neat without further dilution. The application illustrates the use of Shimadzu Color Analysis Software and the UV-2600 spectrophotometer for quick and easy spectral acquisition and interpretation into a meaningful color value.

■ Background

Maple syrup is one of the most commonly used sweeteners produced in the USA and Canada. Different grades of maple syrup are assigned primarily by color. The color of maple syrup is a result of the time of season that the maple sap is collected from maple trees. In general, the later in the season the sap is collected, the darker the color of the resulting maple syrup.

Currently, the United States has three categories of Grade A syrup referred to as Light, Medium, and Dark Amber. Light amber is the lightest of the three followed by Medium and then Dark. However, Vermont has a grade referred to as "Fancy", which has been reported to be lighter in color than the three U.S. Grade A classifications. An additional classification is Grade B, which is darker than Grade A Dark Amber and considered unsuitable for consumer labelling by some vendors. However, consumers are seeking ways to purchase the Grade B syrup because of its sweeter taste, leading to some manufacturers labelling it for sale and allowable for consumption purposes.

The United States Department of Agriculture is providing a path for a universal classification grading system, which is scheduled to be released and made active for consumers beginning in 2015. The new system will remove the Grade B classification and classify maple syrup as Golden Color, Amber Color, Dark Color, and Very Dark Color. Currently, U.S. grading classifications are made by comparing the maple syrup to color glass standards. In addition to the U.S. grade standards, some states use a spectroscopic method to determine the color of maple syrup. This spectroscopic method differentiates maple syrup grades by the % transmittance at a wavelength of 560 nm. Table 1 outlines the classifications of maple syrup both at a state and federal level, along with the proposed new rating program slated for implementation January 1st 2015[1].

Table 1: Federal and State Classifications of Maple Syrup[1]

Current U.S. Standard	Vermont and Ohio	New Hampshire	New York	Maine	Canada all Provinces	Proposed Option, Jan. 1st 2015
U.S. Grade A Light Amber	Vermont Fancy ≥ 75.0% T, Ohio Light	Grade A Light Amber	Grade A Light Amber	Grade A Light Amber ≥75.0%T	Canada No. 1 Extra Light ≥75.0%T	**Grade A Golden Delicate Taste ≥75.0%T**
U.S. Grade A Medium Amber	Grade A Medium Amber 60.5-74.9% T	Grade A Medium Amber	Grade A Medium Amber	Grade A Medium Amber 60.5-74.9%T	Canada No. 1 Light 60.5-74.9%T	**Grade A Amber Rich Taste 50-74.9%T**
U.S. Grade A Dark Amber	Grade A Dark Amber 44.0-60.4%	Grade A Dark Amber	Grade A Dark Amber	Grade A Dark Amber 44.0-60.4%T	Canada No. 1 Medium 44.0-60.4%T	**Grade A Dark Robust Taste 25-49.9%T**
U.S Grade B for Reprocessing	Grade B 27.0-43.9%T	Grade B	Extra Dark for Cooking or Grade B for Reprocessing	Grade A Extra Dark Amber 27.0-43.9%T	Canada No. 2 Amber 27.0-43.9%T	**Grade A Very Dark Strong Taste <25.0%T**
U.S. Grade B for Reprocessing	Commercial Grade <27.0%T	Grade B	Extra Dark for Cooking or Grade B for Reprocessing	Commercial Grade <27.0%T	Canada No. 3 Dark <27.0%T	**Processing Grade any Color Class, any off-flavored syrup.**

Color is a complex quality and may be more accurately interpreted by the concept of color scales rather than the %T value at a single wavelength. Multiple color scales are used in various lab settings depending on the user's protocol. One commonly used color scale is CIE $L*a*b*$. In this color scale, color values are calculated from a mathematical combination of %T. $L*$ out of the CIE $L*a*b*$ color scale measures the lightness of a sample. An $L*$ value of 100 represents the maximum brightness of a color, whereas an $L*$ value of 0 represents the minimum brightness of a color. $a*$ measures the red or green components of a given sample. Positive values of $a*$ represent a more red color component, whereas negative values lean more towards a dominant green component. Similarly, the $b*$ value measures the yellow or blue components of a sample. Positive values of $b*$ represent a stronger yellow, whereas negative values represent more blue in the sample[2].

■ Experimental

Four separate samples labelled as "Vermont Fancy", "Grade A Medium Amber", "Grade A Dark Amber", and "Grade B", were received as is from a maple syrup sampling kit. Transmittance spectra were collected using standard 10 mm quartz cuvettes with an empty cuvette as a reference with no additional sample preparation. Along with the four samples obtained from the kit, ten commercial samples from different parts of the U.S. were analyzed.

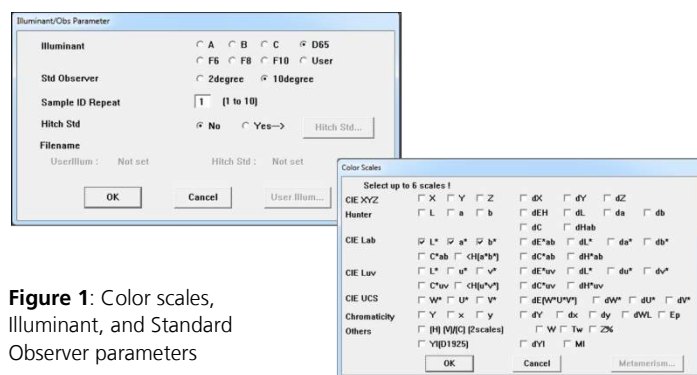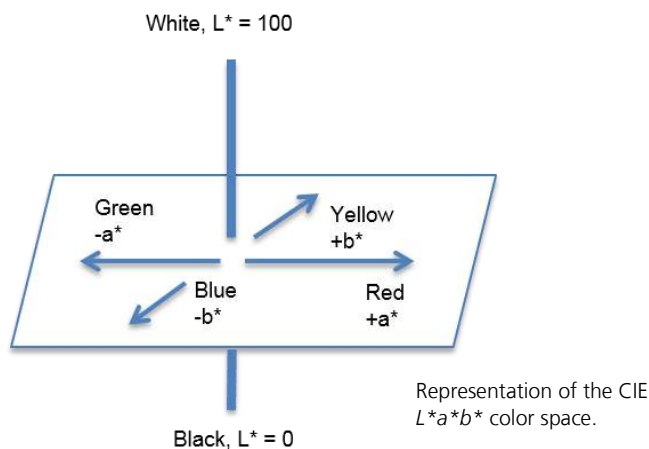Experimental parameters for the color calculation are given in Figure 1.

Figure 1: Color scales, Illuminant, and Standard Observer parameters

White, L* = 100

Green -a*

Yellow +b*

Blue -b*

Red +a*

Black, L* = 0

Representation of the CIE $L*a*b*$ color space.

■ Results and Discussion

Spectra of the four different pure maple syrup samples are shown in Figure 2, with corresponding CIE $L*a*b*$ values and the %T at 560 nm presented in Table 2. The transmittance spectra are similar in profile and demonstrate a decrease in magnitude going from the lighter Vermont Fancy to darker Grade B.
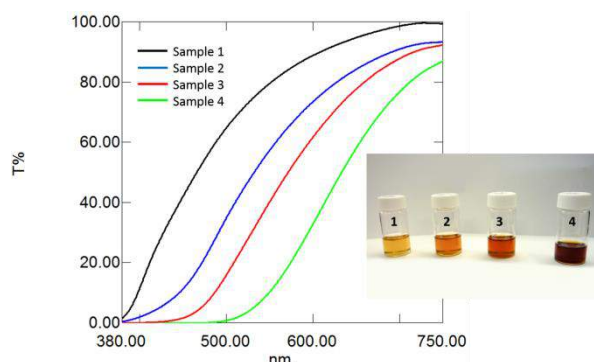

Figure 2: Transmittance spectra of maple syrup samples from sampling kit

As shown in Table 2, the %T at 560 nm decreases as the samples become darker. This trend is in good agreement as supported by the decreasing $L*$ values obtained, which indicate lightness. However, this alone does not offer any insight into the color of the sample.

Under the new classification system scheduled to go into effect in 2015, terms such as "Golden", "Amber", and "Dark" will be used to name the maple syrup. By visually inspecting the samples, the colors range from light yellow to a reddish brown between Vermont Fancy and Grade B. As previously discussed, positive $a*$ values indicate a more red component in the overall color determination, along with a positive $b*$ value, which corresponds with a more yellow sample. The color "Amber" is a yellowish-orange color and is halfway between yellow and orange on the color wheel. Thus, the values for $a*$ and $b*$ increase going from Vermont Fancy to Medium Amber and Dark Amber, as expected.

As shown in Table 2, the value of $b*$ for Grade B drops slightly as compared to Dark Amber, but rises significantly for $a*$ from 19.13 to 41.60. This is to be expected after visual inspection of Grade B since it is a dark color with a very intense red component, and less of a yellow component. This additional insight into the colors present in the maple syrup is gained through the use of the Shimadzu Color Analysis Software.

In addition to the samples analyzed from the sampling kit, ten separate commercial samples labelled as "Pure Maple Syrup" with various classification grades were analyzed for this Application News. Table 3 summarizes the results obtained for analyzing these products.

Table 2: *CIE L*a*b* values and %Transmittance (560 nm) for samples from sampling kit measured on the Shimadzu UV-2600*

Sample ID	Sample Classification	L*	a*	b*	%T at 560 nm
1	Vermont Fancy	90.49	0.40	33.31	81.61
2	Grade A Medium Amber	79.17	7.80	61.61	60.83
3	Grade A Dark Amber	69.33	19.13	83.67	44.64
4	Grade B	45.87	41.60	77.78	13.69

Table 3: CIE *L*a*b** values and %Transmittance (560 nm) for samples from sampling kit, along with commercial samples measured on the Shimadzu UV-2600

Sample ID	Sample Classification	L*	a*	b*	%T at 560 nm
Sampling Kit					
1	Vermont Fancy	90.49	0.40	33.31	81.61
2	Grade A Medium Amber	79.17	7.80	61.61	60.83
3	Grade A Dark Amber	69.33	19.13	83.67	44.64
4	Grade B	45.87	41.60	77.78	13.69
Commercial Samples	**Classification Label**				
5	U.S. Grade A Light Amber	84.46	4.51	59.49	71.31
6	*Grade A Medium Amber*	*70.96*	*16.72*	*79.39*	*47.05*
7	U.S. Grade A Dark Amber	69.71	20.72	91.23	45.81
8	U.S. Grade A Dark Amber	67.26	16.97	83.47	41.73
9	U.S. Grade A Dark Amber	67.96	23.32	94.77	42.93
10	Grade A Dark Amber	70.38	19.77	88.68	46.78
11	U.S. Grade A Dark Amber	67.98	19.16	84.89	42.64
12	U.S. Grade A Dark Amber	66.32	18.05	82.72	40.07
13	U.S. Grade A Dark Amber	73.31	13.76	75.29	51.08
14	U.S. Grade B	52.62	22.69	79.41	22.75

Although the %T values are reported in Table 3, it is important to keep in mind that the majority of these samples were classified under the U.S. grading system. The U.S. system does not rely on %T for classifying maple syrup. Rather, the U.S. system relies on the color of the sample as compared to colored glass standards, which further supports the importance of color analysis[1].

The color results obtained for the commercial samples demonstrate that as the syrup becomes darker, the lightness value decreases. In addition to the lightness value, L*, it is observed that as the amber color darkens, the red component increases, and the yellow component decreases. Thus, a more complete picture of the color of the sample is established for each material.

Interestingly, sample #6, which is classified as "Grade A Medium Amber" on the packaged bottle, demonstrated transmittance and color values close to that of a dark amber maple syrup. More specifically, the color values and %T are similar to samples 3 and 7-13. Visually comparing the samples, #6 has the appearance of an Amber color more close to that of dark amber, rather than medium. The transmittance spectrum of sample 6 is shown in Figure 3, overlaid with the spectra from the sampling kit in Figure 2.
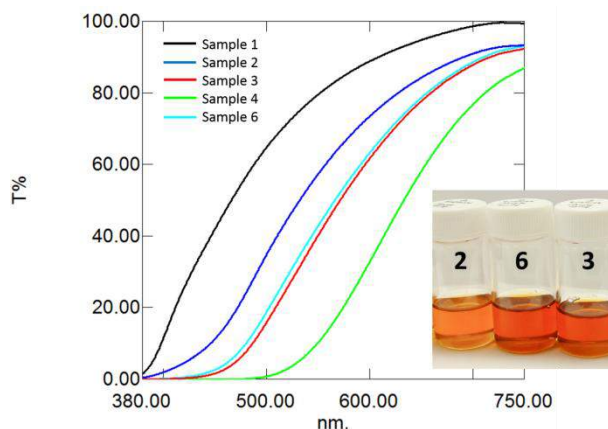
Figure 3: Transmittance spectra of maple syrup samples

■ **Conclusion**

The Shimadzu UV-2600 with Color Analysis software offers an accurate and effective means for obtaining a meaningful color value for maple syrup. The software and spectrophotometer together offer the ideal solution for any QA/QC laboratory requiring the analysis of finished products.

■ **References**
1. Federal Register/Vol. 79, No. 88/ Wednesday, May 7, 2014. "United States Standards of Maple Sirup".
2. Hunter, R.S., Harold, R.W. "The Measurement of Appearance". Second Edition. John Wiley & Sons.

Redefining spectrometric niches

High absorbance readings in UV analysis of Tertiary-Butyl-Catechol (TBC) without colorimetric derivatization

Figure 2: Chemical structure of TBC (Tertiary-Butyl-Catechol)
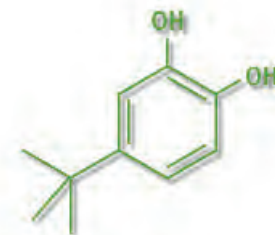

Figure 1: The Shimadzu UV-2700 UV-Vis-NIR spectrophotometer

UV-VIS spectroscopy has been a fundamental tool for most laboratories since it was first used routinely nearly 70 years ago. The technique is widely applied in research, quality control and assurance laboratories in the chemical and pharmaceutical industries.

The UV-VIS market has been divided into sections created by the limitations of the component quality of diffraction gratings, detectors and source lamps. The 'normal' banding consists of instruments which are able to read in the order of 2 - 4 absorbance (abs). 'Research' machines extend this range to 4.5 - 5 abs through the use of pre-monochromators to further reduce stray light. Beyond this is a further niche of 'Reference' grade instruments using double monochromators and advanced wavelength drives to reach as high as 7 - 8 abs.

Smaller, lighter and more powerful

With the launch of the new Lo-Ray-Ligh™ grating, Shimadzu has completely redefined the conventional spectrophotometer niches. This new grating offers dramatic reduction of stray light enabling a single monochromator (as in the UV-2600) to deliver > 5 abs performance, and a double monochromator system (UV-2700) to reach > 8 abs – in an instrument which is physically smaller and lighter than most conventional double-beam systems. The grating also offers a wider wavelength range than any earlier generation grating, permitting the UV-2600 to read up to 1,400 nm with the ISR-2600 Plus integrating sphere option which contains an additional InGaAs detector (Indium Gallium Arsenide).

This new development gives spectroscopists a new choice. It is no longer necessary to invest in a very high specification double grating, double monochromator system to cover this absorbance range. The UV-2700 is much more compact, just a third of the size of conventional reference instruments and with a fraction of the costs.

Application example

The following example shows how to reduce costs not only from the instrument but also from the application side. A chemical company has been using a method for determination of TBC, an inhibitor of polymerization reactions applied to increase the handling time for bonding agents, which involves a reaction with NaOH to produce a red color. The color has been used for quantitation as it exhibits lower absorbance reducing the need for dilution. Direct measurement of TBC
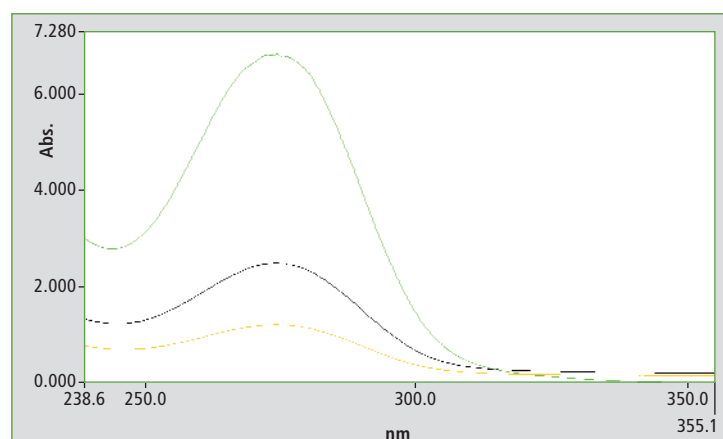

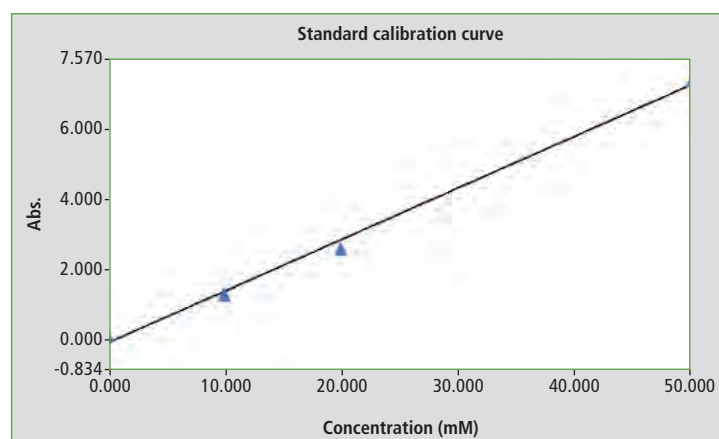Figure 3: High absorbance spectra from TBC

Figure 4: Calibration curve from TBC method, high absorbance against concentration in mM

at 275 nm has not been possible using conventional 0 - 4 abs UV-VIS instruments as the highest concentrations of TBC at 50 mM have an absorbance of nearly seven Abs.

Using the UV-2700, it is possible to directly measure the absorbance peak of TBC at 275 nm. The following figure shows the absorbance traces of 10, 20 and 50 mM TBC (axis scale 0 - 8 abs).

The figure shows that it is possible to scan a sample which has a maximum absorbance of 6.87 at 275 nm. The ability to quantitate this product directly is demonstrated by a plot of the concentration vs. absorbance from the standard quantitation software in Shimadzu UVProbe.

The relationship of absorbance to concentration remains linear through to very high absorbance. In order to read at very high absorbances, the Shimadzu UV-2700 offers a 'High Absorbance' scan mode which can be used in conjunction with rear-beam attenuation to allow measurement of light intensities less than one ten millionth of normal open beam energy.

Summary

The Shimadzu UV-2700 is an affordable and compact instrument which dramatically increases the concentration range of highly absorbing species which can be directly observed in UV spectroscopy. It offers a performance previously available only in reference grade, double monochromator instruments which were too large and too expensive for most laboratories.

Instrumentation
UV-2700, UVProbe software, Attenuator, standard 1 cm square cell holder, 1 cm square quartz cell

New tool for healthcare and cosmetic products

SPFCalculator software for Shimadzu UV-VIS instrumentation

A new UV-VIS instrumentation software for the healthcare and cosmetic segments outperforms the new regulations to be applied from July 2013. These adjustments will be fixed by the European Community, relating to the production and marketing of cosmetics [1]. Other regulations are the Colipa [2], FDA [3], Boots Star Rating [4] and JCIA (Joint Commission International Accreditation - Health Organisation). All of them are part of the SPFCalculator Software which even helps to calculate some physical properties. This product has been designed in cooperation with the Aqualis software house in Milano, Italy.

The SPFCalculator presents 17 parameters requested for the qualification of a sun protection product. The program includes more information on the sun screen product than is required by the guidelines. The calculator is easy to handle and just needs a simple training for users. The software can be updated based on changes in the regulations. The seventeen parameters which can be calculated are shown in table 1.

Users can easily test the sun protection product and change its formulation where necessary, before carrying out the very expensive in vivo measurements.

Shimadzu can provide a complete easy to handle solution: a package containing the UV-2600 instrument, the ISR-2600 integrating sphere in combination with UVProbe and the SPFCalculator. It is a total solution in accordance with European Cosmetics Associations requirements. The strength of the package is that other parameters such as color, appearance, quality of packaging etc. can be determined using the same combination.

References

[1] Regulation (EC) No 1223/2009 of the European Parliament and of the Council of 30 November 2009 on cosmetic products
[2] Colipa, (European Cosmetics Trade Association) 'In Vitro Sun Protection Methods' group
[3] Sunburn Protection Factor (SPF). Food and Drug Administration (United States). 2009-04-30; 'Questions and Answers: FDA announces new requirements for over-the-counter (OTC) sunscreen products marketed in the U.S.', updated 6/23/2011
[4] Measurement of UVA: UVB Ratio According to the Boots Star Rating System (2008 Revision), Boots, Nottingham, UK, 2008

UVAPF0	UVAPF	Ratio (UVAPF/SPFlabel)	UVA dose
Exposure energy	Conversion factor	Exposure time	Critical lambda (pre-irradiation)
Critical-lambda (after-irradiation)	UVA-I/UV FDA	Critical lambda FDA	Star rating FDA
UVA/UVB pre-irradiation Boots	UVA/UVB after-irradiation Boots	Critical lambda boots	Boots star rating
Japan PA rating			

Table 1: Parameter selection for the SPF report

Production quality contr

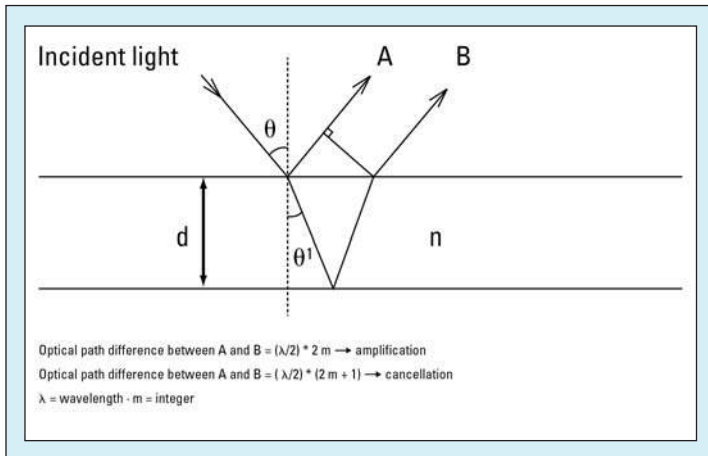## Film thickness determination using UV spectroscopy

Figure 1: Principle of interference

T he UV spectroscopy can be applied for the non-destructive determination of layer thicknesses of thin films. This determination is based on the simple physical phenomenon of interference, resulting from standing waves between two phase boundaries. In order to make this possible in UV spectroscopy, the materials under investigation must exhibit layer thicknesses of approximately 0.3 to 60 µm. The refractive index of the material must be known to be able to carry out this determination.

Reflectance spectroscopy and transmission measurement

There are basically two UV measuring modes – reflectance and transmittance spectroscopy – which enable interference measurement in application areas such as thin films deposited onto materials or transparent films consisting of a single material.

Thin films can be present on non-transparent carrier materials. The uniformity of the surface film can be determined using reflectance spectroscopy. The sample surface must be smooth and mirror-like. Rough surfaces are not suitable, as the diffuse reflectance taking place at the surface prevents the formation of an interference pattern.

A typical example of this application is film thickness determination of wafers during chip production, where process control of the thicknesses of the applied SiO_2 films is critical. Wide variations in film thickness result in high failure rates during further processing.

The transmission mode is applied for thin films on a transparent substrate, for instance in the manufacture of foils. In the transmission mode it is also possible to analyze films consisting of only one material.

Theory

An example is presented to explain the physical principle of reflectance spectroscopy. Light striking a film at an angle of incidence θ invokes an interaction/interference of the incident surface A with an angle of reflectance of the opposite surface B (bottom), as shown in Figure 1, which results in a spectrum with interference patterns (Figure 2). Counting the number of peaks (or valleys) in this pattern in a fixed wavelength range, the film thickness can be calculated according to the following equation:

$$d = \frac{\Delta m}{2\sqrt{n^2 - \sin^2 \theta}} \times \frac{1}{\left(\frac{1}{\lambda_2} - \frac{1}{\lambda_2}\right)}$$

where d is the film thickness, Δm is the number of peaks in the fixed wavelength range, n is the index of refraction, θ is the angle of incidence of the light on the sample surface, and λ_1 and λ_2 are the initial and final wavelength of the respective range.

The calculation for two samples, a 10 µm polyvinyl chloride film and a 46 µm polycarbonate film, with different film thickness is
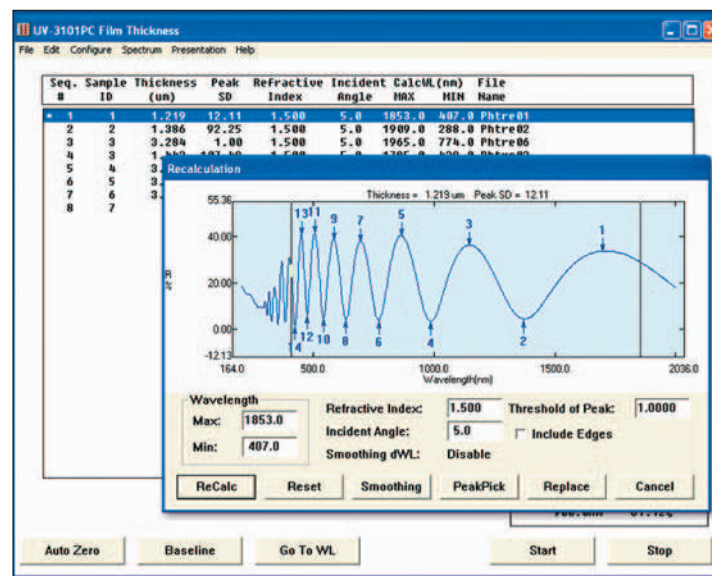

Figure 2: Screenshot of the film thickness software and an example of the selection criteria for film thickness determination
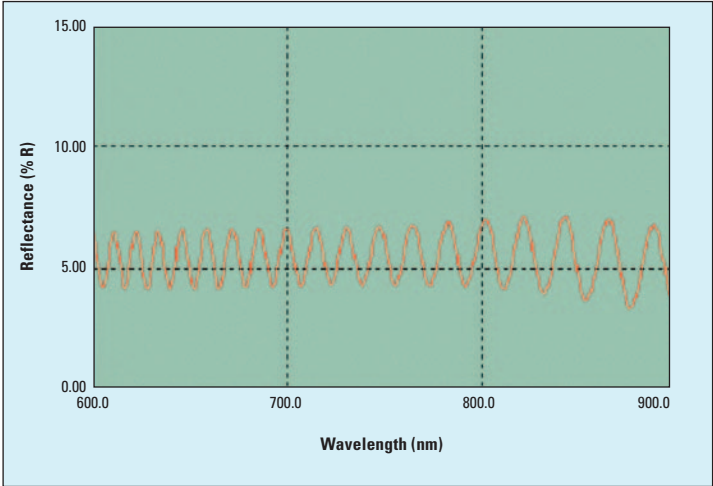
ol

Figure 3: Reflectance measurement of a polyvinyl chloride film with a
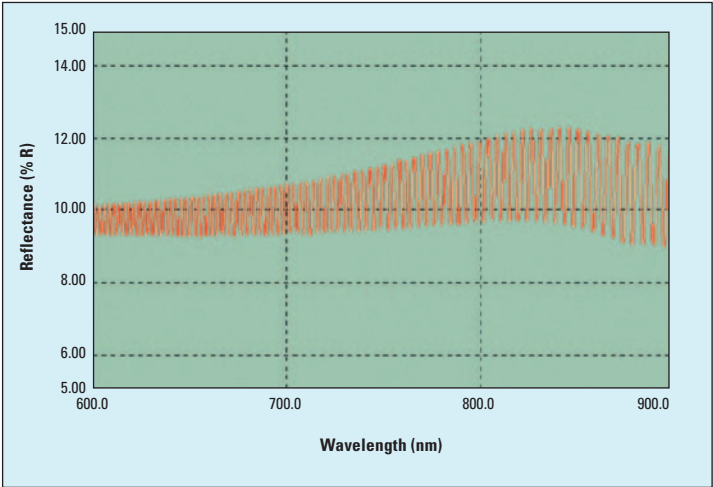film thickness of 10 μm

Figure 4: UV reflectance spectrum of a polycarbonate film with a
film thickness of 46 μm

presented below. Figure 3 shows the interference pattern of the 10 μm PVC film in the wavelength range of 600 to 900 nm. This is compared with the higher film thickness sample of 46 μm. The result is an excellent example demonstrating that thin films lead to wide amplitudes and thicker films to narrower amplitudes.

The calculation can be easily carried out using the film thickness determination tool featured in the software. When all physical parameters such as refractive index, angle of incidence and wavelength range are known, the film thicknesses are calculated automatically (Figure 2).

Most valued features of the TOC-Control V software

Now also Vista compatible
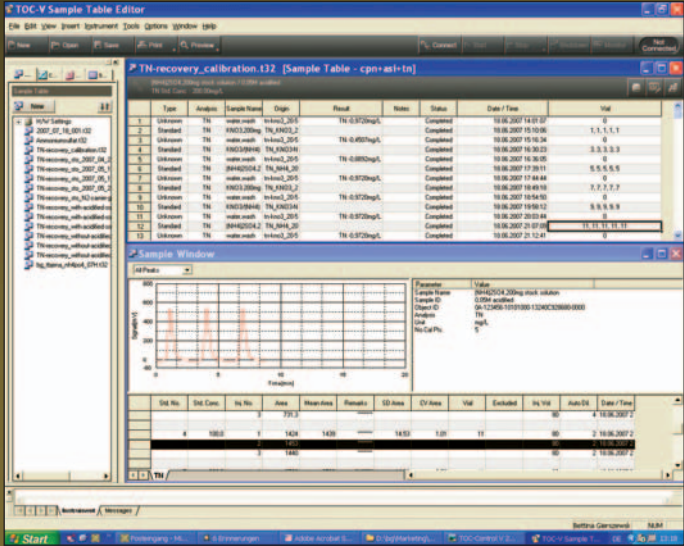
TOC-Control V software 2.1

An update (version 2.1) for Windows Vista is now available for the TOC-Control V software successfully introduced last year. Among the features most valued by our users are:

Adding additional samples during ongoing operation
Any number of samples, calibration curves or control samples may be added in the edit mode. Previously measured samples can be recalculated and reports can be printed. During activation of the edit mode the ongoing measurement cycle continues running.

Other users can take over during ongoing operation
In access-controlled systems, it is important that change of personnel during shift operation allows users to log in and out without interrupting the ongoing measuring cycle. This can be configured in the user authorization rights for each user.

Simplified recalculation in a single step
In the past, recalculation of previously measured samples using another calibration curve had to be carried out individually for each sample. In the TOC-Control V version 2.00 software, however, the respective samples are tagged in the sample table before a new calibration curve is selected and the recalculation is carried out.

Simple operation
Sample tables can be established via a simple "drag & drop" operation. Using the mouse, the desired elements are dragged into the sample table from a list of the established calibration curves, measuring methods, control samples and measuring sequences. The right mouse button contains many functions which greatly simplify operation.

The use of shorter "Wizards" enables even faster establishment of calibration curves and measuring methods as well as improved templates for sample tables in routine analyses.

Everything within view

Quality control of camera objectives with UV-2600 and MPC-2600

With the introduction of the new generation of LO-RAY-LIGH® gratings in Shimadzu's new UV-2600/UV-2700 UV-VIS spectrophotometer series, many application areas in the field of optics can now be covered. In addition to single optical elements such as lenses and glasses, composite materials or single-coated systems and even entire assemblies can now be analyzed. Camera objectives are small optical benches, equipped with different lenses and glasses with protective coatings or surface finishes. The quality of an objective is determined by its light intensity and low optical aberrations.

The light intensity can be determined spectroscopically. By combining the UV-2600 or UV-2700 with a MPC-2600 extra large sample compartment, non-destructive analysis of entire camera objectives is possible. This sample compartment is equipped with a V-shaped holder, ensuring stable positioning of the objective. The holder can be positioned in all three dimensions, so that the analytical irradiation hits the center of the objective optics and passes through the optical bench, while the spectrophotometer measures the incident light intensity, which is displayed in the form of transmittance spectra. These spectra show not only the light throughput in percentages but also the transmission range as a function of wavelength for visible and ultraviolet light.

Quality determination of objectives and camera accessories

Using this combination of instruments, it becomes possible to establish a quality determination process that allows production control of a production series.

Figure 1: Two camera objectives from different manufacturers, featuring a standard lens and a macro lens

In addition, it is also possible to check the specifications that characterize the objective. The goal is, after all, to manufacture high-quality objectives. There are several criteria in photography that can be met by implementing such quality control:

- the visible range of an objective for the image quality of the colors, or depth of field in the photographs
- the quality of the coatings on glasses and lenses
- sensitivity in the red or blue ranges.

In addition, a UV-VIS spectrophotometer can be used to qualify camera accessories such as polarizing filters or UV filters.
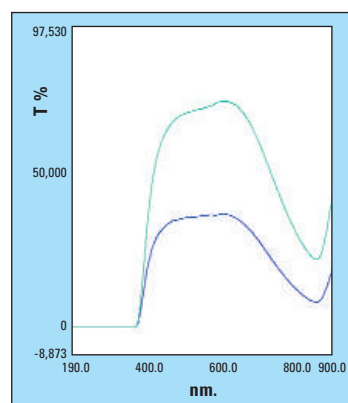
Testing two objectives

In the experiment shown here, two objectives from different manufacturers were tested. Since the objectives have been designed for different uses, they have different characteristics:
1. Fixed lens system, 50 mm F/1.2
2. Macro lens, 28 - 300 mm F3.5 - 6.3 DG Macro (F = focal length, 1.2 or 3.5 - 6.3 are aperture values.)

The objectives were measured using the UV-2600 and MCP-2600 sample compartment. The objectives were placed on the V-table of the MPC-2600 and were brought to the measuring position. The measuring assembly simulates the incident light for imaging within the camera. The objectives were measured with the incident light from outward to inward.

The detector (photomultiplier) is located in an integrating sphere (Ulbricht sphere) and displays the transmittance, i.e. the light of the transmittance of the object (objective). Furthermore, absorptions by sealings can be expected, as well as effects of reflections and antireflective coatings.

Discussion of the spectra

When the focal length is increased, the light transmittance decreases due to the reduction of the field of view, as can be seen in Figure 2. The spectra displayed are the light transmittance at 28 mm (70.6 %) and 300 mm (37 %). Due to the reduced light transmittance, taking a photograph using the zoom setting needs a longer exposure time, a larger aperture or additional lighting in order to obtain more light intensity.

The quality of the objectives varies according to the function of the

objective. An objective with fixed focal length can result in good light transmittance with few components. Figure 3 shows two very different representative examples.

The light transmittance of the fixed focal length results in a value of 86.7 % while the variable focal length results in a transmittance of up to 70.6 %. Assuming the loss of 4 % of the original energy at all surfaces based on the physics of flat glass, it might be concluded that the fixed objective consists of 4 glass components.

With extrapolation, four glass components should result in a loss of approx. 15 % of transmittance. This corresponds approximately to the measured value of 86.7 %. But this is, of course, a rough estimate for an unknown object in which other aspects, e.g. filtering surface coatings, can have an influence.

Both objectives are distinguished by their wavelength range. The objective with fixed focal length
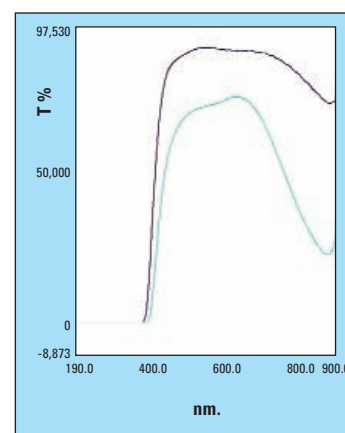
Figure 3: UV-VIS spectra and comparison of the light transmittance of a fixed objective (black) of 50 mm with a zoom objective (green) at a setting of 25 mm

features a high light transmittance. In addition, a profile maximum at approx. 520 nm corresponding to the green wavelength range is apparent. In comparison, the zoom objective is optimized for wavelengths in the red range (approximately 620 nm).

Figure 2: UV-VIS spectra of a zoom objective at a setting of 25 mm (green) and 300 mm (blue)

SHIMADZU
Excellence in Science

Application News

Spectrophotometric Analysis

Haze Evaluation of Plastic Sheets and Films – Haze Measurement Using ISR-1503 Integrating Sphere Attachment –

No.A525

Plastics are broadly grouped into thermosetting plastics and thermoplastics, and thermoplastics are further grouped based on properties such as heat resistance and mechanical strength. Apart from these mechanical and thermal properties are the optical properties of plastics that include transmittance, reflectance, and haze. Haze refers to the proportion of diffuse transmittance to total transmittance, and is used to evaluate material surface treatment (roughness and matte). Materials used for solar cells may also have a periodic structure (textured structure) on their surface to increase dispersion and contain light. Measuring the haze of plastic materials is defined by international standard ISO 14782, while the same content is reproduced in Japanese Industrial Standard (JIS) K 7136.[1,2] This article describes analyzing plastics of different properties using Shimadzu UV-3600 Plus UV-VIS-NIR spectrophotometer with ISR-1503 integrating sphere attachment to calculate their haze and solar transmittance.

■ ISR-1503 Optical System and Haze Measurement

Fig. 1 shows the UV-3600 Plus and ISR-1503. Fig. 2 shows the ISR-1503 optical system. The optical system of the ISR-1503 is designed to enable horizontal sample placement when measuring transmittance/0 degree reflectance to allow measurement of film and tapered samples without special immobilization. Fig. 3 shows the method used to measure total transmittance and diffuse transmittance, which are properties used to calculate haze. Total transmittance is determined by measuring both light transmitted straight through the sample and light diffused inside the sample. Diffuse transmittance is determined by measuring only diffuse light after removing the standard white board from the integrating sphere, as shown by the bottom image in Fig. 3. τ_1 and τ_2 in JIS K 7136 correspond to measured total transmittance[Note 1] (τ_1 being 100 % transmittance without sample placement). τ_3 and τ_4 correspond to measured diffuse transmittance[Note 1] (τ_3 being almost 0 % transmittance without sample placement). Haze is defined as the ratio of diffuse transmittance to total transmittance, and can be calculated with the following equation. Haze (%) = [(τ_4 / τ_2) - τ_3 (τ_2 / τ_1)] × 100

Fig. 1 UV-3600 Plus with ISR-1503 Installed
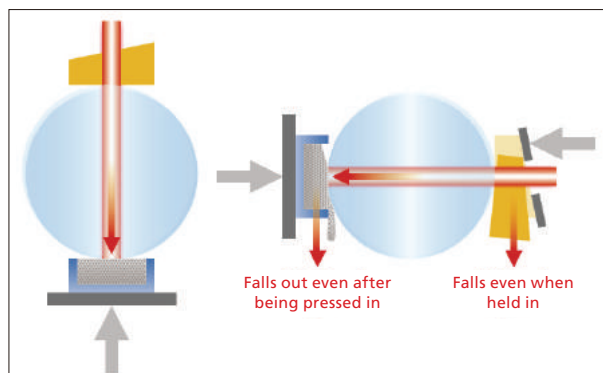

Falls out even after being pressed in

Falls even when held in

**Fig. 2 Left: Optical System of ISR-1503,
Right: Optical System of Conventional Integrating Sphere
(Lateral View of Integrating Sphere)**

Standard White Board

Reference Light

Measured Light

Sample

Standard White Board

Detector (Top/Bottom of Integrating Sphere)

Reference Light

Measured Light

Sample

Standard White Board

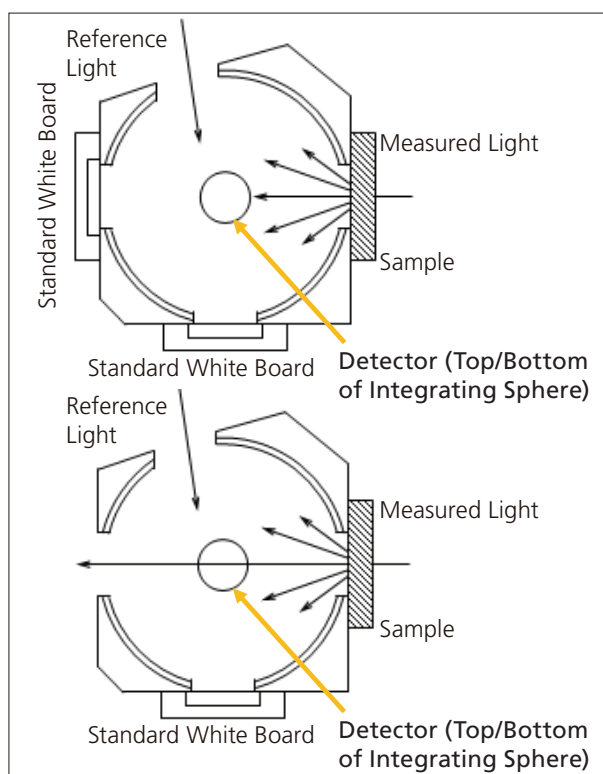Detector (Top/Bottom of Integrating Sphere)

**Fig. 3 Top: Total Transmittance Measurement
(Corresponds to τ_2 Measurement Method
from JIS K 7136)
Bottom: Diffuse Transmittance Measurement
(Corresponds to τ_4 Measurement Method
from JIS K 7136)**

Sample Spectra Measurement

Fig. 4 shows the plastics of different materials with different surface treatments that were analyzed. Samples No. 1 to 5 are sheets of approximately 2 to 3 mm thickness. Samples No. 1 to 3 are made of polymethyl methacrylate (PMMA), No. 2 has a matte treatment, and No. 3 has a textured structure in a striped pattern. No. 4 is made from polyethylene terephthalate (PET), and No. 5 is made from polyvinyl chloride (PVC). No. 6 and 7 are films of approximately 0.3 mm thickness and made from PVC with a plasticizing agent additive (phthalate ester). No. 7 has been given a surface treatment. No. 8 and 9 are films of approximately 0.03 mm thickness. No. 8 is made from polypropylene (PP) and No. 9 is made from polyethylene (PE). Samples were cut to sizes allowing their analysis with the ISR-1503 (maximum dimensions of W176 × D168 × T20 mm), and analyzed using the conditions shown in Table 1.
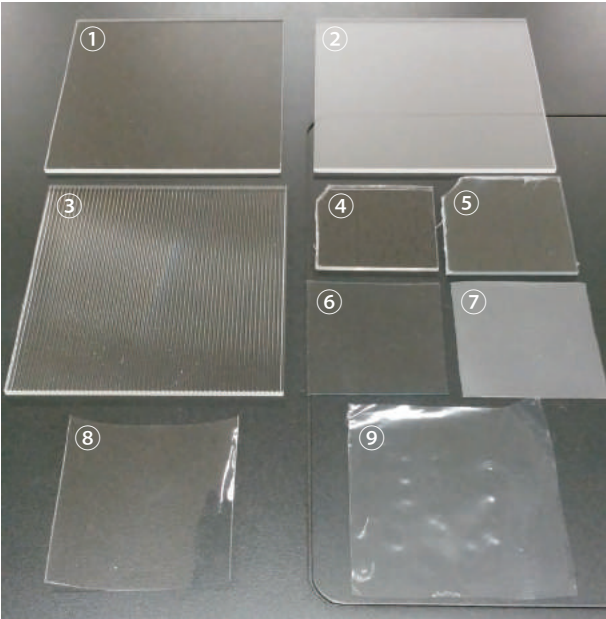

Fig. 4 Plastics of Different Materials and Surface Treatments
  1: PMMA (Clear), 2: PMMA (Matte), 3: PMMA (Textured),
  4: PET, 5: PVC, 6: PVC (Clear), 7: PVC (Surface Treated),
  8: PP, 9: PE

Table 1 Measurement Conditions

Instruments Used	: UV-3600 Plus and ISR-1503
Measurement Wavelength Range	: 200 nm to 2500 nm
Scanning Speed	: Intermediate
Sampling Pitch	: 1.0 nm
Photometric Value	: Transmittance
Slit Width	: (20) nm
Light Source Switching Wavelength	: 290 nm
Detector Unit	: External (3 Detectors)
Detector Switching Wavelength	: 870 nm/1650 nm
Grating Switching Wavelength	: 850 nm
S/R Changeover	: Reverse
Stair Correction	: Effective

Fig. 5 shows the total transmittance spectra and diffuse transmittance spectra of samples No. 1 to 3. Samples No. 1 to 3 are all made of PMMA. The total transmittance spectra show all samples with around 90 % transmittance at long wavelengths above 400 nm. The diffuse transmittance spectra show around 40 % transmittance for the matte treatment sample (No. 2) and around 70 % transmittance for the textured structure sample (No. 3). This shows the surface treatment of samples results in light diffusion. Fig. 6 shows total transmittance spectra in the range 200 to 2500 nm. The results show that PMMA absorbed light at long wavelengths above 1000 nm. Samples No. 1 to 3 show absorption at almost the same wavelengths since they are made of the same material.
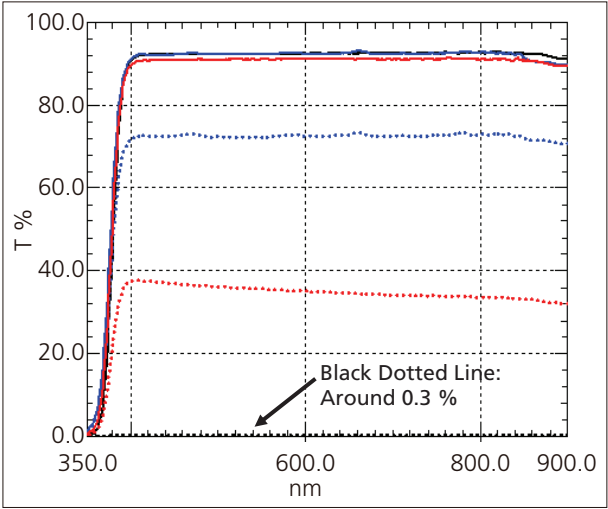

Fig. 5 Solid Lines: Total Transmittance,
  Dotted Lines: Diffuse Transmittance (PMMA)
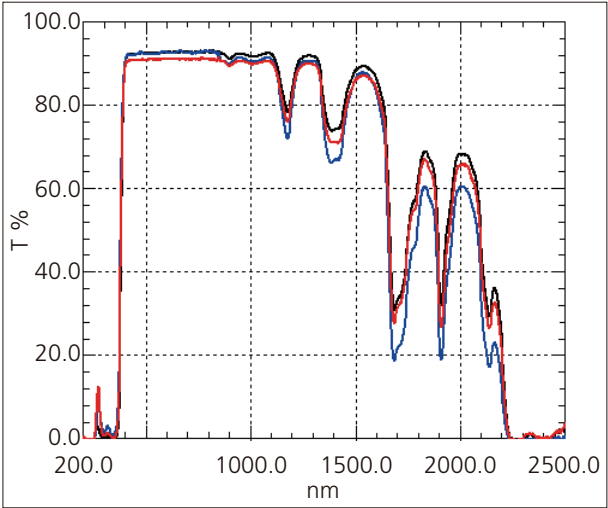 **Black: No. 1 Clear, Red: No. 2 Matte, Blue: No. 3 Textured**

Fig. 6 Total Transmittance Spectra (PMMA)
  Black: No. 1 Clear, Red: No. 2 Matte, Blue: No. 3 Textured

Fig. 7 shows the total transmittance spectra and diffuse transmittance spectra of samples No. 5 to 7. The main material used in samples No. 5 to 7 is PVC. The total transmittance spectra show film samples with around 90 % transmittance at long wavelengths larger than 400 nm. The sheet samples were shown to absorb light at around 600 nm. The diffuse transmittance spectra show evidence of light diffusion for surface treated sample No. 7, with around 40 % transmittance.

Fig. 8 shows total transmittance spectra in the range 200 to 2500 nm. The results show samples of the same material absorbed light at almost identical wavelengths, and the degree of absorption differed depending on sample thickness.

Fig. 9 shows total transmittance spectra and diffuse transmittance spectra for samples No. 4, 8, and 9. The total transmittance spectra show all samples with around 90 % transmittance at long wavelengths larger than 400 nm. The spectra also show around 90 % transmittance for thin film samples (No. 8 and 9) at wavelengths of 350 to 400 nm. The spectra also show low diffuse transmittance for all samples.

Fig. 10 shows total transmittance spectra in the range 200 to 2500 nm. The results show the material in sample No. 4 absorbed light at long wavelengths above 1000 nm. This shows the thin film samples displayed high transmittance at almost all wavelengths.
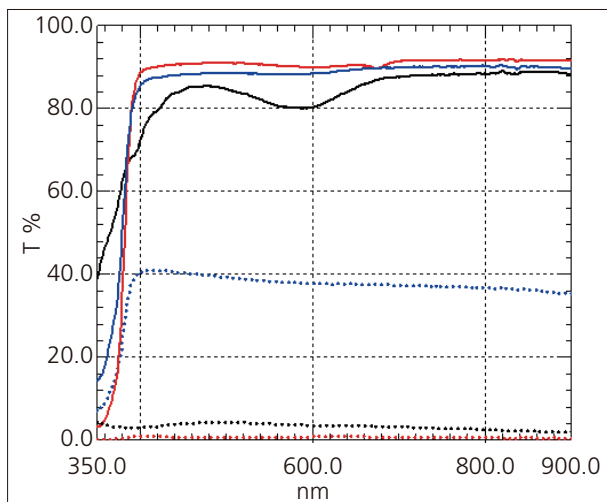

**Fig. 7 Solid Line: Total Transmittance,
Dotted Line: Diffuse Transmittance (PVC)
Black: No. 5 Sheet, Red: No. 6 Film (Clear),
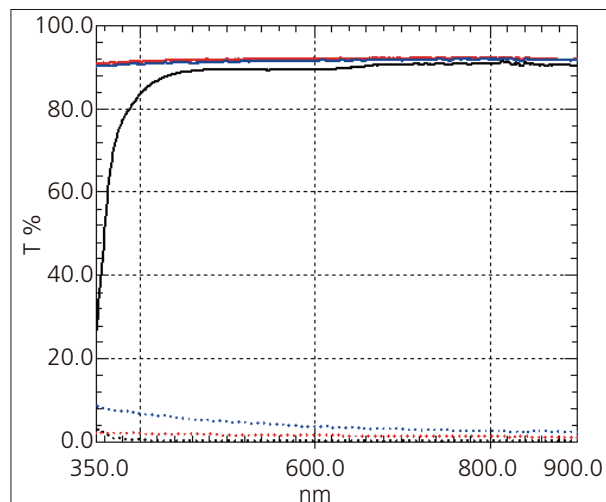Blue: No. 7 Film (Surface Treated)**

**Fig. 9 Solid Line: Total Transmittance,
Broken Line: Diffuse Transmittance
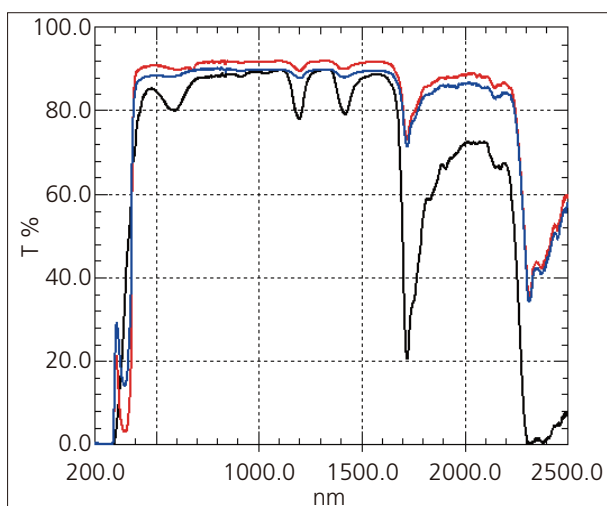Black: No. 4 PET Sheet, Red: No. 8 PP Film,
Blue: No. 9 PE Film**

**Fig. 8 Total Transmittance (PVC)
Black: No. 5 Sheet, Red: No. 6 Film (Clear),
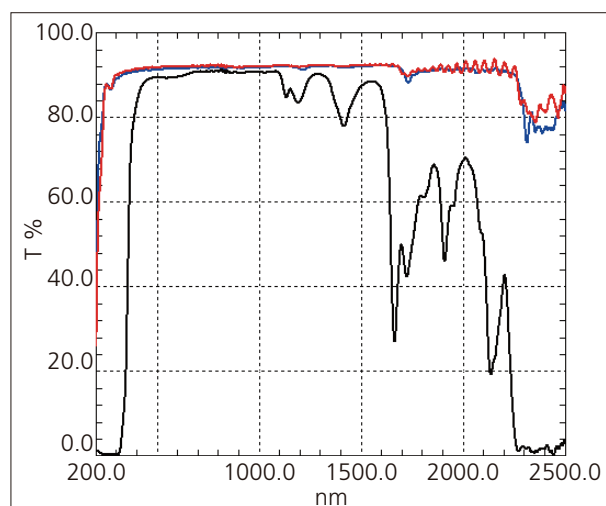Blue: No. 7 Film (Processing)**

**Fig. 10 Total Transmittance
Black: No. 4 PET Sheet, Red: No. 8 PP Film,
Blue: No. 9 PE Film**

Table 2 Haze and Visible Light/Solar Transmittance

Sample Type	No.	Material	Thickness (mm)	Haze (%)	Visible Light Transmittance (%)	Solar Transmittance (%)
Plate	1	PMMA (Clear)	2.08	0.18	92.49	87.92
	2	PMMA (Matt)	2.16	38.76	91.06	86.32
	3	PMMA (Textured)	3.15	78.28 [*3]	92.36	86.85
	4	PET	1.99	0.13	89.38	86.53
	5	PVC [*1]	2.15	4.45	81.93	83.63
Film	6	PVC (Clear) [*2]	0.303	0.50	90.35	89.04
	7	PVC (Processing) [*2]	0.303	43.11 [*3]	88.46	87.58
	8	PP	0.031	1.53	91.92	91.95
	9	PE	0.035	4.37	91.41	91.55

*1: Carboxylated, *2: Phthalic ester, *3: Values for reference only; JIS K 7136 applicable for measurement of samples with 40 % or lower haze

Color analysis software was used to calculate τ_1, τ_2, τ_3, and τ_4 based on total/diffuse transmittance spectra. Color analysis software can output results in a variety of formats, including the L*a*b* color system, Munsell color system, and XYZ color system. τ_1, τ_2, τ_3, and τ_4 correspond to the Y value (color value) in the XYZ color system calculated based on a D_{65} standard illuminant. Haze results calculated based on each τ value are shown in Table 2. The results show surface treated samples No. 2 and 7 with a haze of around 40 %. They also show a high haze for sample No. 3 with its textured structure. Some haze was also measured in sheet sample No. 5 PVC, and thin film samples No. 8 and 9.

Visible light/solar transmittance results calculated using solar transmittance software are also shown in Table 2[Note 2]. All samples, including those with surface treatment, showed visible light/solar transmittance of around 80 to 90 %. We can predict that degree of light diffusion changes without almost no change in sample luminosity.

■ **Conclusion**

Total transmittance and diffuse transmittance of different plastics were measured using Shimadzu UV-3600 Plus with ISR-1503 attachment. Haze and visible light/solar transmittance of each sample were also calculated with software and analytical results.

Spectral, haze, and visual light/solar transmittance measurement is expected to be applied to evaluate and confirm the properties of ever more sophisticated materials and products in the future.

Note 1: JIS K 7136 assumes use of a single beam and for this reason requires a compensation port in the integrating sphere. The method used in this article is not entirely compliant with JIS K 7136, as the UV-3600 Plus uses a double beam and the ISR-1503 has no compensation port. The assumption was made that these factors did not affect haze results.

Note 2: The solar transmittance software calculates solar transmittance in the range of 300 to 2100 nm. A user defined function allows solar transmittance to be calculated in the range of 300 to 2500 nm.

References
1) ISO 14782 Plastics — Determination of haze for transparent materials
2) K 7136 Plastics — Determination of haze for transparent materials

SHIMADZU

Shimadzu Corporation

www.shimadzu.com/an/

Application News

No.A526

Spectrophotometric Analysis

Optical Properties of Films and Glasses Used to Protect Smartphones

Just as new smartphones are constantly being developed and marketed, a variety of accessories are sold alongside them. Films and glasses used to protect smartphone screens are among these accessories, with such products given a variety of optical properties including blue light reduction and screen privacy.
Here, we describe using a SolidSpec-3700DUV UV-VIS-NIR spectrophotometer with variable angle absolute reflectance attachment to measure the optical properties of films and glasses used for smartphone protection.

■ Sample Measurement with Variable-Angle Absolute Reflectance Attachment

Fig. 1 shows the sample compartment of the SolidSpec-3700DUV with a variable angle absolute reflectance attachment. The variable angle absolute reflectance attachment allows for measurement of transmittance and absolute reflectance with light at different angles of incidence on the sample. Please refer to Application News No. A390 and A394 for detailed information about the variable angle absolute reflectance attachment.
Four commercially available protective films and four glass screen protectors designed for smartphones were obtained as samples. The four protective films and four glasses were designed for screen privacy, high hardness, blue light reduction, and clarity. Transmittance at different angles of incident light and 12-degree absolute reflectance were measured using the conditions shown in Table 1. A polarizer and quartz depolarizer[Note 1] were used to depolarize any polarized light during measurement. Fig. 2 shows transmittance spectra with light at an angle of incidence of 0 degrees.

Table 1 Analytical Conditions

Instrument Used	: SolidSpec-3700DUV, large polarizer assembly, variable angle absolute reflectance attachment, quartz depolarizer[Note 1]
Measurement Wavelength Range	: 250 nm to 850 nm
Scanning Speed	: Low speed
Sampling Pitch	: 1.0 nm
Slit Width	: (12) nm
Light Source Switching Wavelength	: 310 nm

Fig. 2 Transmittance Spectra Measured at 0-Degree Angle of Incidence
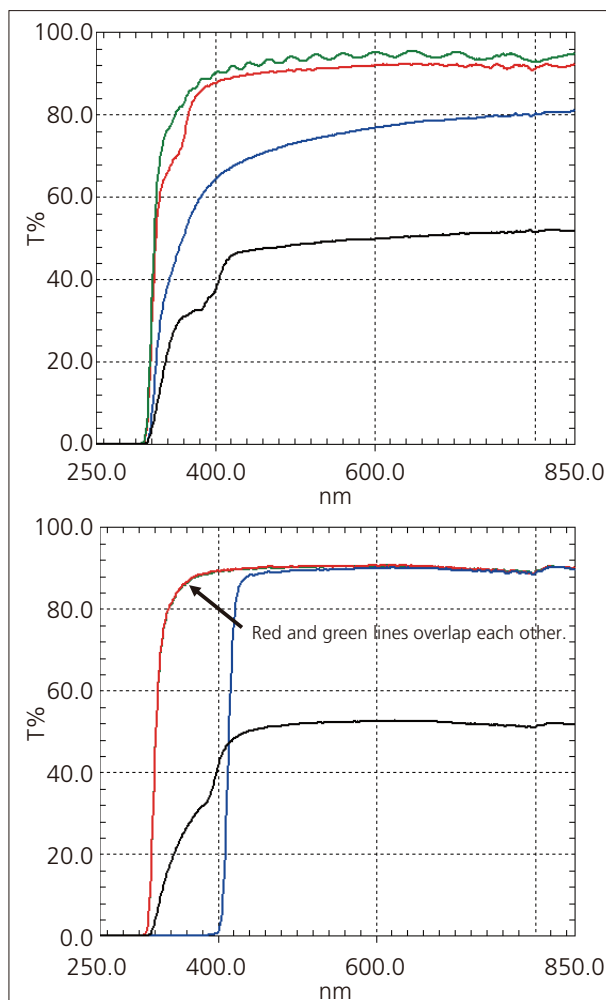Top: Films, Bottom: Glasses, Black: Screen Privacy, Red: High Hardness, Blue: Blue Light Reduction, Green: Clarity

Fig. 1 Sample Chamber of SolidSpec-3700DUV with Variable Angle Absolute Reflectance Attachment

The film designed for screen clarity had the highest transmittance out of the four films, and the film designed for blue light reduction gradually reduced transmittance from 600 nm across the short wavelength region. The film sample designed for screen privacy exhibited around 50 % transmittance from a 0-degree angle of incident light. The glass samples designed for screen clarity and hardness exhibited almost identical transmittance spectra. The glass designed for blue light reduction showed a sudden drop in transmittance from around 400 nm in the short wavelength region. Similar to the film designed for screen privacy, the glass designed for screen privacy exhibited around 50 % transmittance from a 0-degree angle of incident light. Fig. 3 shows visible light transmittance[1] at different angles of incident light[Note 2]. Visible light transmittance is the transmittance of daylight as prescribed by the Japanese National Committee of CIE. Visible light transmittance is easily calculated by the solar transmittance analysis software used, since it comes with the spectral distribution of daylight as prescribed by the CIE. Visible light transmittance was almost unchanged at different angles of incident light for samples that were not designed for screen privacy. However, for samples designed for screen privacy, visible light transmittance fell to around 10 % at an angle of incident light of 30 degrees.
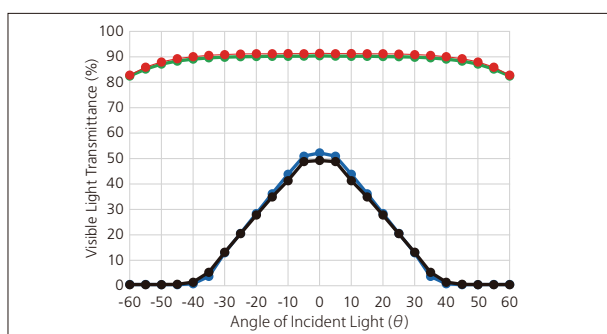

Fig. 3 Relationship between Angle of Incident Light and Visible Light Transmittance
Black: Screen Privacy (Film), Red: High Hardness (Film), Blue: Screen Privacy (Glass), Green: High Hardness (Glass)

Visible light reflectance, which is defined in a similar way to visible light transmittance, is defined at an angle of incidence of less than 15 degrees. Absolute reflectance spectra were measured at a shallow angle of incidence of 12 degrees, at which transmittance begins to decrease with screen privacy protectors. The results obtained are shown in Fig. 4. The film designed for screen privacy showed a reflectance of around 3 % at all wavelengths, and the film designed to reduce blue light reduced reflectance in the short wavelength region. Despite being almost the same thickness as the film designed for high hardness, the film designed for screen clarity produced interference waveforms. This fact leads to an assumption that the films designed for high hardness and screen clarity have a different

refractive index and are made of different materials. The glass designed for screen privacy produced around 5 % reflectance at all wavelengths, while the other glasses exhibited around 7 % reflectance. The glass protector designed for blue light reduction was the only glass to show a drop in reflectance from around 400 nm in the short wavelength region.
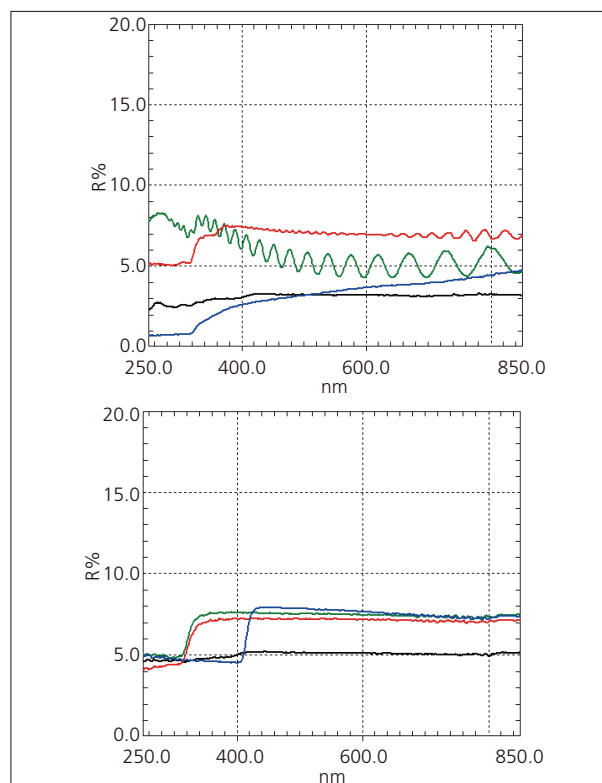

Fig. 4 Absolute Reflectance Spectra Measured at 12-Degree Angle of Incident Light, Top: Films, Bottom: Glasses
Black: Screen Privacy, Red: High Hardness, Blue: Blue Light Reduction, Green: Clarity

■ **Conclusions**

Film and glass products used to protect smartphone screens were analyzed using a SolidSpec-3700DUV with a variable angle absolute reflectance attachment. The optical properties of each sample were confirmed based on transmittance and reflectance measured at difference angles of incident light.

The spectra obtained from each sample allowed for an evaluation of the sophisticated optical properties of protectors designed for screen privacy, to reduce blue light, and for other purposes.

［Reference］
1) JIS R 3106: Testing method on transmittance, reflectance and emittance of flat glasses and evaluation of solar heat gain coefficient.

Note 1) Sigmakoki DEQ-2OP: Pseudo depolarized light is created by setting the polarization of incident light at 45 degrees to the optical axis.
Note 2) Visible light transmittance results at positive angles of incidence were used for visible light transmittance results at negative angles of incidence.

SHIMADZU

Shimadzu Corporation

www.shimadzu.com/an/

Spectrophotometric Analysis

Quantitation of dsDNA Using the Micro-Volume BioSpec-nano Spectrophotometer

Jeff Head, MS, Mark Talbott, Ph.D., Robert H. Clifford, Ph.D.

No. UV-002

The Shimadzu BioSpec-nano is a low-maintenance micro-volume spectrophotometer designed for the modern life science laboratory. It offers superior detection limits, up to 10 times better compared to the competition, making it the perfect instrument for quantitation of DNA, RNA, Protein analysis, and photometric measurements. The "Drop and Click" design combined with easy sample mounting and automated cleaning offers a rapid 3 second analysis time and a 10 second cycle time between samples. The instrument features 3 different path length settings of 0.2, 0.7, and 5 mm with linear range as shown in **Table 2**. This communication presents data on the detection limits of the BioSpec-nano for analyzing dsDNA.

Path Length	5 mm	0.7 mm	0.2 mm
Detection Limit, ng/µL	0.15	0.40	0.89

Table 1: Detection Limits of BioSpec-nano by Path Length

Path Length	5 mm	0.7 mm	0.2 mm
Linear Dynamic Range, ng/µL	0.63-20	6.58-842.5	13.16-3370

Table 2: Linear Dynamic Range of Shimadzu BioSpec-nano by Path Length
[1] For extended linear range, see the brochure for specifications.

Experimental Conditions

All measurements were carried out using double stranded calf thymus DNA (Sigma, USA, D3664-5X-1MG). A series of dilutions was carried out on the DNA standards providing concentrations in the range of 2 to 3500 ng/µL, and were measured using the 0.2, 0.7, and the optional 5 mm path length cells. Data analysis was carried out using the software provided with the instrument. The formula that was used for determining the concentration was: sample concentration = dilution factor X (OD260-OD320) X Nucleic acid concentration factor (50), where OD is the Optical Density. The nucleic acid concentration factor is set in accordance with the analyte selected. The automatic wiper feature was used to clean the target surface, thus eliminating the need for time-consuming manual cleaning techniques used by other manufacturers. All measurements were repeated 3 times or more. The detection limit was determined with an 85% confidence limit from the following equation[2]:

$$\bar{x} \qquad \sqrt{\frac{}{} - \frac{}{}}$$

where $\Delta\bar{x}_{lim}$ is the detection limit, $t_{\alpha,\varphi}$ is the confidence limit based off of the number of degrees of freedom, s_{xb} is the standard deviation of the blank, n_s and n_b are the number of observations on the sample and blank, respectively.

Results

Figure 1 is a plot of the acquired data using the BioSpec-nano after measuring dsDNA with the 0.7 mm path length setting. As seen from the plot, the instrument demonstrates a linear dynamic range from 6.58 to 842.50 ng/µL.
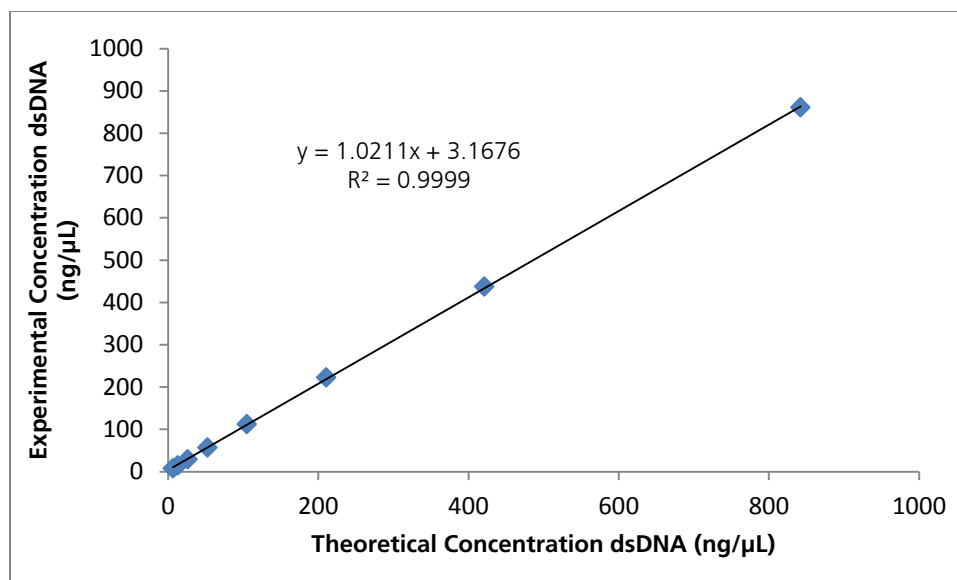
Figure 1: Graph of the experimental concentrations plotted as a function of the theoretical values acquired using the 0.7 mm path length.

Theoretical Concentration	Experimental Concentration				
	Trial 1 ng/µL	Trial 2 ng/µL	Trial 3 ng/µL	Average ng/µL	Standard Deviation ng/µL
842.50	862.38	858.09	861.12	860.53	2.21
421.25	438.78	435.46	436.94	437.06	1.66
210.63	222.92	221.53	221.70	222.05	0.76
105.31	111.68	112.01	113.28	112.32	0.84
52.66	57.29	55.37	56.91	56.52	1.02
26.33	28.07	29.18	28.64	28.63	0.56
13.16	15.48	14.84	13.48	14.6	1.02
6.58	7.52	7.37	7.49	7.46	0.08

Table 3: Average dsDNA concentration values obtained from the BioSpec-nano using a 0.7 mm path length.

Trial 1	Trial 2	Trial 3	Trial 4	Trial 5	Trial 6	Trial 7	Trial 8	Trial 9	Trial 10	Average	Standard Deviation
0.41	0.55	0.19	1.66	1.6	0.9	0.85	0.32	0.03	0.64	0.72	0.55

Table 4: Blank values recorded by the BioSpec-nano in ng/µL for the 0.7 mm path length.

Summary

The BioSpec-nano demonstrates detection limits of 0.15, 0.40, and 0.89 ng/µL for the 5 mm, 0.7 mm, and 0.2 mm pathlengths, respectively. The adjustable path length capability of the BioSpec-nano allowed for measurement of samples across the full concentration dynamic range. Concentrations were calculated by the software in the defined concentration range for each respective path length setting.

References
1. BioSpec-nano Instruction Manual, 206-97213C.
2. Peters, et. al. "Chemical Separations and Measurements-Theory and Practice of Analytical Chemistry," pg. 29.

First Edition: June 2012

SHIMADZU

SHIMADZU

Spectrophotometric Analysis

Quantitation of Protein Using the Micro-Volume BioSpec-nano Spectrophotometer

Andrew Shaff, B.S, Jeff Head, M.S., John Kinyunjui Ph.D, Mark Talbott, Ph.D., Robert H. Clifford, Ph.D.

No. UV-003

The Shimadzu BioSpec-nano is a low-maintenance micro-volume spectrophotometer designed for the modern life science laboratory. It is the perfect instrument for the quantitation of protein. The "Drop and Click" design combined with easy sample mounting and automated cleaning offers a rapid three-second analysis time and a ten-second cycle time between samples. The instrument features three different path length settings of 0.2, 0.7 and 5 mm. The focus of this study is on the quantitation of protein using the 0.2 and 0.7 mm pathlength settings with linear ranges shown in **Table 1**. This communication presents data on the detection limits of the BioSpec-nano for protein analysis.

Pathlength	0.7 mm	0.2 mm
Tested Dynamic Range, mg/mL	0.6-20.5	1.3-20.5
Specified Dynamic Range, mg/mL	0.45-31.8	1.5-114*

Table 1: Linear Dynamic Range of Shimadzu BioSpec-nano by Pathlength
[*1]This report focuses on the lower level range of the instrument.

Pathlength	0.7 mm	0.2 mm
Detection Limit, mg/mL	0.018	.149

Table 2: Detection Limits of BioSpec-nano by Pathlength

Experimental Conditions
All measurements were carried out using protein standard (Sigma, USA, P5619, 2.05 mg/vial). The protein was dissolved in 100 μL of SAFC Biosciences Dulbecco's Phosphate Buffered Saline (DPBS Modified). The molar absorptivity, ε, of the protein standard is 43,824 $M^{-1}cm^{-1}$ with a molecular weight of 66,400 g/mol.[2] An initial stock protein concentration was prepared at 20.5 mg/mL. A series of dilutions were carried out on the protein standard providing samples with concentrations in the range of 1.3 to 20.5 mg/mL for the 0.2 mm pathlength and 0.6 to 20.5 mg/mL for the 0.7 mm pathlength.

All measurements were repeated ten times. The automatic wiper feature was used to clean the target surface, thus eliminating the need for time-consuming manual cleaning techniques. Although the instrument linear range extends to 114 mg/mL, this study focuses on a maximum protein concentration of 20 mg/mL.

Results-Dynamic Range
Table 3 shows the protein concentrations using the 0.2 mm path length setting in the concentration range of 1.3 to 20.5 mg/mL.

Theoretical Concentration (mg/mL)	Experimental Concentration (mg/mL)	%RSD
20.5	20.3	2.8
10.3	10.8	10.4
5.1	5.5	4.7
2.6	2.7	9.4
1.3	1.5	11.0

Table 3: Theoretical and average protein concentrations reported by the BioSpec-nano measured with a 0.2 mm pathlength.

Figure 1: Experimental protein concentrations reported by the BioSpec-nano when using the 0.2 mm pathlength plotted as a function of the theoretical concentrations.

Figure 1 displays the experimental average protein concentration plotted as a function of theoretical concentration using the 0.2 mm pathlength setting. As seen, the BioSpec-nano demonstrates linearity of 1.3 to 20.5 mg/mL when using a pathlength of 0.2 mm.

Table 4 shows the protein concentrations reported by the BioSpec-nano using the 0.7 mm pathlength setting in the concentration range of 0.6 to 20.5 mg/mL.

Theoretical Concentration (mg/mL)	Experimental Concentration (mg/mL)	%RSD
20.5	19.8	1.4
10.3	9.5	7.6
5.1	5.3	14.2
2.6	2.5	27.5
1.3	1.6	26.3
0.6	0.7	6.9

Table 4: Theoretical and average protein concentrations reported by the BioSpec-nano measured with a 0.7 mm pathlength.
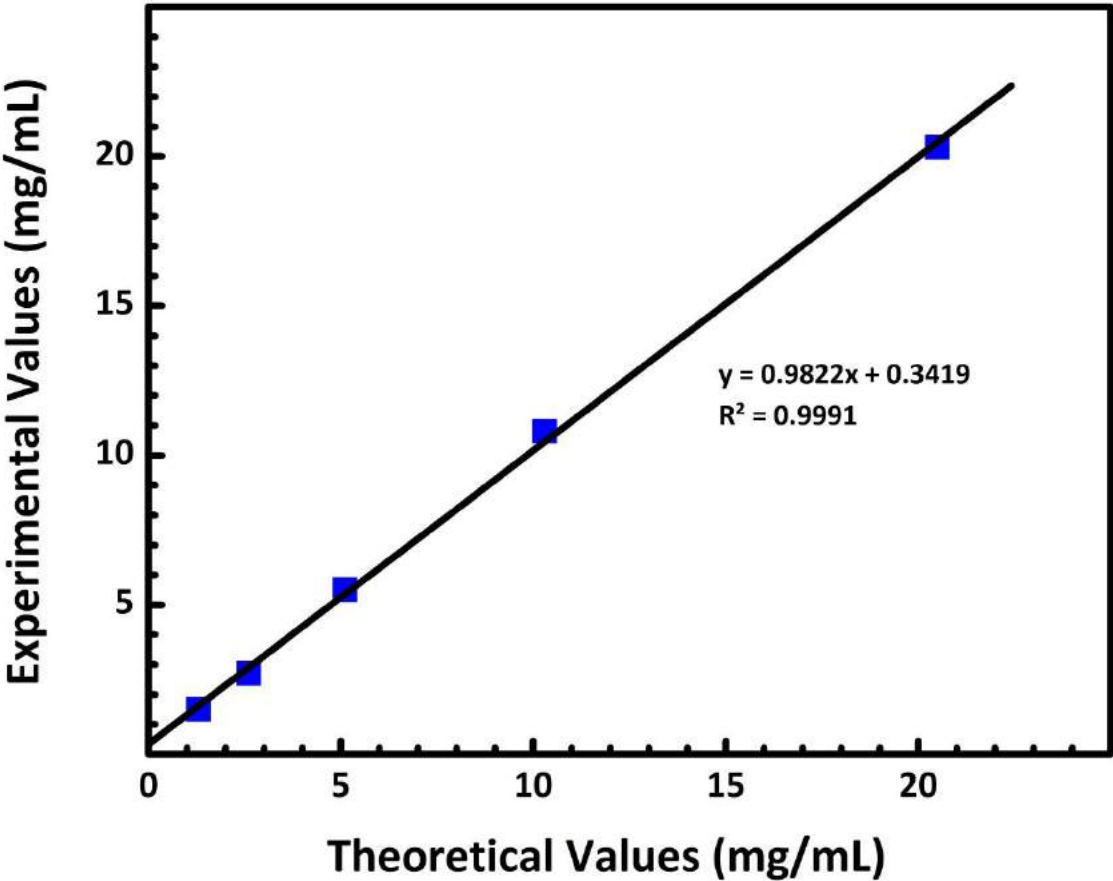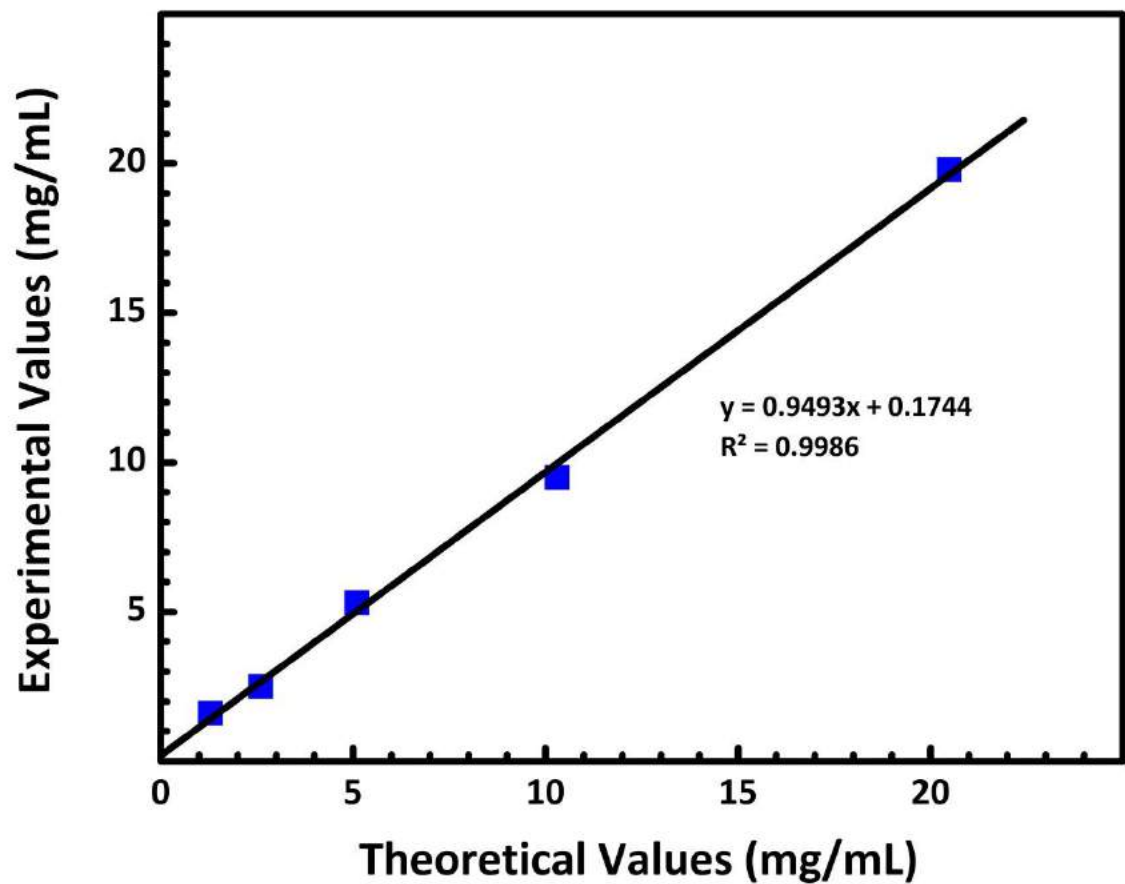
Figure 2: Experimental protein concentrations reported by the BioSpec-nano when using the 0.7mm pathlength plotted as a function of the theoretical concentrations.

Figure 2 displays the experimental average protein concentration plotted as a function of theoretical concentration using the 0.7 mm pathlength setting. As seen from Figure 2, the BioSpec-nano demonstrates a linear range of 0.6 to 20.5 mg/mL when using a pathlength of 0.7 mm.

Results-Detection Limits
The detection limits listed in table 2 were determined with an 85% confidence limit from the following equation[3],

$$\Delta \bar{x} \qquad \sqrt{ - }$$

where $\Delta \bar{x}_{lim}$ is the detection limit, $t_{\alpha,\varphi}$ is the confidence limit based off of the number of degrees of freedom, s_{xb} is the standard deviation of the blank, n_s and n_b are the number of observations on the sample and blank, respectively. **Table 5** displays the average and standard deviation values of the blank measurements recorded by the BioSpec-nano when measuring SAFC Biosciences Dulbecco's Phosphate Buffered Saline ten times for each pathlength setting.

Pathlength	Average	Standard Deviation
0.2 mm	0.022	0.304
0.7 mm	0.059	0.036

Table 5: Average and standard deviations for blank measurements for the 0.2 and 0.7 mm pathlengths.

Summary

The BioSpec-nano demonstrates the ability to quantitatively measure the amount of protein in a sample. Using the 0.2 mm pathlength and 0.7 mm pathlength, the detection limits for protein analysis were calculated to be 0.149 mg/mL and 0.018 mg/mL respectively. Protein analysis is commonly carried out in the life sciences laboratories. The need for a rapid and simple analysis tool for protein samples is met with the use of the micro-volume BioSpec-nano. The included software for the BioSpec-nano provides the instrumental capabilities needed for protein analysis in the modern laboratory.

References

1. BioSpec-nano Electronic Instruction Manual, Software Version 2.02.
2. Practical Handbook of Biochemistry and Molecular Biology, Fasman, D.G., Ed. (1992). CRC Press, Boston.
3. Peters, et. al. "Chemical Separations and Measurements-Theory and Practice of Analytical Chemistry". pg. 29.

2. Spectrophotométrie IR

SHIMADZU
Excellence in Science

Application News

No.**A486**

Spectrophotometric Analysis

Introduction of Quest Single-Reflection ATR Accessary

The ATR (Attenuated Total Reflectance) method is a technique that is widely used for verification testing and contaminant analysis. Here, we introduce the Quest, a new, high-sensitivity single reflection ATR accessory.

■ What Is Quest?

The Specac's Quest is a single-reflection ATR accessory designed for mid- and far-infrared spectroscopic measurement. The internal optical system consists solely of an array of mirrors, thereby permitting extremely simple replacement of the crystal plate. The types of crystal include, in addition to diamond, both ZnSe and Ge crystals. The diamond crystal utilizes a Type III a diamond disk, which features extremely good physical and chemical stability, and permits a maximum measurement range[*1] from 10,000 to 40 cm^{-1}.

Further, a torque limiter built into the clamp eliminates concern about damaging the crystal by preventing the over-application of pressure when bringing the sample and crystal into contact. In addition, the clamp mechanism adopts a swing system, permitting extremely simple placement of the sample, as well as simplifying cleaning.

Fig. 1 shows an overview of the Quest.

Fig. 1 Overview of Quest

■ Sample Measurement Conforming to JP/EP/USP

We conducted analysis of L-alanine and L-arginine, amino acids that require verification testing conforming with the Japanese Pharmacopoeia (JP), European Pharmacopoeia (EP), and United States Pharmacopeia (USP). The measurement conditions are shown in Table 1.

Table 1 Instruments and Analytical Conditions

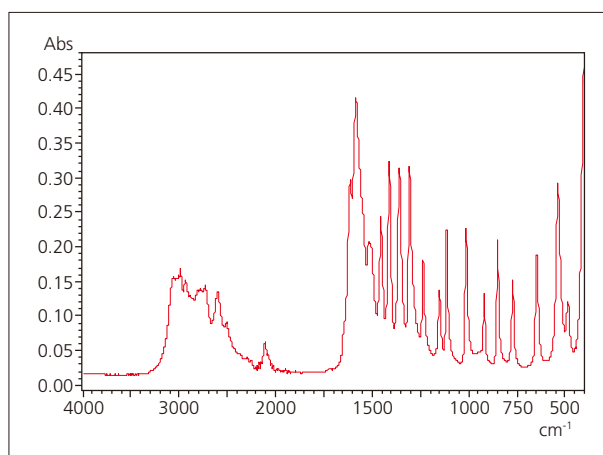|	
Instruments	: IRAffinity-1S, Quest
Resolution	: 2 cm^{-1}
Accumulation	: 45
Apodization	: Sqr-Triangle
Detector	: DLATGS

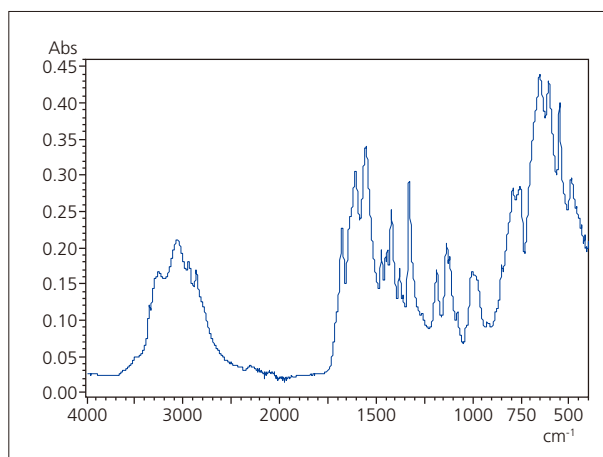**Fig. 2 ATR Spectrum of L-Alanine**

Fig. 3 ATR Spectrum of L-Arginine

The measurement results of Fig. 2 and Fig. 3 demonstrate that good ATR spectra are obtained over the measurement range (from 4,000 to 400 cm^{-1}) specified in each of the Pharmacopoeia.

■ ATR Measurement in Far-Infrared Region by Quest

Measurement of spectra in the far-infrared region is typically conducted by the transmission method, but this requires sample pretreatment that includes dilution and thin film preparation, etc. Measurement by the ATR method, on the other hand, requires no particular pretreatment, thereby permitting easy measurement in the far-infrared region.

Here, we acquired ATR spectra in the far-infrared region[1].

The measured samples consisted of anhydrous caffeine powder and polyvinylidene chloride (PVDC) film. The measurement conditions are shown in Table 2. To avoid interference due to water vapor absorption in the far-infrared region, purging with either nitrogen or dry air is required at the time of measurement.

Table 2 Instruments and Analytical Conditions

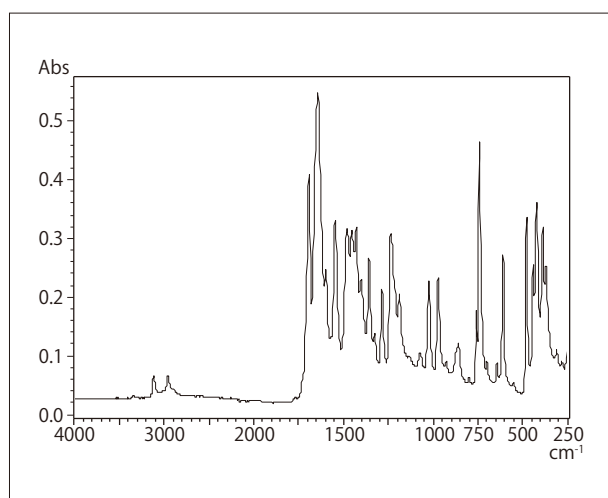|	
Instruments	: IRTracer-100, Quest, Far IR kit, Purge control kit
Resolution	: 4 cm^{-1}
Accumulation	: 100
Apodization	: Sqr-Triangle
Detector	: DLATGS

Fig. 4 FIR-ATR Spectrum of Anhydrous Caffeine

[1] Two types of diamond plate are available with the Quest, a high-throughput type for mid-infrared analysis and an extended wavelength range type for mid- and far-infrared analysis. For this Application News, the extended wavelength range type was used.
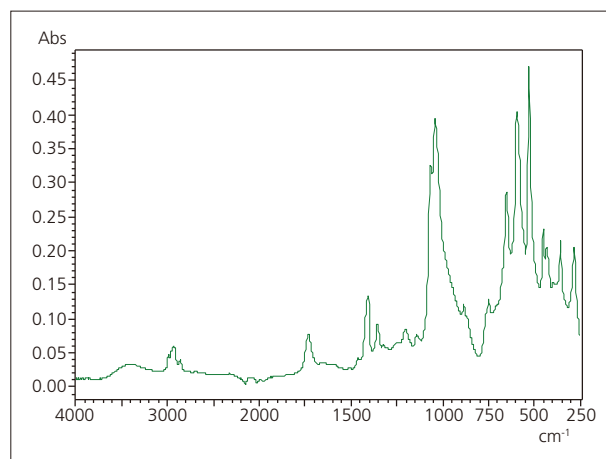

Fig. 5 FIR-ATR Spectrum of PVDC

The measurement results of Fig. 4 and 5 demonstrate that good ATR spectra can be obtained over the wavelength range from 4,000 to 240 cm^{-1}. Also, to compare results using the transmission and ATR methods, spectral measurements of the PVDC sample were conducted in the far-infrared region using both methods.
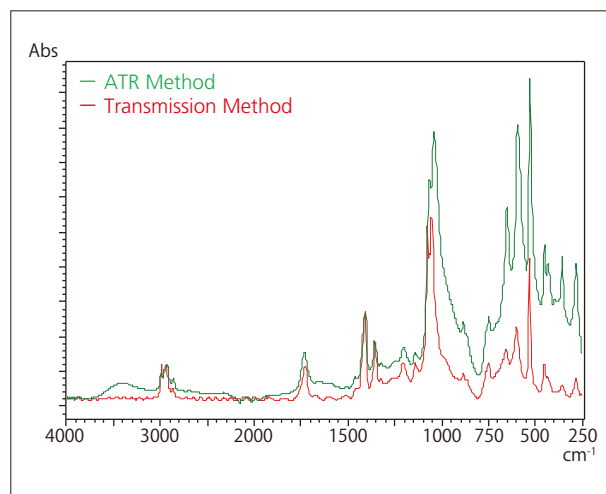

Fig. 6 Comparison of FIR-ATR Spectra of PVDC

The measurement results of Fig. 6 demonstrate that ATR spectra just as good as spectra obtained by the transmission method can be obtained over the wavelength range from 4,000 to 240 cm^{-1}. Note that for the purpose of data comparison, the peak intensities in the vicinity of 1,360 cm^{-1} are aligned.

■ Conclusion

Here, we introduced examples of ATR measurement in the mid- and far-infrared regions using the new Quest ATR single-reflection accessory.

Especially in the far-infrared region, the transmission method was predominantly used until recently, but the ATR method, which requires no pretreatment, is likely to attract greater attention and become an effective technique for applications associated with the far-infrared region.

SHIMADZU

Shimadzu Corporation

www.shimadzu.com/an/

SHIMADZU
Excellence in Science

Application News

No.A501

Spectrophotometric Analysis

Analysis of Thermally Degraded Plastics Using Thermally Degraded Plastics Library

-Applications to Contaminant Analysis-

■ Introduction

In daily life, we encounter a variety of natural products and manufactured goods. In fields such as food products, pharmaceuticals, and machinery, effort is put into quality assurance, striving to prevent the incorporation of contaminants. However, the incorporation of contaminants does inadvertently occur due to unforeseen factors and problems.

While there are many types of contaminants, the plastic parts used in production line, specific environments, and the vicinity become brittle due to aging and thermal degradation, making their incorporation in part a possibility.

FTIR is optimal for the analysis of such plastic contaminants. However, the infrared spectrum of degraded plastic differs from the spectral pattern before degradation. Accordingly, in searches using commercially available plastics libraries, even if a search result has top ranking, it can inadvertently consist of the spectral pattern for a different substance, making identification and qualification difficult.

In this article, we introduce an example of the changes to the infrared spectrum of a plastic degraded by heat, and a sample search using a library containing data created by changing the heating temperature and time beforehand.

■ Changes to the Spectrum of a Polyethylene Film Due to Thermal Degradation

A polyethylene film was wrapped in aluminum foil, and then heated on a hot plate. As it was heated in air, the polyethylene film was subject to oxidative degradation.

Fig. 1 is a photograph of the polyethylene film before heating, and then after heating at 200 °C for two hours. Before heating, it was transparent. After heating, however, it evidently turned brown.

Fig. 2 (top) shows the respective infrared spectra. The measurements were performed using the single bounce ATR method. Polyethylene has a repeating $-(CH_2)_n-$ structure, so before heating, peaks due solely to this structure are visible near 3000 cm^{-1}, 1400 cm^{-1}, and 700 cm^{-1}.

As a result of heating, in addition to the original peaks, there are peaks in the 1700 cm^{-1} to 1750 cm^{-1} range due to -C=O, and peaks in the 1100 cm^{-1} to 1200 cm^{-1} range due to -C-O-. These are likely due to oxidative degradation. Fig. 2 (bottom) shows the spectra for polystyrene film before and after an identical heat treatment. Identical changes are visible here as well.
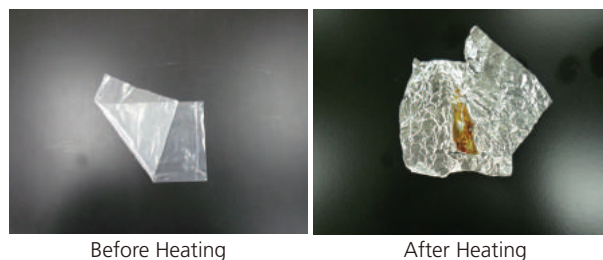

Before Heating   After Heating

Fig. 1 Polyethylene Film Before Heating, and After Heating at 200 °C for 2 Hours

Abs
— Polyethylene, 200 °C, 2 hours
— Polyethylene, unheated

4000 3600 3200 2800 2400 2000 1800 1600 1400 1200 1000 800 cm^{-1}
Polyethylene, unheated

Abs
— Polystyrene, 200 °C, 2 hours
— Polystyrene, unheated

4000 3600 3200 2800 2400 2000 1800 1600 1400 1200 1000 800 cm^{-1}
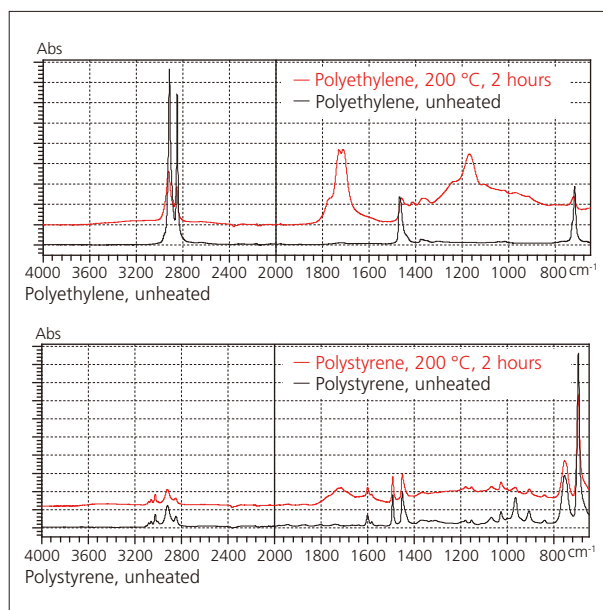Polystyrene, unheated

Fig. 2 Top: Infrared Spectra of Polyethylene Film Before Heating (Black) and After Heating at 200 °C for 2 Hours (Red). Bottom: Polystyrene Film Before Heating (Black) and After Heating at 200 °C for 2 Hours (Red)

■ Analysis of a Contaminant on a Plated Part

A semi-transparent light brown contaminant was visible on a plated product. This area was measured, and the spectrum in Fig. 3 was obtained. A search of the spectrum was performed using a standard library directly, but no equivalent spectra were found.

As shown in Fig. 2, a portion is similar to heated plastic, so it is presumed to be plastic that had been changed by heating.

■ Searches Using Thermally Degraded Plastics Library

As in Figs. 2 and 3, with heating, the infrared spectral pattern is changed due to oxidation. Typical search libraries contain the infrared spectra for plastic samples measured in an unheated state. As a result, if a search is performed directly, there is a risk that the results obtained will be different than for plastic samples after heating.

This article introduces the Thermally Degraded Plastics Library, a proprietary library compiled by Shimadzu. It consists of spectra obtained by measuring samples at the Industrial Research Institute of Shizuoka Prefecture's Hamamatsu Technical Support Center. The library contains 13 plastics, both unheated and thermally degraded at temperatures from 200 °C to 400 °C.

Fig. 4 shows the results of a search utilizing these. It is evident that the heated plastics have top ranking.

In addition, this library contains infrared spectra changed by heating temperature and heating time, which will be useful for estimating the thermal history of a plastic.

Note that this library is not intended for searches of heating time and heating temperature, but is considered for investigating the thermal history of a sample.

■ Conclusion

It is evident that qualitative analysis of plastics that have undergone thermal changes can easily be performed by searching the Thermally Degraded Plastics Library.

This library will prove useful in contaminant analysis.

Table 1 FTIR Analysis Conditions

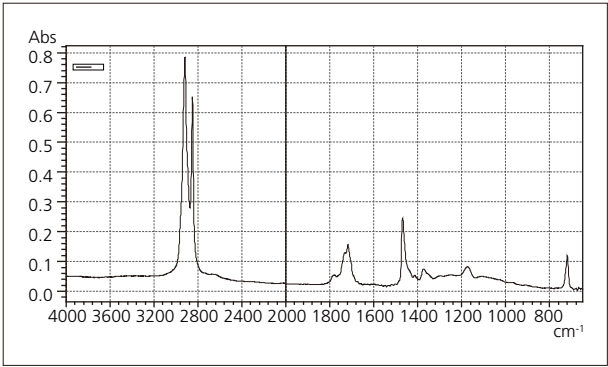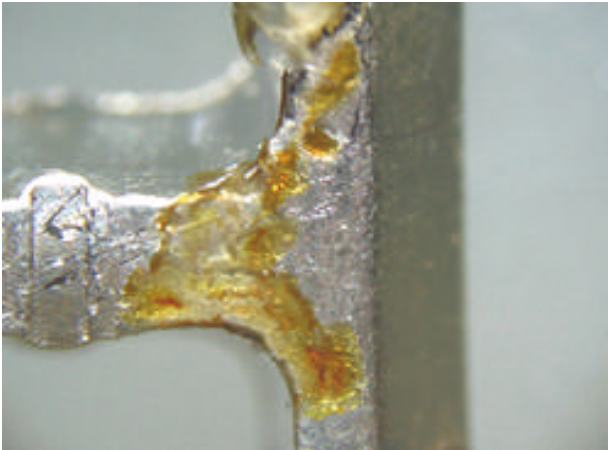|	
Instrument	: IRTracer-100
	MIRacle10
Resolution	: 4.0 cm^{-1}
Accumulation	: 100
Apodization	: Happ-Genzel
Detector	: DLATGS

Fig. 3 Photograph of a Contaminant on a Plated Part (Top); Measured Infrared Spectrum (Bottom)
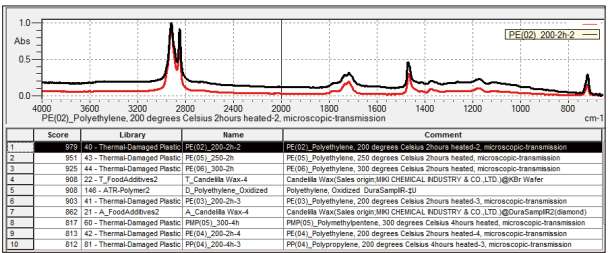

Fig. 4 Search Results Using the Thermally Degraded Plastics Library

SHIMADZU

Shimadzu Corporation

www.shimadzu.com/an/

SHIMADZU
Excellence in Science

Application News

Spectrophotometric Analysis

Quantification of Natural Sugars in Baby Food Products by MID FTIR Spectroscopy

No. FTIR-1401

R.I. Clifford, Jeff Head, M.S., John Kinyanjui, Ph.D., Mark Talbott, Ph.D.

■ Introduction

No other food products focus consumer attention as those that are prepared for consumption by children. Of current interest are the natural and added sugar contents of processed baby foods and juices. Identification and quantification of natural sugars was investigated in baby food products by mid-IR Fourier Transform Infrared (FTIR) spectroscopy. Using Horizontal Attenuated Total Reflectance (HATR), neat baby food samples were analyzed without need for extensive sample preparation. By use of the HATR technique it was demonstrated that high sensitivity could be easily achieved without significant effect from water content. Factor space chemo-metric analysis was used to establish a robust method that allowed the confident measurement of sugar concentrations in these food products. The method was developed using a training matrix of three naturally occurring sugars, fructose, glucose, and sucrose. The method was confirmed using a verification matrix and was found to be readily applicable to the evaluation of sugar quantities occurring in commercial baby food products. Several commercial products were analyzed with this method and quantities of fructose, glucose, and sucrose were determined.

■ Analytical Concept – FTIR Analysis

Baby food samples pose a unique challenge for FTIR analysis because of the strong IR absorption by water. Figure 1 shows the FTIR absorption spectra of water (red) and a 5% aqueous glucose solution (black) acquired using a Horizontal Attenuated Total Reflection (HATR) accessory with a trough liquid plate.[1, 2, 3] The strong absorption bands due to water can be seen between 3800 – 2800, 1700 – 1550, and below 900 cm^{-1}. However, absorption from the glucose can be seen in the fingerprint region between 1486 and 963 cm^{-1}. This water-free absorption region suggests that quantitative sugar analysis in aqueous solutions may be feasible.

FTIR spectra of aqueous solutions of 5% fructose (blue), 5% glucose (green), and 5% sucrose (black) are shown in figure 2. The sugars have characteristic absorption bands that appear in the 1486 – 963 cm^{-1} range. The absorption bands overlap making quantitation by least squares or traditional multivariate analysis routines difficult.

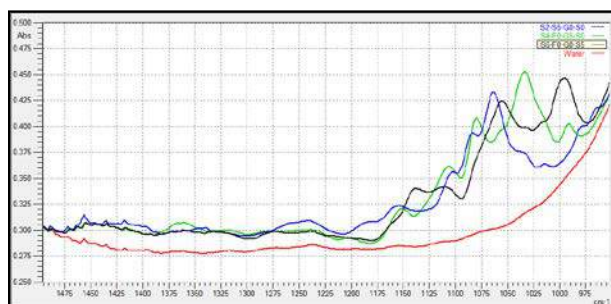**Figure 2**: FTIR spectra of 5% aqueous solutions of water (red), fructose (blue), glucose (green), and sucrose (black)

Figure 1: FTIR spectra for water and a 5% aqueous glucose

■ **Analytical Concept – Factor Space**

Chemometric factor-space analysis was utilized to establish simultaneous calibration curves for the three-sugar aqueous mixtures. Partial Least Squares (PLS) was selected as the factor-space routine of choice. The use of a factor-space analysis routine increased the number of dimensions in the analysis.[4] This allowed for each sugar component to be assigned to a specific dimension or factor-space. In addition, noise in the spectra (e.g. water absorption) was also treated by the additional dimensions. By using the factor-based routines, the components that attributed to analytical noise (e.g. water absorptions) could readily be identified and separated out in the quantitation.

A training set of samples was prepared to cover the full 3-dimensional quantitative space required for analysis of the baby foods. Since there were three sugar components of interest, fructose, glucose, and sucrose, a three dimensional training matrix was created (figures 3 and 4). Aqueous sugar samples were prepared to cover the eight corners of the matrix, the face centered positions of the matrix, and the matrix center.
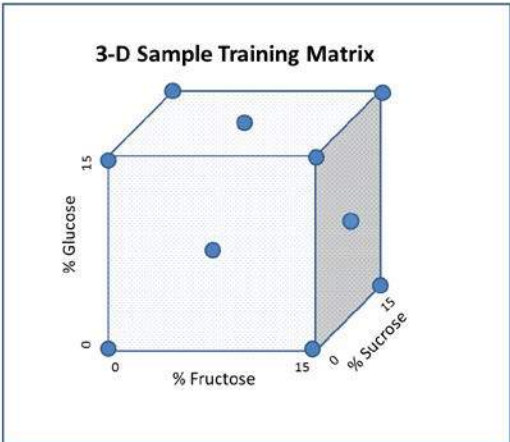

Figure 3: 3-Dimensional cube showing placement of training matrix calibration samples

In addition to the training matrix, a verification matrix (figure 5) of aqueous sugar samples was prepared using random concentrations of each of the three sugars, fructose, glucose, and sucrose. The verification matrix was used to evaluate the validity of the calibration method.

Sugar Concentration (Mass Percent)

Sample	Fructose	Glucose	Sucrose
1	0.00	0.00	0.00
2	5.08	0.00	0.00
3	10.06	0.00	0.00
4	0.00	5.00	0.00
5	0.00	10.22	0.00
6	0.00	0.00	4.97
7	0.00	0.00	9.94
8	4.92	4.91	0.00
9	0.00	5.10	4.95
10	4.95	0.00	4.91
11	10.10	10.55	0.00
12	0.00	9.83	9.88
13	10.21	0.00	10.03
14	5.10	5.06	5.04
15	10.11	9.84	9.94
16	3.84	7.83	2.68
17	7.94	5.03	1.75
18	1.83	4.67	0.73
19	0.48	2.94	3.07
20	4.95	6.39	1.47
21	3.99	2.66	7.21
22	3.56	3.53	9.63
23	4.97	4.96	9.95
24	10.13	5.05	5.05
25	4.92	9.84	4.94
26	14.95	0.00	0.00
27	0.00	14.99	0.00
28	0.00	0.00	14.72
29	15.14	15.26	0.00
30	15.31	0.00	15.24
31	0.00	15.15	15.16
32	14.97	14.98	7.59
33	14.89	7.45	14.97
34	7.53	15.14	15.21

Sugar Concentration (Mass Percent)

Sample	Fructose	Glucose	Sucrose
35	1.39	12.90	0.70
36	9.58	13.77	1.16
37	2.33	13.55	14.71
38	12.92	3.95	2.58
39	6.86	10.63	9.23
40	9.90	10.82	9.89

Figure 4 (top): Actual training matrix for aqueous sugar standards
Figure 5 (bottom): Verification matrix of random aqueous sugar standards

■ Calibration Results

FTIR Absorbance spectra were acquired of the training matrix standard samples using parameters of 4 cm^{-1} resolution, Happ-Genzel apodization, and the averaging of 32 scans. Figure 6 shows the spectra and demonstrates the complexity of the overlapping absorption bands.
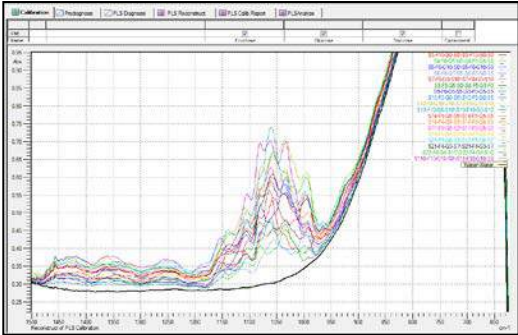

Figure 6: FTIR spectra of training matrix aqueous sugar standards

A Partial Least Squares (PLS) algorithm was utilized to establish a calibration curve for each of the three sugar components. It was found that good correlation could be achieved without the use of pre-processing methods such as smoothing, derivatives, or zero corrections. In addition, the use of five factors accounted for all of the noise in the spectra and provided good calibration curves with acceptable R^2 values (figure 7).

PLS Calibration Report			
Calibration Table:	Quant_1to25_a.irqc		
Algorithm:	PLS I		
Number of components:	3		
Number of references:	25		
Range[1]:	963.00 - 1486.00		
Preprocess:			
Scale:	None		
Component:	Fructose	Glucose	Sucrose
Number of factors:	5	5	5
Correlation coeff.:	0.999	0.9987	0.9986
Square of correlation coeff.:	0.998	0.9973	0.9973
MSEP:	0.0019	0.0026	0.0026
SEP:	0.0441	0.0506	0.0513
X Leverage warnings:	3	3	3
Y Residual warnings:	1	0	2

Figure 7: PLS Calibration Report showing R^2 values for each sugar calibration curve

To further demonstrate that the use of 5 factors was appropriate, the P Loadings for each sugar component were examined. As seen from the graphs (figure 8), the P Loading of the 5th factor resembles a random noise spectrum, suggesting that all of the spectral noise had been accounted for.

Figure 8: P Loading graphs for each sugar supporting the selection of five factors

■ Calibration Validation

Once the calibration curve for each sugar component were established, FTIR spectra were acquired of the verification matrix of samples using the same acquisition parameters as was used for the training matrix (figure 9).

Results of the verification matrix showed average residuals for each sugar of 0.004% and established that the calibration method was valid.

Spectrum	Fructose	Resid. 1	Glucose	Resid. 2	Sucrose	Resid. 3
S35-F1-G13-F1	1.638	0.005	13.088	0.005	1.076	0.005
S36-F10-G14-S1	9.41	0.003	14.036	0.003	1.762	0.003
S37-F2-G14-S15	1.589	0.005	13.591	0.005	15.156	0.005
S38-F13-G4-F3	12.189	0.006	3.411	0.006	2.642	0.006
S39-F7-G11-S9	6.636	0.002	10.813	0.002	9.655	0.002
S40-F10-G11-S10	9.213	0.003	11.151	0.003	10.175	0.003
Average		0.004		0.004		0.004

Figure 9: Verification Matrix results demonstrating the validation of the PLS calibration method

■ Sugar Component Analysis of Baby Foods

Commercial baby food samples from three major manufactures were acquired for fructose, glucose, and sucrose analysis. The baby foods selected consisted of pureed fruits and vegetables and fruit juices.

FTIR spectra for each baby food were acquired neat without any pretreatment using the HATR accessory and the spectral acquisition parameters noted previously (figure 10). The fructose, glucose, and sucrose sugar contents were calculated using the calibration established for each sugar from the factor-spaced analysis.
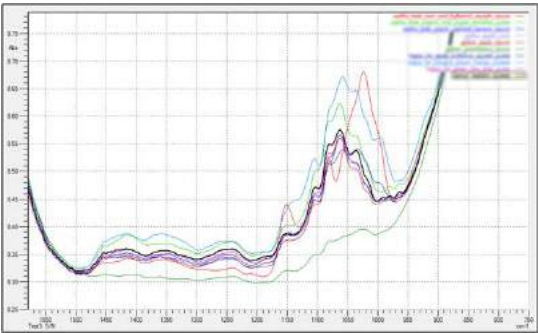

Figure 10: FTIR acquired for the neat commercial baby food samples

Examination of the calculated residuals from the calibration suggested very good fits with the various sugar calibration curves (figure 11). Baby foods that were more fruit based appeared to give better residual values, whereas baby foods that were more vegetable based generally gave higher residuals.

A total sugar concentration for each baby food was calculated from the sugar content provided on the nutrition label of each package. The calculated total sugar value from the nutritional label was compared to the total sugar value calculated from the FTIR quantitative spectral analysis. The measured total sugar values showed a high bias when compared to the reported total sugar values for all samples (figure 12).

Baby Food Analyzed	Measured % Fructose	Measured % Glucose	Measured % Sucrose	Total Measured Sugars (%)	Reported Total Sugar Conc. (%)
corn_and_butternut_squash_sauce	-3.25	10.55	4.52	11.82	2.65
organic_fruit_yogart_smoothie_puree	8.80	4.43	0.93	14.15	10.00
peach_oatmeal_banana_sauce	3.51	5.08	2.31	10.90	4.42
apple_sauce	7.01	2.79	1.45	11.24	9.73
greenbeans_sauce	0.68	2.34	0.36	3.37	2.65
banana_peach_mango_pureee	5.59	5.78	5.32	16.69	9.17
rasberry_pureee	7.12	4.29	0.66	12.06	9.17
apple_butternut_squash_puree	7.08	3.11	1.45	11.64	7.50
banana-peach-coconut_prune	6.90	7.61	3.38	17.88	10.00
green_pea_pear_puree	7.14	3.16	1.17	11.47	7.50
apple_juice	6.59	3.54	1.42	11.55	11.02

Figure 12: Total measured sugar comparison to that listed on the nutritional labels for each commercial baby food sample

Spectrum	Fructose	Resid. 1	Glucose	Resid. 2	Sucrose	Resid. 3
corn_and_butternut_squash_sauce	-3.25	0.05	10.55	0.05	4.52	0.05
organic_fruit_yogart_smoothie_puree	8.80	0.02	4.43	0.02	0.93	0.02
peach_oatmeal_banana_sauce	3.51	0.01	5.08	0.01	2.31	0.01
apple_sauce	7.01	0.01	2.79	0.01	1.45	0.01
greenbeans_sauce	0.68	0.01	2.34	0.01	0.36	0.01
banana_peach_mango_pureee	5.59	0.01	5.78	0.01	5.32	0.01
rasberry_pureee	7.12	0.01	4.29	0.01	0.66	0.01
apple_butternut_squash_puree	7.08	0.01	3.11	0.01	1.45	0.01
banana-peach-coconut_prune	6.90	0.01	7.61	0.01	3.38	0.01
green_pea_pear_puree	7.14	0.01	3.16	0.01	1.17	0.01
apple_juice	6.59	0.01	3.54	0.01	1.42	0.01

Figure 11: Measured sugar concentration results for the commercial baby food samples

■ Conclusion

FTIR Analysis, using a horizontal attenuated total reflection accessory, was demonstrated to be a suitable method to acquire FTIR spectra of commercial baby foods without sample pretreatment or concern for IR water absorption.

Chemometric Partial Least Squares (PLS) routines were used to establish and validate calibration curves for fructose, glucose, and sucrose concentrations in aqueous solutions.

Commercial baby food samples were analyzed for fructose, glucose, and sucrose sugar content. Residual data from the calibration suggested that the baby food samples were within the calibration algorithm's area of analysis. A comparison was made of the total sugars measured to those reported on the nutritional labels of the baby food packages.

This data demonstrates that FTIR analysis of baby foods offers a quick and efficient means of sugar analysis for QA/QC applications.

■ References

1. Jagdish, T., & Irudayaraj, J. (2004, June). Quantification of saccharides in multiple floral honeys using Fourier transform infrared microattenuated total reflectance spectroscopy. *J. Agric Food Chem*, *52*(11), 3237-43.
2. Tucker, M., Nguyen, Q., & Eddy, F. (2001). Fourier Transform Infrared Quantitative Analysis of Sugars and Lignin in Pretreated Softwood Solid Residues. *Applied Biochemistry and Biotechnology*, *91 - 93*, 51-61.
3. Cadet, F., & Offmann, B. (1997). Direct Spectroscopic Sucrose Determination of Raw Sugar Cane Juices. *J. Agric. Food chem.*, *45*(), 166-171.
4. Kramer, R. (1998). *Chemometric Techniques for Quantitative Analysis*. New York, NY: Marcel Dekker Inc.

Application News

Quantification and Identification of Various Sugars in Maple Syrup by MID FTIR Spectroscopy

No. FTIR-1403

Jeff Head, M.S., John Kinyanjui Ph.D., Mark Talbott, Ph.D.; Robert Clifford, Ph.D.

■ Introduction

Maple syrup is a commonly used sweetener that is heavily produced in the United States and Canada. Grocery stores keep their shelves well-stocked with multiple types and varieties for the average consumer. This food product can be purchased as either pure or as the cheaper alternative, which contains additives such as corn syrup. Corn syrup is a common additive to syrup products in the production process[1].

Pure maple syrup is comprised of various phenolics, flavor components, and sugars, mostly sucrose. In addition to sucrose, the sugars fructose and glucose may be present in smaller quantities. Typically, pure maple syrup contains 98% sucrose, and less than 2% fructose and glucose. Unlike maple syrup, corn syrup is comprised primarily of glucose. Figure 1 shows the FTIR spectra of the various sugars and syrups under consideration for this application news.
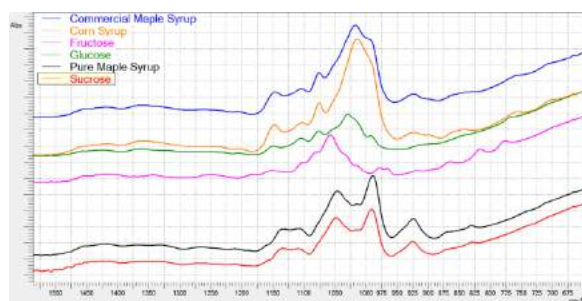

Figure 1: FTIR spectra of syrups and various sugars

Identification and quantification of natural sugars was investigated in maple syrup by MID FTIR spectroscopy. Using attenuated total reflectance (ATR) samples were analyzed with the Shimadzu IRTracer-100 FTIR spectrophotometer. Factor space chemometric analysis was used to establish a robust method that allowed the measurement of sugar concentrations in maple syrup. The method was developed and is discussed extensively in Application News No. FTIR-1401. Several types of maple syrup were analyzed with this method and quantities of fructose, glucose, and sucrose were determined.

IRTracer-100

■ Experimental

Maple syrup was diluted in water and dropped directly onto a ZnSe ATR crystal for analysis. During acquisition 32 spectra were averaged for each sample, using a resolution of 4 cm^{-1} on the Shimadzu IRTracer-100.

■ Results and Discussion

Using chemometric analysis, Table 1 summarizes the % W/W concentrations of sucrose, fructose, and glucose, present in various maple syrup samples.

For the commercial maple syrup, the amount of glucose present is significantly greater than that of the pure maple syrup, suggesting the presence of corn syrup. This is in good agreement with the ingredients label for each commercial sample which list corn syrup as a major component.

Table 1: Calculated concentrations of Fructose, Glucose, and Sucrose for various maple syrup samples

Sample ID	Sample Name	%Fructose (W/W)	%Glucose (W/W)	%Sucrose (W/W)
Vermont Sampling Kit				
1	Vermont Fancy	3.3%	0%	96.7%
2	Grade A Medium Amber	2.9%	0%	97.1%
3	Grade A Dark Amber	3.7%	0%	96.3%
4	Grade B	6.9%	0%	93.1%
Commercial Pure Maple Syrup				
5	U.S. Grade A Light Amber	0%	0%	100%
6	Grade A Medium Amber	0%	0%	100%
7	U.S. Grade A Dark Amber	3.2%	0%	96.8%
8	U.S. Grade A Dark Amber	5.8%	0%	94.2%
9	U.S. Grade A Dark Amber	8.9%	0%	91.1%
10	Grade A Dark Amber	5.4%	0%	95.5%
11	U.S. Grade A Dark Amber	6.1%	0%	93.9%
12	U.S. Grade A Dark Amber	6.4%	0%	93.6%
13	U.S. Grade A Dark Amber	0%	0%	100%
14	U.S. Grade B	4.5%	0%	95.5%
Commercial Maple Syrup				
15	Sample 1	0%	**68.1%**	31.9%
16	Sample 2	2.8%	**94.4%**	2.8%
17	Sample 3	8.1%	**87.7%**	4.2%
18	Sample 4	15.2%	**79.5%**	5.3%
19	Sample 5	23.4%	**58.9%**	17.7%

■ Conclusion

For the commercial maple syrup, the amount of glucose present is significantly greater than that of the pure maple syrup, suggesting the presence of corn syrup. This is in good agreement with the ingredients label for each commercial sample which list corn syrup as a major component.

This application news demonstrates that FTIR analysis is a viable tool for the quantification and identification of various natural sugars present in food products, such as maple syrup. Chemometric techniques allow for the quantitative analysis of fructose, glucose, and sucrose present, with minimal sample preparation. The IRTracer-100 coupled with an ATR accessory provides the ideal solution for any QA/QC environment requiring the quantitative analysis of components present in finished products.

■ Reference

1. Nollet, L.M.L. "Handbook of Food Analysis, Methods and Instruments in Applied Food Analysis". 2nd Edition, Revised and Expanded. Marcel Dekker, Inc. 2004.

SHIMADZU
Excellence in Science

Application News

Thermal and Spectrophotometric Analysis

Analysis of Polyimide CFRP by TG-FTIR

No.A474

Epoxy resin is typically used in carbon fiber composite materials (carbon fiber reinforced plastic: CFRP), however, due to its limited heat resistance, high heat-resistant CFRP materials using polyimide resin are being developed. Here, we introduce the results of combined Thermogravimetric (TG) - Fourier Transform Infrared Spectroscopy (FTIR) analysis of thermoplastic polyimide and thermosetting polyimide prepregs, polyimide matrices impregnated with carbon fibers and formed into sheets ready for processing.

■ Polyimide / Carbon Fiber Composites

CFRPs containing the base material epoxy have a temperature limit of approximately 120 °C, and are therefore not applicable for use in high-temperature materials. Studies using polyimide resin in CFRP materials which display excellent heat resistance are presently underway, but due to problems in workability, methods to improve their thermoplasticity are being considered. In this study, we analyzed thermoplastic polyimide and thermosetting polyimide prepregs by TG-FTIR to identify the types of gasses they generate.
(Samples provided by the Advanced Composite Research Center, Aerospace Research and Development Directorate, Japan Aerospace Exploration Agency (JAXA).)

■ TG-FTIR System

Figure 1 shows an overview of the system used for measurement. The system comprises a DTG-60, a simultaneous TG - differential thermal analysis (DTA) instrument, and an IRAffinity-1 FTIR spectrophotometer connected via a gas cell and heated transfer line.

Fig. 1 Overview of TG-FTIR System

Table 1 Instrument and Analytical Conditions

FTIR	Instrument	: IRAffinity-1/IRTracer-100
	Resolution	: 8 cm^{-1}
	Accumulation	: 10
	Interval	: 30 sec
	Detector	: DLATGS
DTG	Instrument	: DTG-60
	Heating Rate	: 20 °C/min
	Hold Temperature	: 800 °C
	Atmosphere	: N$_2$

■ Analytical Results

Measurements of thermoplastic and thermosetting polyimide prepreg samples weighing 36.8 mg and 30.9 mg, respectively, were conducted under the conditions shown in Table 1. Figures 2 and 3 show the TG-DTA curves obtained for the samples. Glass transitions are clearly observed in the vicinity of 250 °C in both DTA curves. Furthermore, in the TG curves, a slight weight loss is noticeable in the vicinity of 200 °C – 400 °C (between 500 to 1000 seconds). Also visible is the onset of decomposition, signified by the beginning of the large weight loss around 550 °C (at about 1500 seconds) in the TG curves. This decomposition onset temperature is a measure of heat resistance, which is higher in the thermosetting prepreg.
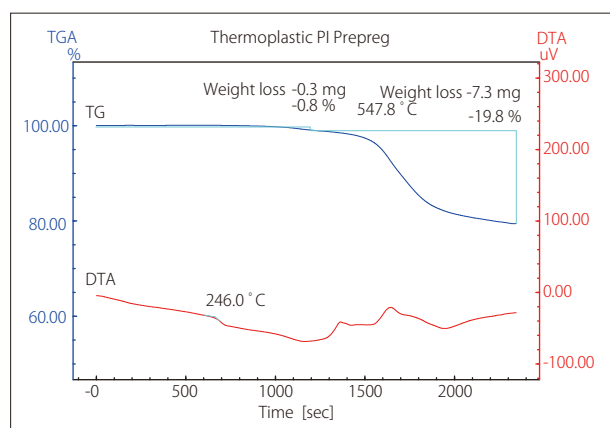
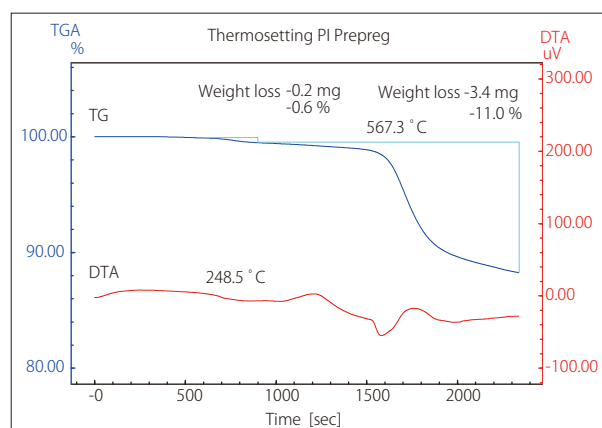**Fig. 2 TG-DTA Curves of Thermoplastic Polyimide Prepreg**

Fig. 3 TG-DTA Curves of Thermosetting Polyimide Prepreg

Figures 4 and 5 show 3D infrared spectra of the two samples. The infrared spectra were analyzed to identify the components corresponding to the slight weight losses seen in the first half of the TG curves of the thermoplastic and thermosetting polyimide prepregs. Search results associated with the first arrow-marked positions in the infrared spectra of Figure 4 position (1) and Figure 5 position (2) are shown in Figures 6 and 7, respectively. The result shown in Figure 6 suggests that the gas generated at position (1) might be a phthalate ester. For position (2), the IR spectrum of NMP (N-methyl-2-pyrrolidone) shows good agreement in Figure 7, which is consistent, because NMP is used as a solvent to dissolve the thermosetting polyimide. Not only does residual NMP create voids during forming, it also lowers the glass transition temperature.

Also conducted was an infrared spectral search for the gas components that were generated in the latter stage of the analysis, Figure 5 position (3). As indicted in Figure 8, they were confirmed to consist of phenol, CO_2 and CO. These components are assumed to be aromatic polyimide decomposition products, and were present in thermoplastic polyimide as well.

As the above results show, combined TG-FTIR analysis is a powerful method for confirming the presence of residual solvents and identifying chemical products associated with thermal transitions.
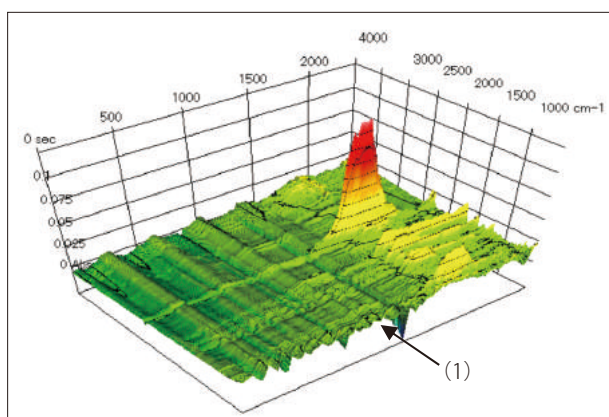

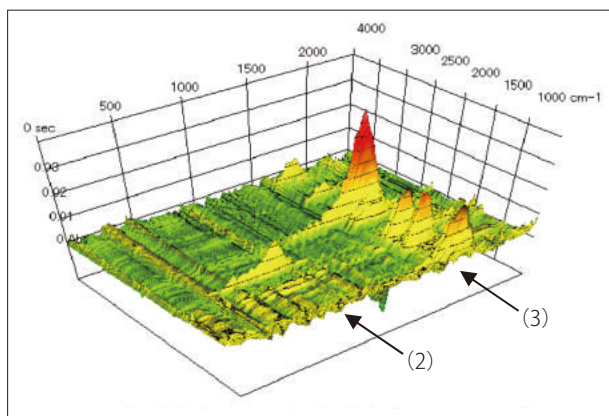**Fig. 4 3D Display of IR Spectra of Thermoplastic Polyimide Prepreg**

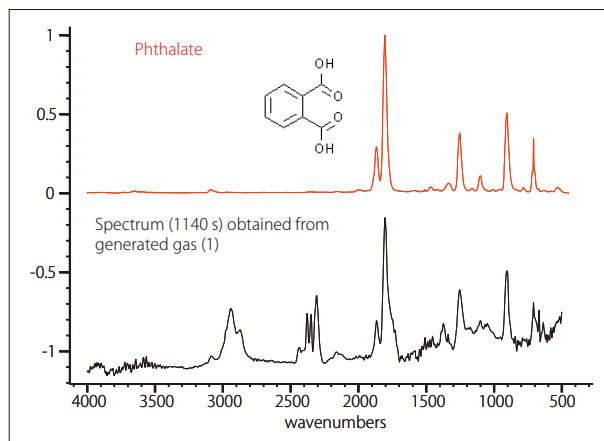**Fig. 5 3D Display of IR Spectra of Thermosetting Polyimide Prepreg**
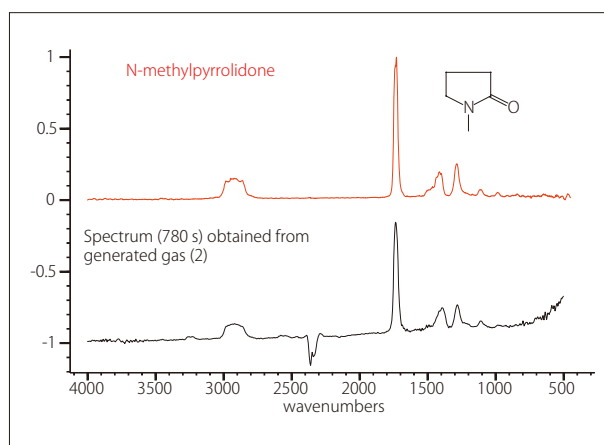

Fig. 6 Search Result for Generated Gas (1)

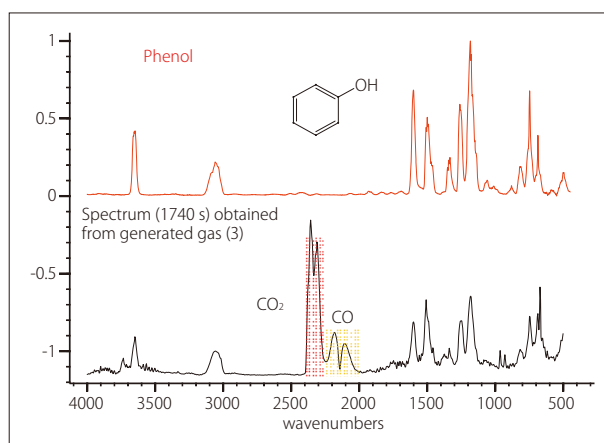
Fig. 7 Search Result for Generated Gas (2)

Fig. 8 Search Results for Generated Gas (3)

First Edition: Nov. 2013

SHIMADZU

Shimadzu Corporation

www.shimadzu.com/an/

![SHIMADZU Excellence in Science]

Application News

No.A476

Spectrophotometric Analysis

Advanced ATR Correction to Convert ATR Spectra to Transmission Spectra

The ATR method is used not only for verification testing, it is a technique that is widely used for contaminant analysis. Comparing the spectrum acquired by the ATR technique with that obtained using transmission spectroscopy, the values indicated on the respective vertical and horizontal axes, in principle, are slightly different. Accordingly, an appropriate correction must be applied to the vertical and horizontal axes of the ATR spectrum when matching the ATR spectrum to a transmission spectrum or database to obtain more accurate results. Here, we introduce an advanced ATR correction processing feature which permits an ATR spectrum to approximate a transmission spectrum, along with an evaluation of the result.

■ Penetration Depth Dependency of Absorbance and Transmittance for ATR Spectrum[1]

When acquiring the infrared spectrum of a given sample, the sample's thickness and concentration must be optimized to prevent the occurrence of saturation when using the transmission method. On the other hand, when using the ATR method, an infrared spectrum of a sample depth measuring just a few μm from the sample surface can be acquired via close contact between the sample and prism, so optimization such as that with the transmission method is unnecessary. However, in the case of a spectrum acquired by the ATR method, the penetration depth of infrared light (dp) is not constant over the entire wavenumber range. Thus, when comparing spectra acquired using the ATR and transmission techniques, the lower the wavenumber region the greater will be the depth using the ATR method, resulting in peaks showing a trend of greater intensity. Shown below is the formula for calculating the theoretical penetration depth of infrared light using the ATR method.

$$dp = \frac{\lambda / n_1}{2\pi \sqrt{\sin^2 \theta - (n_2 / n_1)^2}}$$

Here, θ is the angle of incidence of infrared light, λ is the wavelength, and n1 and n2 are the refractive indices of the ATR prism and sample, respectively. Thus, it is clear from this expression that the penetration depth of infrared light (dp) is proportional to the wavelength (λ). However, the above expression holds true only if there is no peak in the infrared spectrum.

■ Peak Shift in ATR Spectrum[1]

When an infrared spectrum is acquired, typically, various peaks are obtained. If, indeed, a peak is obtained, its absorbance (A) is expressed by the following expression.

$$A = (\log_{10} e) \frac{n_2}{n_1} \frac{E_0{}^2}{\cos \theta} \frac{dp}{2} \alpha$$

Here, E_0 is the evanescent wave of the electric field, and α is the extinction coefficient corresponding to the sample thickness. It is clear from this expression that the penetration depth of the infrared light is different before and after the peak, and that a peak shift occurs in the lower wavenumber side when compared with spectra obtained by the transmission method.

■ Advanced ATR Correction

Shimadzu's Advanced ATR correction feature permits correction corresponding to changes in the ordinate / abscissa mentioned above. This process simultaneously corrects for:

1. Peak intensity changes due to wavelength dependence of infrared light penetration depth
2. Peak shift to lower wavenumbers caused by anomalous dispersion of the refractive index
3. Deviation from Lambert-Beer's law due to polarization characteristics

■ ATR Spectrum of Polycarbonate

Fig. 1 shows the infrared spectra of polycarbonate obtained using the ATR method and transmission method, respectively, and Table 1 shows the measurement conditions that were used. Here, the intensity of the transmission spectrum was corrected so that the absorbances would match in the vicinity of 1190 cm^{-1} to permit easier comparison with the ATR spectrum.
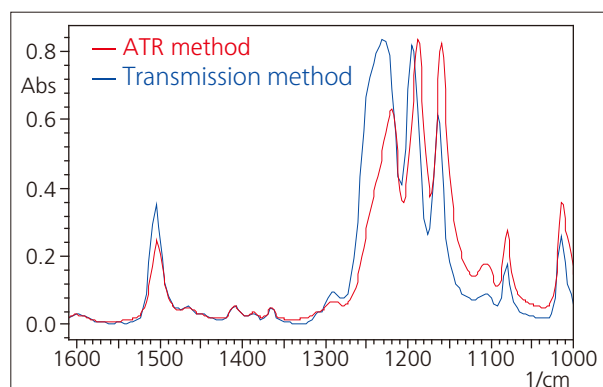

Fig. 1 ATR Spectrum and Transmission Spectrum of Polycarbonate

Table 1 Instrument and Analytical Conditions

Instruments	: IRTracer-100, DuraSamplIR-II (ATR), MHP-1 (Transmission)
Resolution	: 4 cm^{-1}
Accumulation	: 45
Apodization	: Happ-Genzel
Detector	: DLATGS

It is clear from Fig. 1 that not only the peak intensities, but the peak positions as well are quite different using the two methods. Next, Fig. 2 shows an overlay of the ATR spectrum of Fig. 1 (red trace) in which ordinate correction of the penetration depth of the infrared light (ATR ordinate correction) has been applied, together with the transmission spectrum. It is obvious that the transmission spectrum cannot be approximated using ATR ordinate correction.
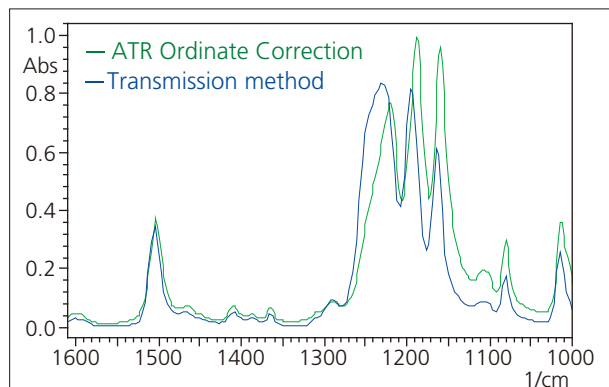

Fig. 2 Effect of ATR Ordinate Correction

Finally, Fig. 3 shows the overlaid ATR and transmission spectra, in which the Advanced ATR correction introduced here was applied to the ATR spectrum (red trace).
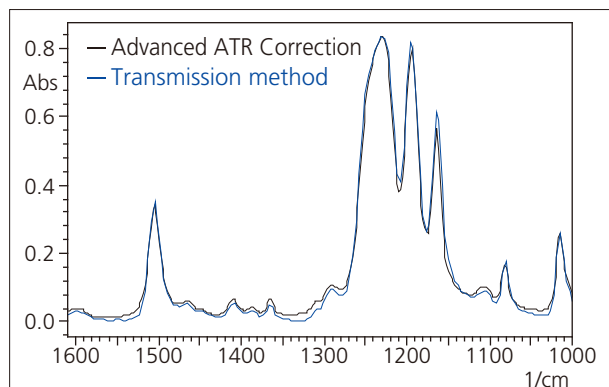
Fig. 3 Effect of Advanced ATR Correction

Comparing the spectrum processed using the Advanced ATR correction with the transmission spectrum, it is clear that extremely good approximation of peak intensities and peak shapes is obtained.

■ **Influence on Search Result**

We investigated the effect on the ATR spectrum hit rate during a search of a database created by the transmission method. Fig. 4 shows the search results obtained without correction of the acquired ATR spectrum, Fig. 5 shows the search results after ATR ordinate correction, and Fig. 6 shows the search results following advanced ATR correction. As can be seen from the results, the number of first place hits rose from 844 points, to 858 points and to 957 points, using no correction, ATR ordinate correction and Advanced ATR correction, respectively.
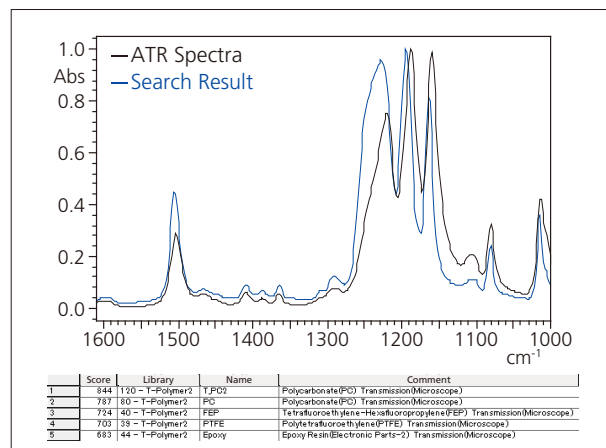

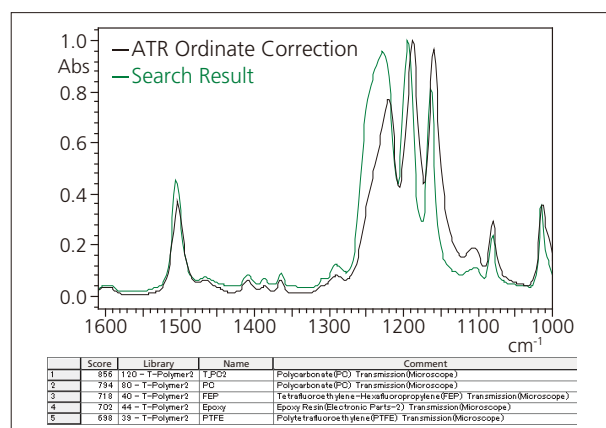**Fig. 4 Search Result Without Correction**

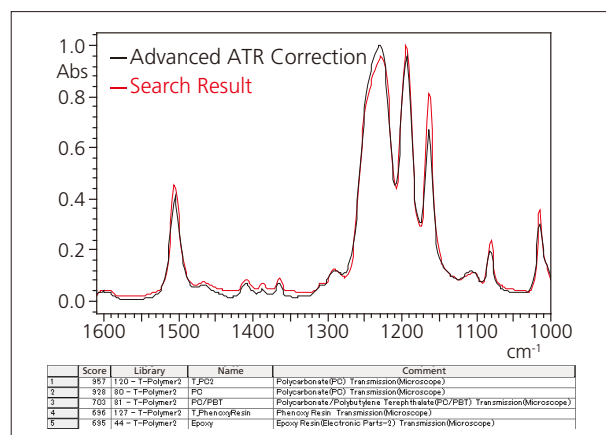**Fig. 5 Search Result after ATR Ordinate Correction**

Fig. 6 Search Result after Advanced ATR Correction

■ **Conclusion**

Advanced ATR correction processing permits a spectrum obtained by the ATR method to approximate a spectrum obtained by the transmission method. This correction process makes it possible to obtain high-accuracy verification results even on the ATR spectrum hit rate during a search of a database created by the transmission method.

1) Materials Analysis by Infrared Spectroscopy Fundamentals and Application Koichi Nishikida, Reikichi Iwamoto, et al, Kodansha Ltd..

SHIMADZU

Shimadzu Corporation

www.shimadzu.com/an/

SHIMADZU
Excellence in Science

Application News

No.A485

Spectrophotometric Analysis

Spectral Characteristics Dependent on ATR Crystal Selection – Differences in Properties (Shape, Hardness, Refractive Index) According to Sample –

ATR (Attenuated Total Reflectance) is a technique that is widely used in verification testing and contaminant analysis. With this technique, however, peak characteristics such as peak intensity and position, etc., vary depending on the shape of the sample and the type of crystal selected. Here, using a variety of samples and three types of crystals (diamond, ZnSe, Ge), we conducted measurements and describe the typical ATR spectral characteristics associated with the contact status between the crystal and sample, as well as the shape of the sample.

■ ATR Crystal

A variety of materials are used as ATR crystals, including diamond, ZnSe, KRS-5 (thallium iodide and thallium bromide mixed optical crystal), Ge, etc., and depending on the type of crystal selected, differences in peak intensity and position may be observed.

Peak intensity is directly related to the principle underlying the ATR method. The penetration depth of infrared light into the sample using the ATR method can be calculated by expression (1) shown below.

$$dp = \frac{\lambda / n_1}{2\pi \sqrt{\sin^2\theta - (n_2 / n_1)^2}} \quad \ldots\ldots\ldots\ldots(1)$$

$$A = (\log_{10} e) \frac{n_2}{n_1} \frac{E_0{}^2}{\cos\theta} \frac{dp}{2} \alpha \quad \ldots\ldots\ldots\ldots(2)$$

Here, dp is the penetration depth of the infrared beam, λ is the wavelength in air, θ is the angle of incidence of the infrared beam, n_1 is the refractive index of the crystal, and n_2 is the refractive index of the sample.

It is clear from expression (1) that the penetration depth of the infrared light is proportional to the wavelength λ, and is also related to n_1, the refractive index of the crystal (assuming a sample with a constant refractive index). In other words, as the refractive index of the crystal increases, the penetration depth of infrared light will decrease, thus generating weaker peak intensity.

For example, assuming a sample refractive index n_2 of 1.5, the calculated penetration depth of infrared light at a 45° angle of incidence is shown in Fig. 1.

The red trace shows the penetration depth obtained using a crystal consisting of diamond, ZnSe, or KRS-5 with a refractive index of about 2.4, and the green trace using a Ge crystal with a refractive index of about 4.0. Thus, from Fig. 1, it is clear that the depth of infrared light penetration differs greatly depending on the crystal used. In the case of the Ge crystal, as the penetration depth is shallow compared to that of diamond, etc., it is clear that more information pertaining to the sample surface can be obtained. On the other hand, the peak intensity of the obtained ATR spectrum is weaker with the Ge crystal.
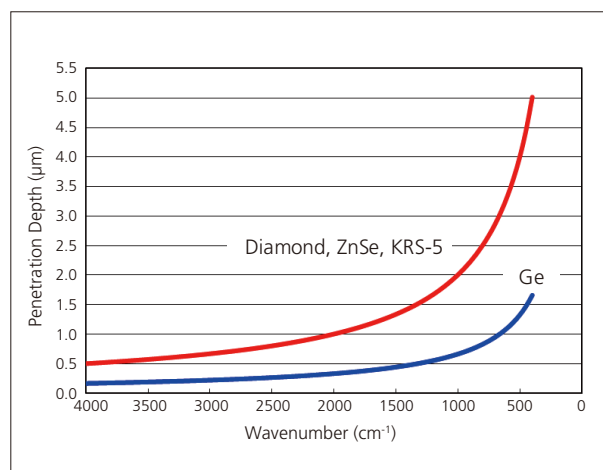

Fig. 1 Theoretical Calculation of Infrared Beam Penetration Depth

In addition, it is also known that in an ATR spectrum, the peak shape and its position change in accordance with expression (2).

Here, A expresses the absorbance, E_0 the evanescent wave electric field, and α the extinction coefficient corresponding to the sample thickness.

E_0 and dp are functions of n_2. n_2 changes greatly (phenomenon referred to as anomalous dispersion) in the presence of strong absorption. This, therefore, causes changes in the shape of the ATR spectrum as well as the peak positions. When a crystal having a low refractive index is used for measurement, there is greater susceptibility to the effects of anomalous dispersion, resulting in peak position fluctuation. But the effects of this abnormal dispersion can be mitigated by using a crystal with a higher refractive index n_1[1], [2].

Thus, fluctuation of peak intensity and peak position occur in the ATR spectrum depending on the refractive index of the crystal, but by approximating the transmission spectrum and utilizing an advanced ATR correction feature, it is possible to compare the ATR spectra measured using different crystals. For more information on the correction feature and its effectiveness, please refer to Application News A476.

■ ATR Measurement of Various Samples

This section describes the characteristics of ATR spectra obtained according to the sample properties (shape, hardness, refractive index) and type of crystal used. Measurements were conducted by single-reflection ATR measurement using three types of crystals, including diamond (with a ZnSe support element), ZnSe, and Ge. The measurement conditions are shown in Table 1.

Table 1 Instruments and Analytical Conditions

Instruments	: IRTracer -100, MIRacle 10
Resolution	: 4 cm^{-1}
Accumulation	: 20
Apodization	: Happ-Genzel
Detector	: DLATGS

■ ATR Measurement of Liquid

As a very good contact can be achieved between a liquid sample and crystal, there is no need to apply pressure. The measurement results using a silicone oil sample are shown in Fig. 2.
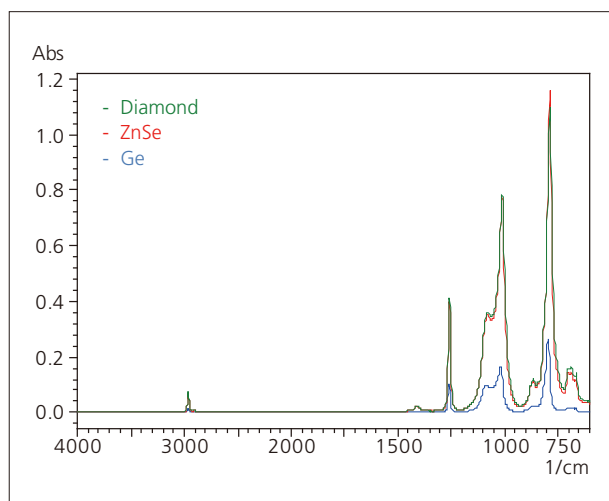
Fig. 2 ATR Spectra of Silicon Oil

Measurement using a diamond and ZnSe provide about the same degree of intensity, but the intensity obtained using Ge is only about one-fourth of that peak intensity. Fig. 3 shows an enlarged view of the peaks in the vicinity of 1,000 cm^{-1}, which are generated due to a Si-O stretching vibration in a silicone oil sample. The peak intensities in this vicinity of 1,000 cm^{-1} match closely.
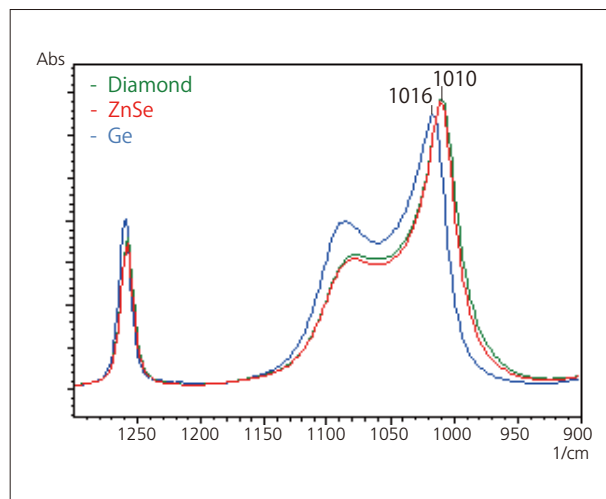
Fig. 3 Enlarged Spectra in Vicinity from 1,300 to 900 cm^{-1}

From Fig. 3, it is evident when comparing these with the Ge crystal, with its large refractive index, that the peak positions using the diamond and ZnSe crystals are shifted to the lower wavelength side by about 6 cm^{-1}. In this way, a peak wavenumber shift generally occurs prominently when using a crystal having a low refractive index.

■ ATR Measurement of Film

Next, we show the measurement results for nylon 6 film in Fig. 4.

When measuring a solid sample, it is necessary to maintain close contact of the sample with the crystal by applying pressure from above. With samples such as film, which permit good contact due to their smooth surface, there is not much difference in the peak intensity obtained using either diamond or ZnSe.
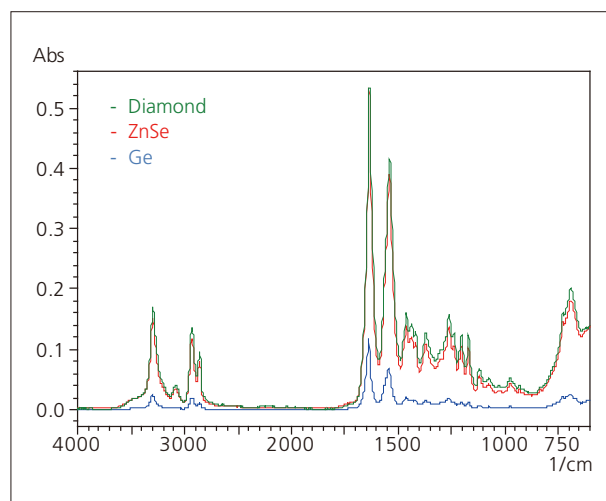

Fig. 4 ATR Spectra of Nylon 6 Film

■ ATR Measurement of Powder

Next, the measurement results for anhydrous caffeine powder are shown in Fig. 5.

As in the case of film, there is not much difference in the contact and peak intensity obtained using either diamond or ZnSe. In such a case, the contact can be improved by grinding the powdered sample more finely.
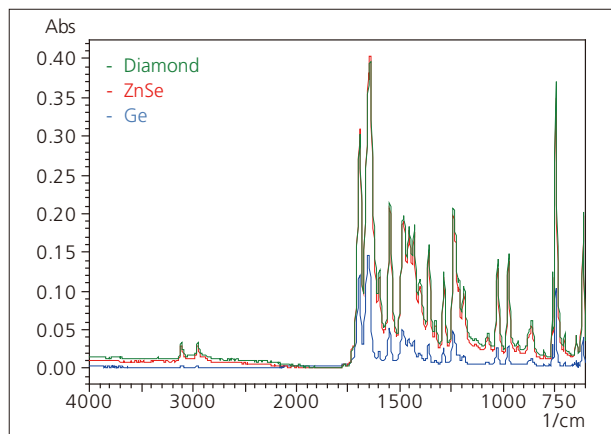

Fig. 5 ATR Spectra of Anhydrous Caffeine Powder

■ ATR Measurement of Resin Pellet

Resin pellets are generally cylindrical in shape, so the contact status can be expected to vary depending on how the sample is placed. Fig. 6 shows the results of measurement of an acrylonitrile butadiene styrene (ABS) resin pellet.
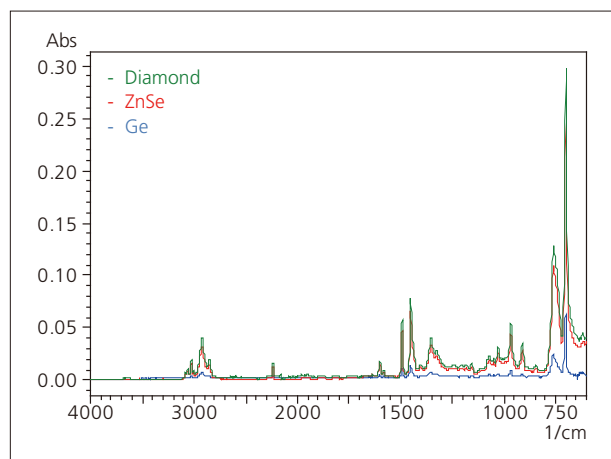
Fig. 6 ATR Spectra of ABS Resin

Comparing the results obtained using diamond and ZnSe crystals, it is diamond that clearly shows the stronger peak intensity. This may be attributed to stronger attachment using diamond, which presumably offers closer contact.

■ ATR measurement of Internal Coating of Aluminium Can

Aluminium cans are coated both internally and externally, but it is the inner surface coating that must meet the more stringent criteria as specified by the Food Sanitation Law, due to the direct contact of that surface with beverages. Fig. 7 shows the results of measurement of epoxy resin coated on the inner surface of a can in order to prevent corrosion. The measurement sample was prepared by cutting off a piece of the aluminium can, and then flattening the excised piece for measurement.
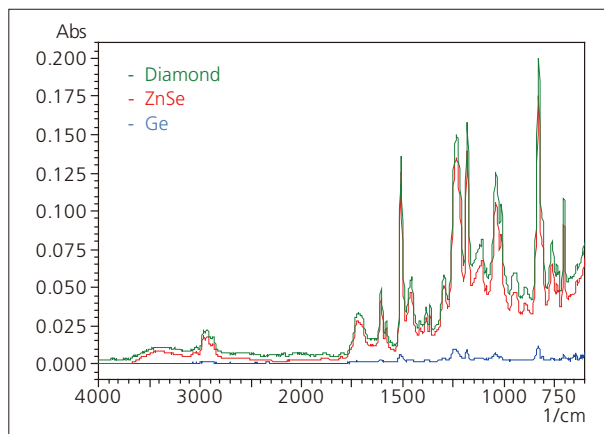

Fig. 7 ATR Spectra of Internal Coating of Aluminium Can

In Fig. 7, the difference in peak intensity between that obtained with the diamond and ZnSe crystals is clearly evident. As for Ge, a bigger difference in peak intensity occurs than the expectations from the difference in theoretically-derived penetration depth. It is presumed that this might be attributable to insufficient flattening of the piece of can used as the specimen, which resulted in imperfect contact between the sample and crystal.

Thus, when conducting measurement of a sample whose properties prevent close contact with the crystal, care is required due to large differences in peak intensity depending on the selected crystal.

■ ATR Measurement of Black Rubber

Carbon black is often added to rubber as an augmentation agent, but as the amount of added carbon black increases, the greater becomes the refractive index of the rubber sample. Also, carbon exhibits absorption throughout the infrared region, and in accordance with ATR principle (penetration depth dependence on wavelength), the baseline rises in the lower the wavenumber region, with greater light penetration. The results of measurement of acrylonitrile butadiene rubber (NBR) containing carbon 10 wt% using three types of crystals are shown in Fig. 8.
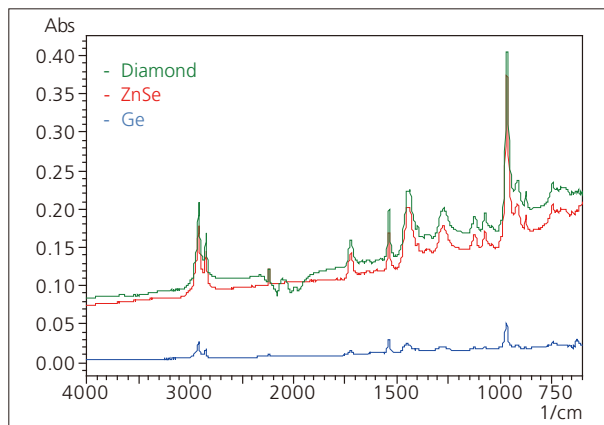

Fig. 8 ATR Spectra of NBR Containing 10 wt% Carbon

Regarding the results using the diamond and ZnSe crystal, compared to that using Ge, there is clearly a large rise in the baseline. Further, comparing the results using the diamond and ZnSe crystals, there is an evident dip in the vicinity from 2,400 to 2,000 cm^{-1} with the diamond crystal. This is due to absorption by the crystal itself (residual absorption by the diamond), and because this phenomenon is commonly seen in measurement of elastic samples such as rubber in which a diamond crystal is used, caution is necessary.

In addition, to check the ATR spectrum of a high-carbon content sample, we conducted measurement of NBR rubber with a carbon content of 30 wt% using three types of crystals. The measurement results are shown in Fig. 9 to 11.

Fig. 11 ATR Spectrum of NBR Rubber Containing 30 wt% Carbon (ATR Crystal: Diamond / ZnSe)
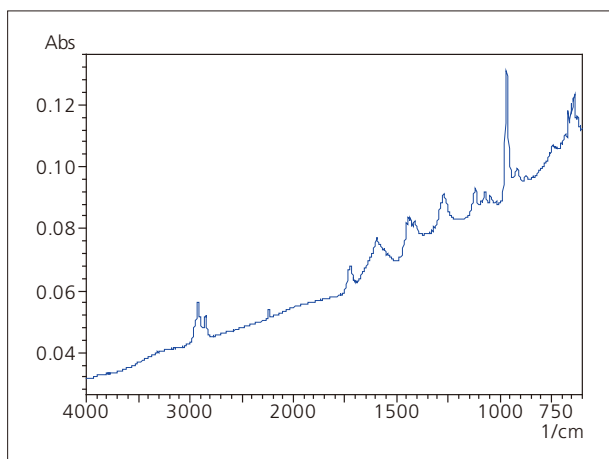
Fig. 9 ATR Spectrum of NBR Rubber Containing 30 wt% Carbon (ATR Crystal: Ge)

Comparing Fig. 8 and figures from Fig. 9 to 11, the baseline rise increases further as the carbon content increases.

Also, peak distortion is noticeable (circled areas in figures) in the spectra generated using the diamond and ZnSe crystals, both of which have a relatively low refractive index. This is due to the increase in the refractive index of the samples as the carbon content increases to the point that the total reflectance method conditions of expression (1) are no longer satisfied. As a result of this phenomenon, the peak position shifts to the lower wavelength side of the original position. Further, when the refractive index of the sample is increased, the peak is generated in the reverse direction, thereby complicating qualitative analysis due to the abnormally generated spectrum. Considering these various factors, the Ge crystal may be more suitable for the analysis of samples having a high refractive index.

■ Conclusion

Here, a variety of samples were measured using three different crystals, and the differences in the resulting peak intensities and positions could be observed and compared. The information and data presented in this Application News are intended to assist in the selection of the optimal crystal in accordance with the sample being analyzed.

Reference:
1) Koichi Nishikida, Reikichi Iwamoto, et al., Kodansha Ltd. (1986), Material Analysis by Infrared Method: Fundamentals and Applications
2) Tsuguo Sawada et al., Dainippon Tosho Co., Ltd. (1988), New Chemical Library / Spectroscopic Analytical Chemistry

Fig. 10 ATR Spectrum of NBR Rubber Containing 30 wt% Carbon (ATR Crystal: ZnSe)

SHIMADZU

Shimadzu Corporation

www.shimadzu.com/an/

Application Note

Analysis of Hydroxyl Value of Polypropylene Glycol Using PLS Method in Near-Infrared Spectroscopy

FTIR
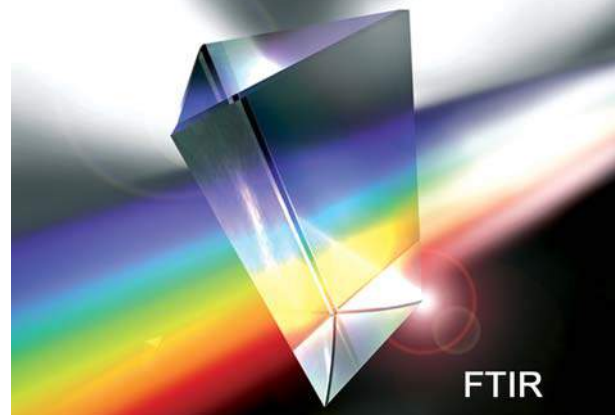
This application introduce examples of iodine value quantitation using near-infrared spectroscopy (NIR) and the PLS method. The NIR for oil and fat substances is promising when applied in the quantitation of acid value, hydroxyl value, saponification value, ester value, etc. This issue introduces examples of the quantification of the hydroxyl value of polypropylene glycol.

Hydroxyl Value

The Japanese Industrial Standards (JIS) section on polyether testing methods for polyurethane (K 1557) explains that "Hydroxyl value is the amount (mg) of potassium hydride equivalent to the hydroxyl group in a 1 g sample". Specifically, hydroxyl value is obtained by esterifying the sample using a phthalic anhydride pyridine solution and then titrating the excess sample with a sodium hydride solution. The analysis – preparation and pre-processing of the equipment and samples needed for titration, etc – requires significant time and effort. Conversely, analysis using NIR requires no complicated procedures and can be conducted easily by performing a transmittance measurement of the sample solution and then applying the PLS quantitative analysis method. While this method is not recognized by the JIS, it can be applied as a quick and simple method of analysis.
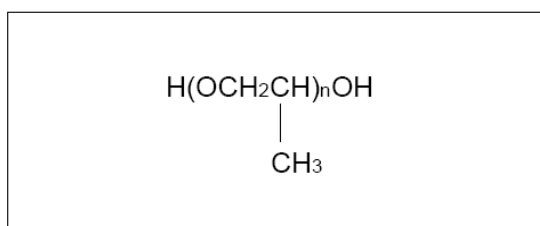
$$H(OCH_2CH)_nOH$$
$$|$$
$$CH_3$$

Fig.1 Structure of Polypropylene Glycol

NIR Spectra of Polypropylene Glycol

Polypropylene glycol (PPG) is a solution manufactured by polymerizing propylene oxide and is the base material for polyurethane. The samples measured for this analysis are structured as shown in Fig.1. The results of a measurement in which we used an infrared transmittance heating cell to analyze 4 types of relative polypropylene glycols having different hydroxyl values are shown in Fig.2. The cell temperature was adjusted to 30 °C. From the figures we see that peaks around 6989 cm^{-1} and 4852 cm^{-1} change intensity.
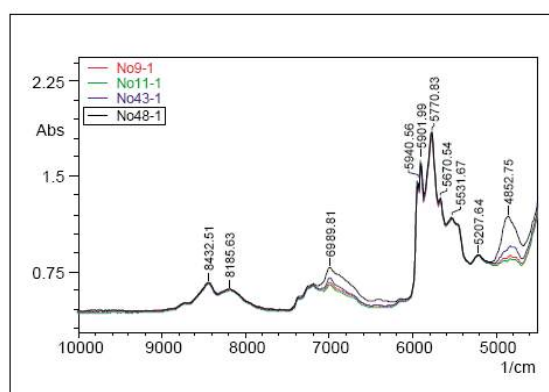

Fig.2 Spectra of Polypropylene Glycol

Table 1 Analytical Conditions

Resolution	: 16 cm^{-1}
Accumulation	: 40
Detector	: InGaAs
Cell Temperature	: 30 °C

Quantitation of Hydroxyl Value with PLS Method

We measured each of the polypropylene glycols shown in Fig.2 (hydroxyl values: 29.8, 35.5, 53.5, 108) 4 times and used the PLS method to create a calibration curve. The PLS quantitative report is shown in Table 2 and Fig.3 shows a plot of

SHIMADZU
Solutions for Science
since 1875

actual values against predicted values. Excellent results were achieved in the hydroxyl value range of 30 – 108. The analytical results of unknown samples based on this report table are shown in Table 3. The average value from the 4 analyses provided a hydroxyl value of 63.376.
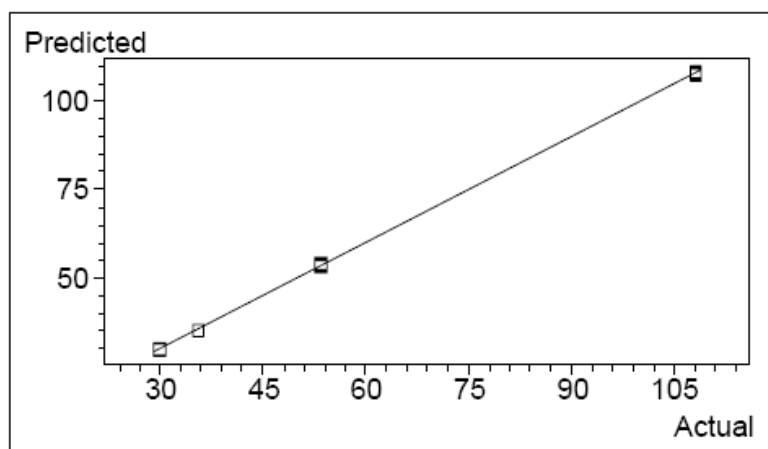

Fig.3 Relationship between actual and predicted hydroxyl value

Table 2 Result Table by PLS

PLS Report table

```
Calibration table :
Algorithm :              PLS 1
Number of components : 1
Number of references :   16
Range [ 1 ] :            4500.00 – 7500.

Centered data :          Yes
Component :              Hydroxyl valule
Number of factors :      3
Correlation coeff. :     0.99996
MSEP :                   0.00008
SEP :                    0.00901
X Leverage warnings :    0
Y Residual warnings :    0
```

Component :	Hydroxyl value					
Reference	Outlier	Actual	Predicted	Diff (%)	ConcResid	SpecResid
No9-1		35.5	35.294	0.582	0.206	0.108
No9-2		35.5	35.244	0.72	0.256	0.099
No9-3		35.5	35.253	0.697	0.247	0.059
No9-4		35.5	35.181	0.899	0.319	0.042
No11-1		29.8	29.614	0.624	0.186	0.056
No11-2		29.8	29.626	0.583	0.174	0.016
No11-3		29.8	30.136	-1.129	-0.336	0.077
No11-4		29.8	30.075	-0.924	-0.275	0.08
No43-1		53.5	53.605	-0.195	-0.105	0.355
No43-2		53.5	53.819	-0.597	-0.319	0.282
No43-3		53.5	53.533	-0.062	-0.033	0.435
No43-4		53.5	54.074	-1.072	-0.574	0.714
No48-1		108	108.263	-0.244	-0.263	0.017
No48-2		108	108.167	-0.155	-0.167	0.015
No48-3		108	107.55	0.417	0.45	0.041
No48-4		108	107.765	0.218	0.235	0.027

Table 3 Analysis Results by PLS

	Spectrum	Hydroxyl value	Residual error.1
1	UK-1	63.475	0.449
2	UK-2	63.330	0.680
3	UK-3	63.430	0.726
4	UK-4	63.267	0.541

Table 1 Analytical Conditions

Resolution	: 4cm^{-1}
Accumulation	: 60
Detector	: DLATGS

References Shimadzu LAAN-A-FT E013 No. A387

Shimadzu Europa GmbH
Albert-Hahn-Str.6-10, 47269 Duisburg

www.shimadzu.eu

SHIMADZU
Solutions for Science
since 1875

SHIMADZU
Excellence in Science

Application News

No.A471

Spectrophotometric Analysis

High Resolution Analysis of Carbon Monoxide (CO) Gas

■ Introduction

FTIR is being used for analysis of gases in various industries, such as the gas manufacturing industry where it is used for production management, and for gas monitoring in such fields as chemical manufacturing and semiconductor manufacturing, etc. When conducting gas analysis by FTIR, the resolution and gas cell path length must be selected depending on the concentration and peak shape of the gas component of interest. Here, using the IRTracer-100, we introduce an example of high resolution measurement of the low-molecular weight gas, carbon monoxide (CO).

Fig. 1 Overlaid Spectra of Water Vapor Measured at Different Resolutions

■ Advantage of High Resolution

To compare spectral differences due to resolution, we measured the infrared spectra of water vapor at resolutions of 0.25 cm^{-1}, 0.5 cm^{-1} and 1 cm^{-1}, respectively. The analytical conditions used are shown in Table 1. Fig. 1 shows an enlarged view of the infrared spectra in the vicinity of 1620 cm^{-1}.
As can be seen here, the peaks that were not separated at 0.5 cm^{-1} and 1 cm^{-1} were clearly separated when measured with a resolution of 0.25 cm^{-1}.
By conducting measurement at high resolution, the spectral peak intensity is noticeably increased, making it easier to distinguish between two peaks that are closely adjacent to one another. This is especially useful in component identification in cases where the mixed gas spectra include similarly shaped, overlapping peaks.
Further, since the lower the molecular weight of the gas, the more pronounced the rotation and vibration of the spectrum, it is more effective to conduct measurement of low-molecular weight gases at high resolution.

■ Quantitation of Carbon Monoxide (CO) Gas

Using CO as an example of a low-molecular weight gas, we measured the spectra of CO gas samples at different concentrations (95 ppm, 191 ppm, 1207 ppm, 2415 ppm), and then generated a calibration curve. In this case, the resolution of 0.25 cm^{-1} was used. The other analytical conditions were as shown in Table 1. For the calibration curve, we used the height of the peak in the vicinity of 2170 cm^{-1}, and primary linear calculations were conducted using the multi-point calibration curve method.
Fig. 2 shows the overlaid spectra of the CO gasses at their respective concentrations, and Fig. 3 shows the calibration curve. The correlation coefficient r = 0.999 for the calibration curve indicated excellent linearity.
Use of a 10 cm gas cell in the quantitation of carbon monoxide gas using a resolution of 0.25 cm^{-1} and a DLATGS detector makes quantitation possible over a wide range of concentrations, from tens to thousands of ppm. When the 0.5 cm^{-1} resolution is used, the lower limit of quantitation will increase due to the lower peak intensity, assuming that the noise remains constant. In actuality, the resolution and number of accumulations must be determined while monitoring the state of the obtained spectrum in order to obtain the optimum lower limit of quantitation.

Table 1 Instrument and Analytical Conditions

Instrument	: IRTracer-100
Resolution	: 0.25, 0.5, 1.0 cm^{-1}
Accumulation	: 30
Apodization	: Happ-Genzel
Detector	: DLATGS
Accessories	: Gas Cell (10 cm) / NaCl Window
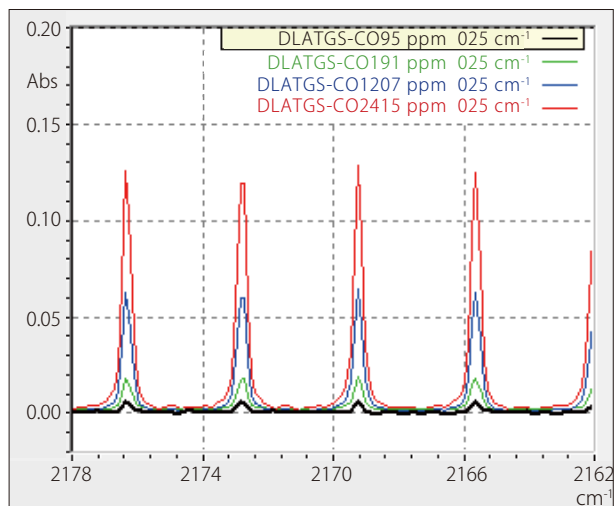
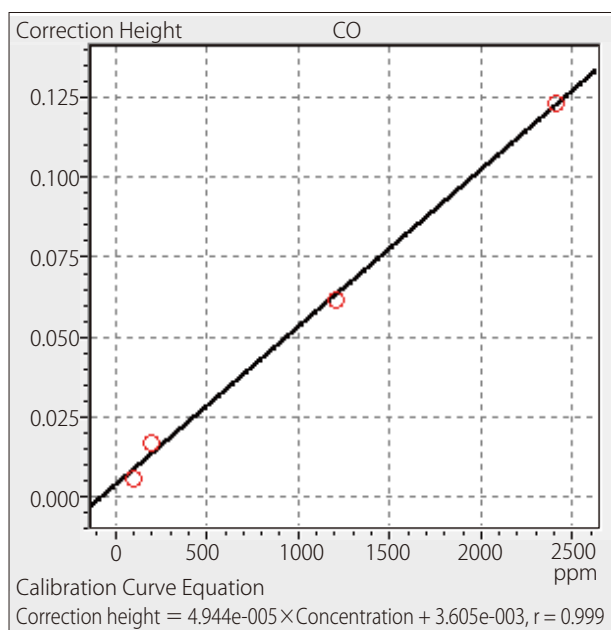**Fig. 2 Overlaid Spectra of CO at Four Concentrations (95, 191, 1207, 2415 ppm)**

Calibration Curve Equation
Correction height = 4.944e-005 × Concentration + 3.605e-003, r = 0.999

Fig. 3 Calibration Curve of CO Using Four Concentrations

the cell is reduced. Therefore, when using a gas cell with a long optical path length for high-resolution measurement, a better spectrum can be obtained with an MCT detector, which can provide high sensitivity detection with low noise.

Fig. 4 shows overlaid spectra of CO gas measured with an MCT detector and a DLATGS detector. Measurement of the 2415 ppm CO gas was conducted using a resolution of 0.25 cm⁻¹, and a gas cell having an optical path length of 10 cm. The red-trace spectrum was obtained using the DLATGS detector, while the black-trace spectrum was measured with the MCT detector.

Due to the high sensitivity of the MCT detector, the light intensity used for this measurement was reduced. However, when compared with the DLATGS detector under the same conditions, a spectrum with less noise was obtained using the MCT detector. Another advantage of the MCT detector is the faster mirror speed compared to that of the DLATGS detector, due to its higher optimum frequency response, which permits a shorter measurement time.
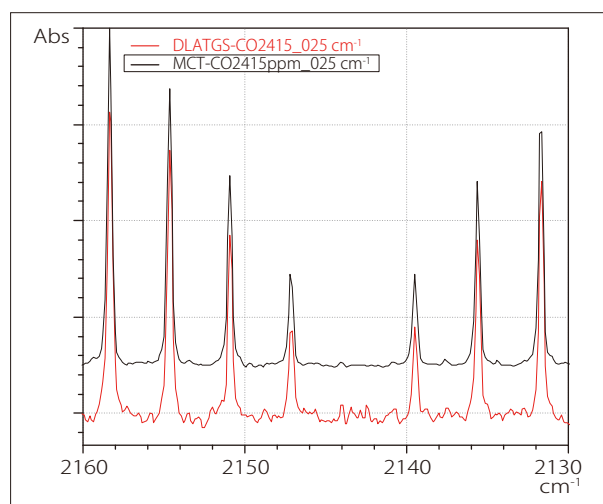
Fig. 4 Spectra of CO Measured with a DLATGS Detector and an MCT Detector

■ Advantage of Optional MCT Detector

The standard detector for the IRTracer-100 is the DLATGS detector, which provides stable detection over a wide wave number range. However, for detection with higher sensitivity, the liquid nitrogen-cooled MCT detector is available as an option.

In measurement at high resolution, the aperture between the interferometer and the light source must be reduced to increase the parallelism of incident light on the interferometer. This results in a reduction in the amount of light reaching the detector. Further, in analysis of a low-concentration gas, there are cases in which a long optical path length cell is required, but as the optical path length increases, the amount of light in

■ Summary

Here, using analysis of CO gas as an example of low-molecular weight gas analysis, we introduced the excellent performance of the IRTracer-100, with its high 0.25 cm⁻¹ resolution and quantitative performance, as well as the advantages of using the optional MCT detector.

Using the IRTracer-100 with the LabSolutions IR software offers stable measurement and simple quantitative operations.

As always, when conducting gas analysis by FTIR, it is necessary to carefully consider various conditions, including the detection limit, corrosiveness, coexisting substances, etc. Please contact your Shimadzu representative for information such as cell selection, etc.

SHIMADZU

Shimadzu Corporation

www.shimadzu.com/an/

SHIMADZU
Excellence in Science

Application News

No.A511

Spectrophotometric Analysis

Investigation of Ultraviolet Degradation of Plastic with Mapping Program

Plastic is degraded by ultraviolet light and heat. However, it is difficult to determine how deep degradation reaches into a material based on its external appearance. The extent of degradation inside a material can be confirmed by cutting cross sections of the material and performing mapping analysis with an infrared microscope.

We describe an analytical technique that confirms the extent of ultraviolet degradation of polypropylene plastic that is used in various everyday products, and compare the results with visual observation of ultraviolet degradation.

■ Polypropylene Plastic

Polypropylene (PP) is created by the polymerization of propylene and is a plastic with excellent mechanical characteristics that include tensile strength, impact strength, and compressive strength, low specific gravity, and the capacity to be easily processed. PP also has excellent heat resistance and chemical resistance, and is used in many products encountered in our daily lives, including daily commodities, home electronic components, food containers, automobile components, and medical equipment.

PP is not particularly weather resistant, and when exposed to sunlight turns white and loses its heat resistance.

■ Procedure for Analysis of Ultraviolet Degraded PP Plastics

First, a microtome was used to cut slices from PP plastics degraded by ultraviolet on one side, creating flat cross-sections (see Fig. 1). Next, the flat cross-sections were held horizontally and reflectance was measured, because the severe degradation made the samples too brittle for ATR measurement. The background measurement was conducted using an aluminum vapor deposition mirror.

Then the state of ultraviolet degradation was confirmed based on the spectra obtained.
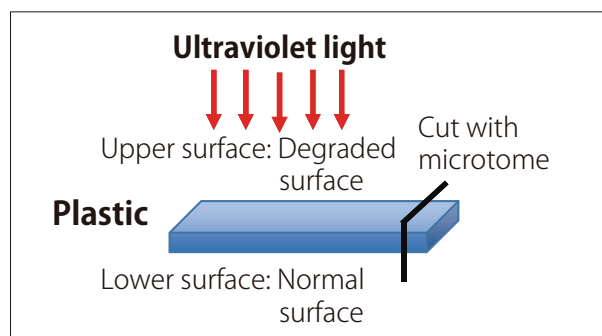
Fig. 1 Flat Cross-Sections from Degraded PP Plastic

Table 1 FTIR Spectroscopy Conditions

Instrument	: IRTracer-100
	AIM-9000
Resolution	: 8 cm^{-1}
Accumulation	: 30
Apodization	: Happ-Genzel
Detector	: MCT
Aperture	: 40 µm × 40 µm
Mapping	: Area
Step	: 40 µm

■ Analysis

Analysis and aperture conditions are shown in Table 1. When setting aperture, the site to be measured is displayed as shown in Fig. 2. Forty-nine points located in a 280 × 280 μm grid pattern shown in Fig. 2 were measured using the analytical conditions shown in Table 1.

■ Analytical Results

Results show the C=O derived peak around 1750 cm^{-1} and the O-H derived peak around 3400 cm^{-1} increase in size with increasing degradation. Fig. 3 shows a map of corrected peak heights around 1750 cm^{-1} and Fig. 4 shows spectra of normal and degraded parts of the sample.

Fig. 3 shows that degradation is more advanced on the left side of the measurement area than on the inner right side. This mapping shows that degradation reaches approximately 200 μm into the material.

■ Conclusion

Degradation of plastics caused by ultraviolet light and heat reaches below the surface. We cut cross-sections of plastic and visualized the depth of degradation using infrared spectrophotometry.

The AIM-9000 infrared microscope and AIMsolution software allowed us to easily view the entire measurement site, and visually observing the sample simultaneous to analysis also enabled us to relate analytical results with our view of the measurement site.

Degraded plastic Surface ⟶ Interior
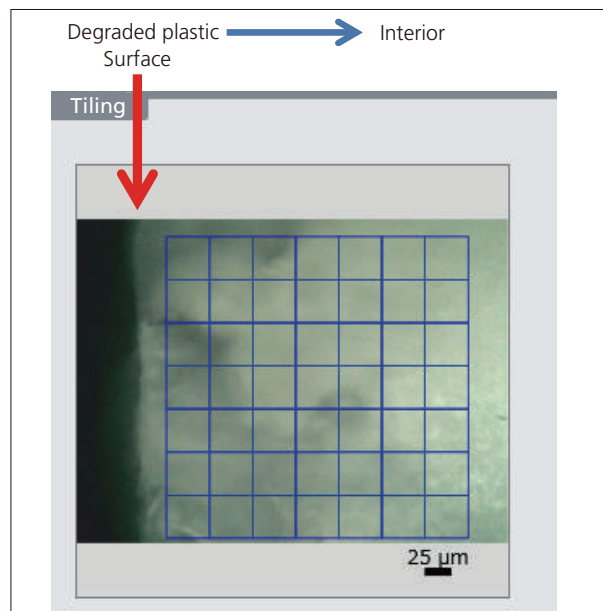
Fig. 2 Image Displayed After Setting Aperture

Peak height (1570.06-2067.69, baseline correction: yes)
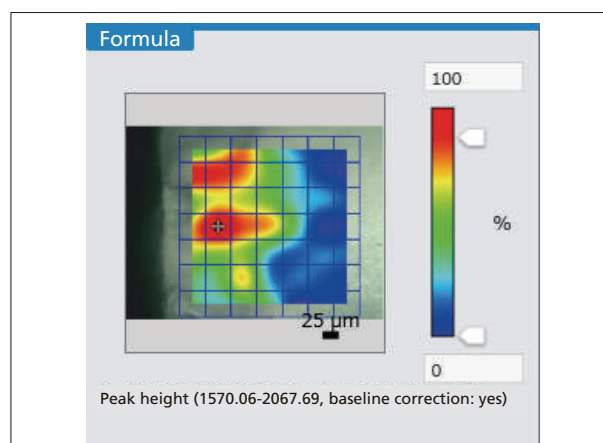
Fig. 3 Mapping Image Obtained at Corrected Peak Height of Around 1750 cm^{-1}

3400 cm^{-1} 1750 cm^{-1}

Abs

4000 3500 3000 2500 2000 1750 1500 1250 1000 750 cm^{-1}
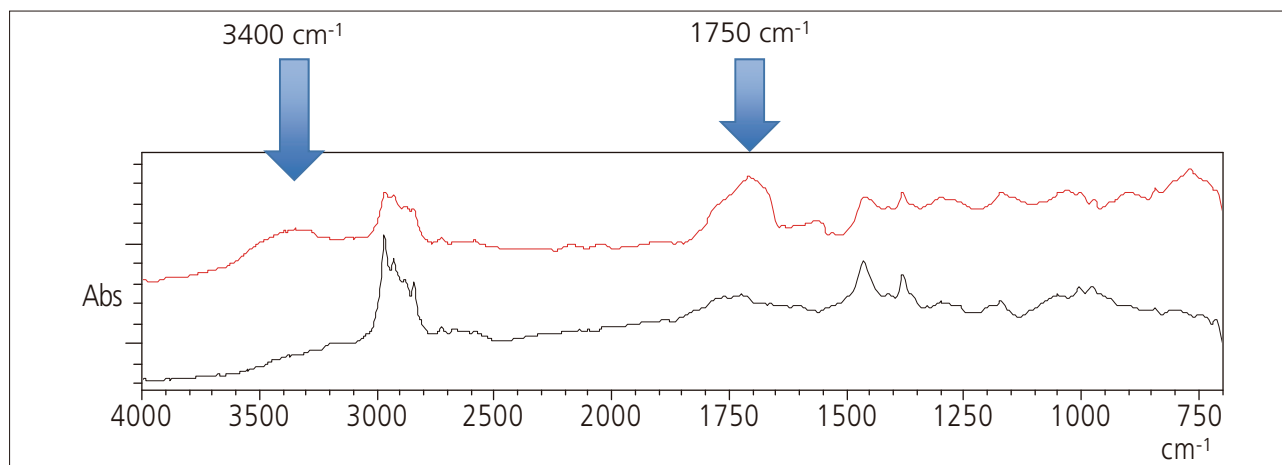
Fig. 4 Infrared Spectra of Normal (Black) and Degraded (Red) Areas

SHIMADZU

Shimadzu Corporation

www.shimadzu.com/an/

SHIMADZU
Excellence in Science

Application News

No.A513

Measuring Micro-Contaminants on Optical Parts: Measurement and Identification by AIM-9000 Infrared Microscope

Due to the miniaturization and increasingly sophisticated functionality of electrical and electronic devices, an increasing number of optical devices are being used today, such as ultra-small and high-performance semiconductor devices and sensors. However, in such miniaturized devices, micron-sized tiny contaminants can cause the devices to malfunction. Therefore, manufacturers need to determine what caused such contaminants to enter the devices, so their recurrence can be prevented.

Shimadzu AIM-9000 infrared microscope features optics that are designed especially for measuring microscopic areas, and allows users to obtain good spectra in short time even for micron-sized tiny contaminants. The following describes an example of using this system to measure micro-contaminants about 10 µm in diameter on the surface of an optical part.

■ Micro-Contaminants on an Optical Part

Fig. 1 shows a microscope photograph of the contaminants on the surface of an optical part installed in an electronic device. The contaminants, which are between about 3 and 10 µm in diameter, are lying scattered on a part surface.

Fig. 1 Microscope Image of Micro-Contaminants (shown with a 10 µm blue box)

■ Measurement

These contaminants were discovered on a shiny, flat, and smooth metal part surface. Therefore, a measurement using specular reflection spectroscopy is appropriate due to no necessity of sampling the part and the low risk of part damage or loss. An infrared spectrum measured from the contaminant using an infrared microscope by specular reflection spectroscopy and corresponding search results are shown in Fig. 2. Measurement conditions are indicated in Table 1. Even for tiny contaminants only about 10 µm across, a spectrum with minimal noise can be obtained using a short measurement time of only about 20 seconds. Results from analyzing the data using the spectrum library included standard with the system determined that the contaminant is probably a lactate.
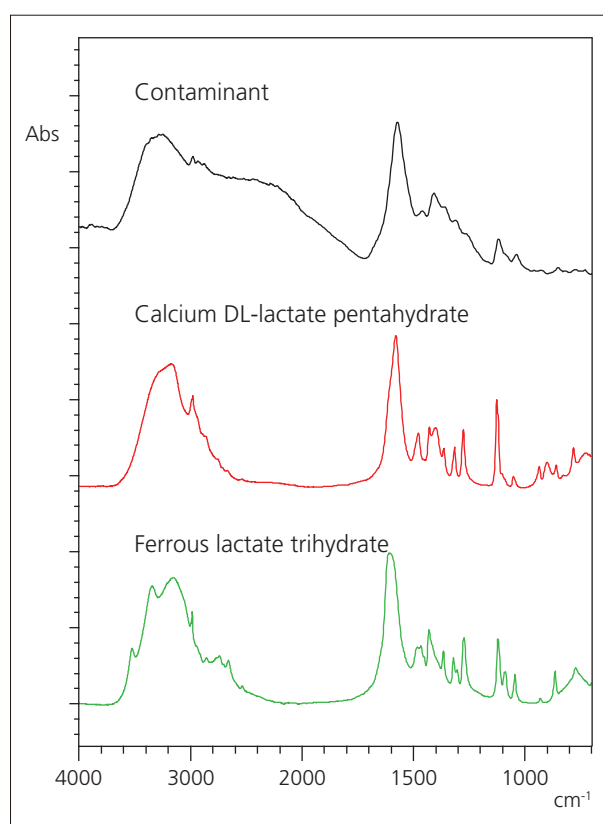

Fig. 2 Infrared Spectrum and Search Results for the Contaminant

Table 1 Measurement Conditions

Instrument	: IRTracer-100, AIM-9000
Resolution	: 8 cm^{-1}
Accumulation	: 40
Apodization	: Happ-Genzel
Detector	: MCT

■ **AIM-9000 Infrared Microscope**

Due to the optics that are designed specifically for measuring extremely small areas, the AIM-9000 infrared microscope achieves the highest signal-to-noise ratios (30,000:1) in its class. That means it can obtain excellent spectra very quickly, even from extremely small contaminants. As an example, results from measuring 10 µm polystyrene beads scattered on a BaF₂ window plate are shown. A microscope photograph of the polystyrene beads is shown in Fig. 3. A comparison of measurements obtained by transmission spectroscopy using both the AIM-9000 and the Shimadzu's previous model is shown in Fig. 4. Measurement conditions are listed in Table 2 and a photograph of the AIM-9000 system connected to an IRTracer-100 infrared spectrophotometer is shown in Fig. 5.
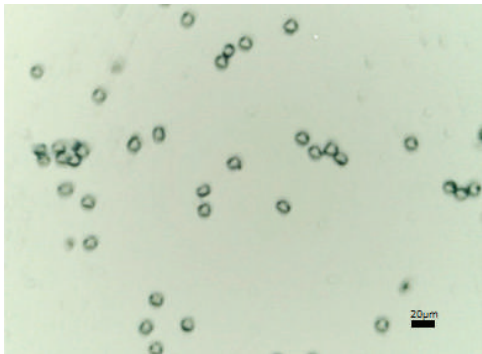
Fig. 3 **Microscope Image of Polystyrene Beads of 10 µm in Diameter**

Table 2 Measurement Conditions

Instrument	: IRTracer-100, AIM-9000, and previous model (AIM-8800)
Resolution	: 8 cm⁻¹
Accumulation	: 40
Apodization	: Happ-Genzel
Detector	: MCT
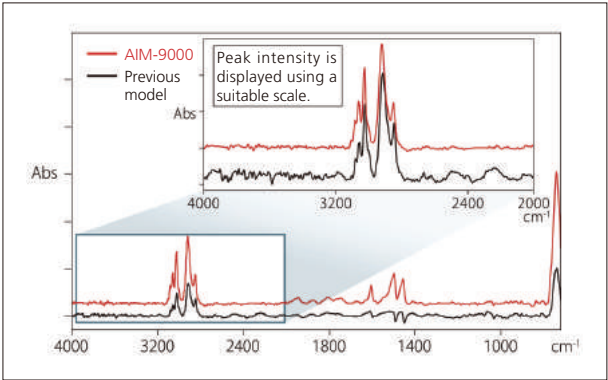
Fig. 4 **Infrared Spectra of Polystyrene Beads of 10 µm in Diameter (with Baseline Correction)**

These results show that the AIM-9000 detects the polystyrene absorption peaks more clearly and with higher intensity. The inset enlargement shows the results from displaying the spectra with peak intensity matched near 2,920 cm⁻¹. It demonstrates how the AIM-9000 can provide superior spectra with less noise than the previous model.

■ **Conclusion**

This article describes measuring micro-contaminants about 10 µm in diameter on the surface of an optical part. The AIM-9000 infrared microscope is ideal for identifying contaminants and analyzing defects in extremely small areas.

Fig. 5 **AIM-9000 Infrared Microscope Connected to IRTracer-100 Fourier Transform Infrared Spectrophotometer**

SHIMADZU

Shimadzu Corporation

www.shimadzu.com/an/

SHIMADZU
Excellence in Science

Application News

No.A514

Spectrophotometric Analysis

Introducing Area Imaging with AIM-9000 and AIMsolution

AIMsolution control software for the AIM-9000 infrared microscope comes with an optional mapping program. Measurements performed with the mapping program integrate seamlessly with normal point measurements, and involve simple configuration of sample image capture, measurement size, aperture size, and measurement pitch all in the same window. The mapping program provides detailed analysis of microscopic sample regions by performing area measurements to analyze the in-plane distribution of components, and line measurements useful for depth-based sample analysis.

An example application is described here that uses the AIMsolution mapping program to perform area measurements.

■ Measurement Sample

A transmission method was used to take area mapping measurements of a pharmaceutical powder that contains a number of components. The sample was first inserted into a diamond cell and compressed to a thickness appropriate for transmission measurements. After compression, the diamond cell was installed on the stage, and area measurements were performed.

A visible image of the entire sample is shown in Fig. 1. The visible image shows areas of different colors in the sample, indicating it is probably a mixture of a number of components.
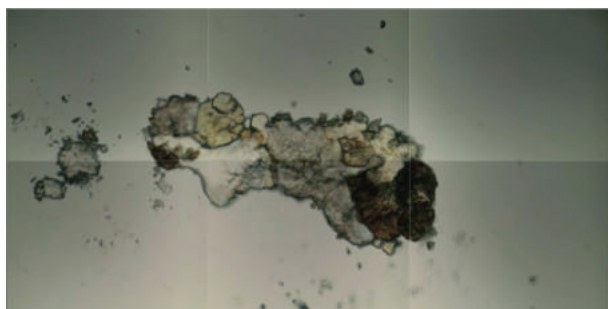
Fig. 1 Visible Image of Sample

Sample measurements were performed in an area of 375 µm (vertical) by 600 µm (horizontal). The measurement area is shown in Fig. 2. A 25 µm by 25 µm aperture size was set at each measurement position. The blue lattice shows the aperture of each measurement position, with the measurement positions being selected to leave no gaps. The yellow box is a background measurement position. Aperture size for background measurements is set automatically to the same aperture size used for sample measurements. Measurements were performed with the parameters shown in Table 1.
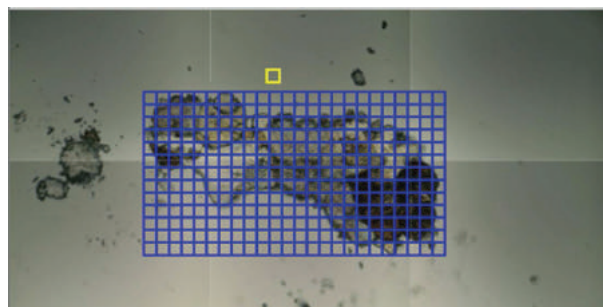
Fig. 2 Image Displayed after Measurement Area Selection

Table 1 FTIR Measurement Conditions

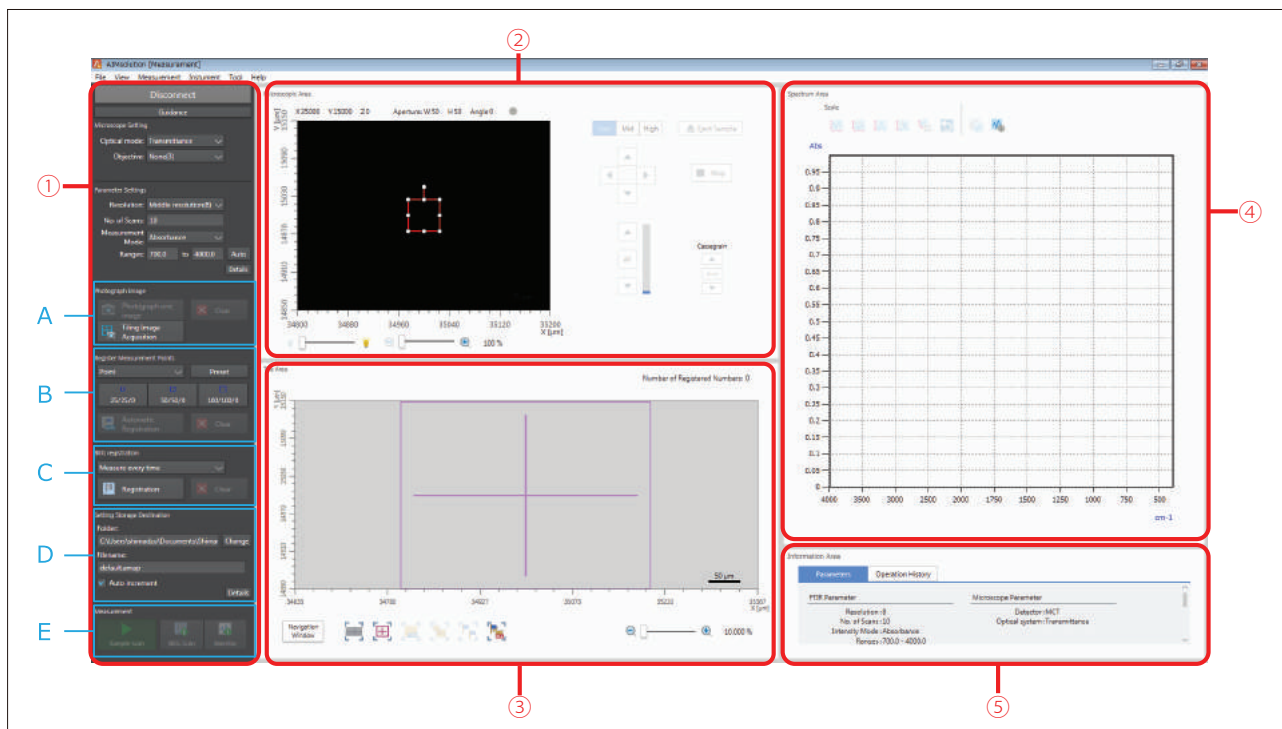|	
Instrument	: IRTracer-100 / AIM-9000
Resolution	: 8 cm^{-1}
Accumulation	: 2
Apodization	: Sqr-Triangle
Aperture Size	: 25 µm × 25 µm
Step	: 25 µm
Detector	: MCT

Fig. 3 Measurement Program Configuration Window

■ **Measurement Procedure**

The AIMsolution measurement program window is shown in Fig. 3.
The window is divided into five areas.

(1) [Measurement Parameter Configuration Area]
Parameters are configured here.

(2) [Microscope Area]
Displays microscopic images. Stage movement and focal adjustment are also performed with buttons in this area.

(3) [Tile Area]
Displays images captured by the microscope side-by-side.
(Displaying images side-by-side is called tiling.)
Specifying positions for area measurement is also mainly performed in this area.

(4) [Spectrum Area]
Displays spectra.

(5) [Information Area]
Information on configured parameters and logs are displayed in this area.

The microscope can be controlled and all necessary information can be viewed in a single window.

A flowchart of the measurement procedure is shown in Fig. 4.
The AIMsolution mapping program is designed to make configuration of area measurements extremely easy. The measurement procedure is very simple, with configuration performed in order of sections A to E of the measurement parameter configuration area.
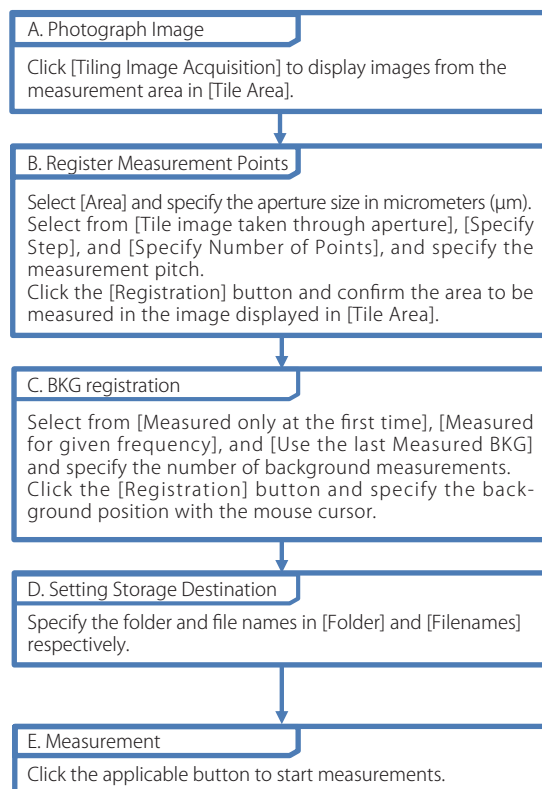
A. Photograph Image

Click [Tiling Image Acquisition] to display images from the measurement area in [Tile Area].

B. Register Measurement Points

Select [Area] and specify the aperture size in micrometers (μm). Select from [Tile image taken through aperture], [Specify Step], and [Specify Number of Points], and specify the measurement pitch.
Click the [Registration] button and confirm the area to be measured in the image displayed in [Tile Area].

C. BKG registration

Select from [Measured only at the first time], [Measured for given frequency], and [Use the last Measured BKG] and specify the number of background measurements.
Click the [Registration] button and specify the background position with the mouse cursor.

D. Setting Storage Destination

Specify the folder and file names in [Folder] and [Filenames] respectively.

E. Measurement

Click the applicable button to start measurements.

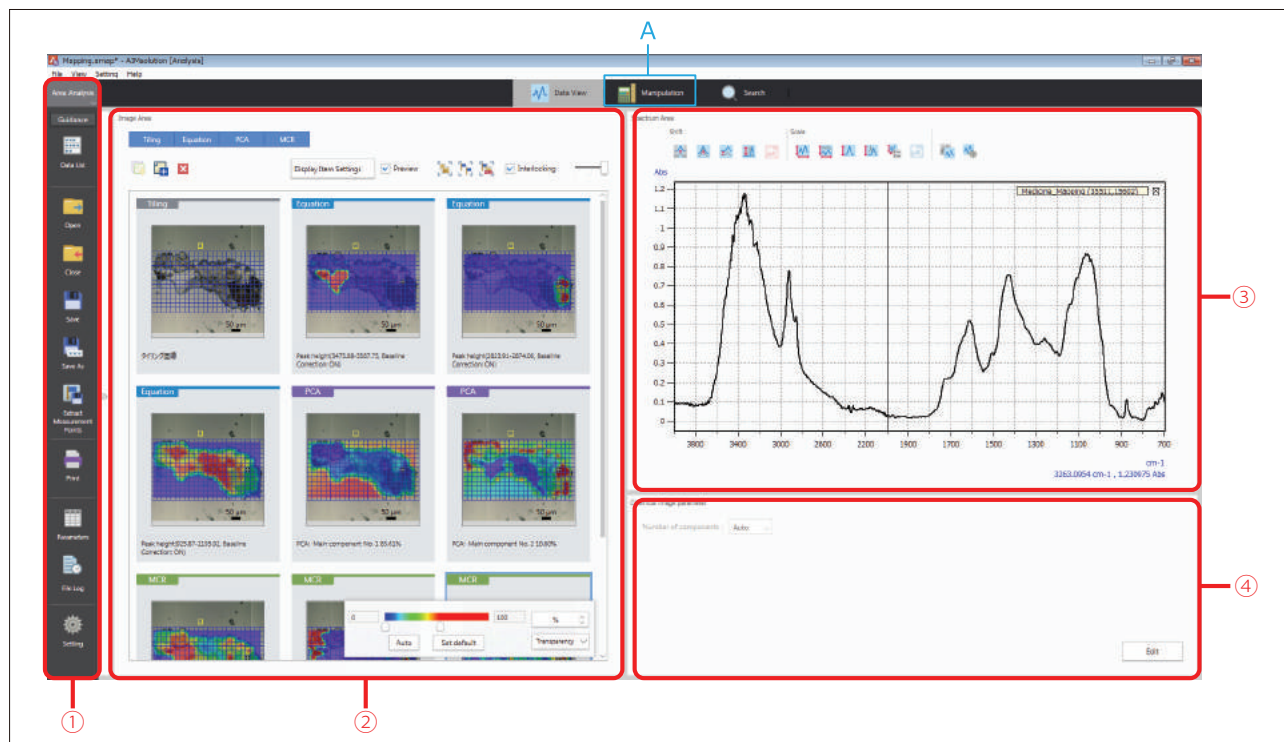**Fig. 4 Flowchart of Sample Measurement**

Fig. 5 Area Data Analysis Program Window

■ Area Data Analysis
(Data Analysis of Area Measurement Results)

Analysis of the area measurement results is performed by the Area Data Analysis part of the analysis program. A view of the Area Data Analysis screen is shown in Fig. 5.

The data analysis screen is divided into 4 areas.

(1) [Toolbar]
   Contains tool icons.

(2) [Image Area]
   Displays tiling images and the results of data analysis (results of calculations).
   The results of data analysis are called chemical imaging.

(3) [Spectrum Area]
   Displays spectra, including measurement point spectra, multivariate analysis loading spectra, and component spectra.

(4) [Chemical Imaging Parameters]
   Displays parameters used during data analysis (computation), and allows them to be edited.
   Wavelength range can be specified for peak height and peak area, and the number of factors for multivariate analysis.

To perform preprocessing of measurement data, change windows by clicking the [Manipulation] button in Fig. 5 (A). Preprocessing included in the software are baseline correction, atmospheric correction, advanced ATR Correction, Kramers-Kronig analysis, and difference (compute difference spectra).

In the default settings, the results of area measurement data analysis are displayed as chemical imaging, with large numbers represented in red and small numbers in blue.

Computing formula factors that can be used to create chemical imaging are as follows: Intensity at specified position, relative intensity at specified position, peak height, relative peak height, peak area, relative peak area, and degree of coincidence.

Other than computing formulae, chemical imaging can also be created using multivariate analysis. Multivariate analyses available to the user are principal component analysis (PCA) and multivariate curve resolution (MCR). PCA and MCR data analyses can be implemented with a single click, without the need to configure complicated parameters.

An example of chemical imaging is shown in Fig. 6. The image in Fig. 6 is created using OH group peak height in the vicinity of 3500 cm^{-1}. The image shows that the left portion of the sample contains a large amount of material with OH groups. Chemical imaging allows distributions to be visually displayed in a way that is easy to understand.
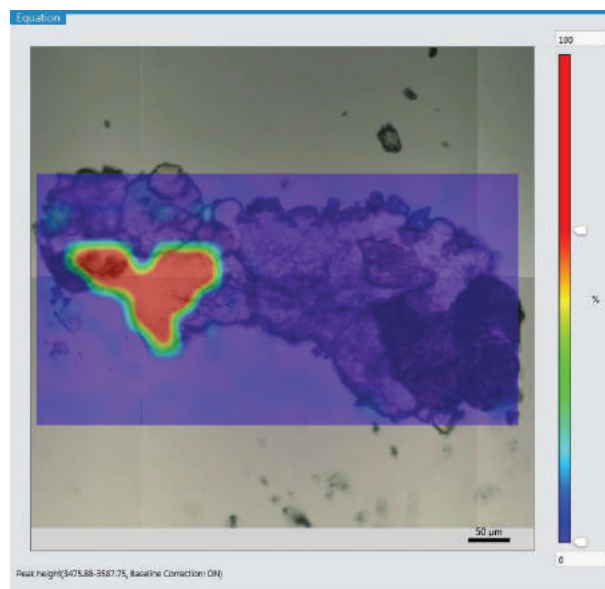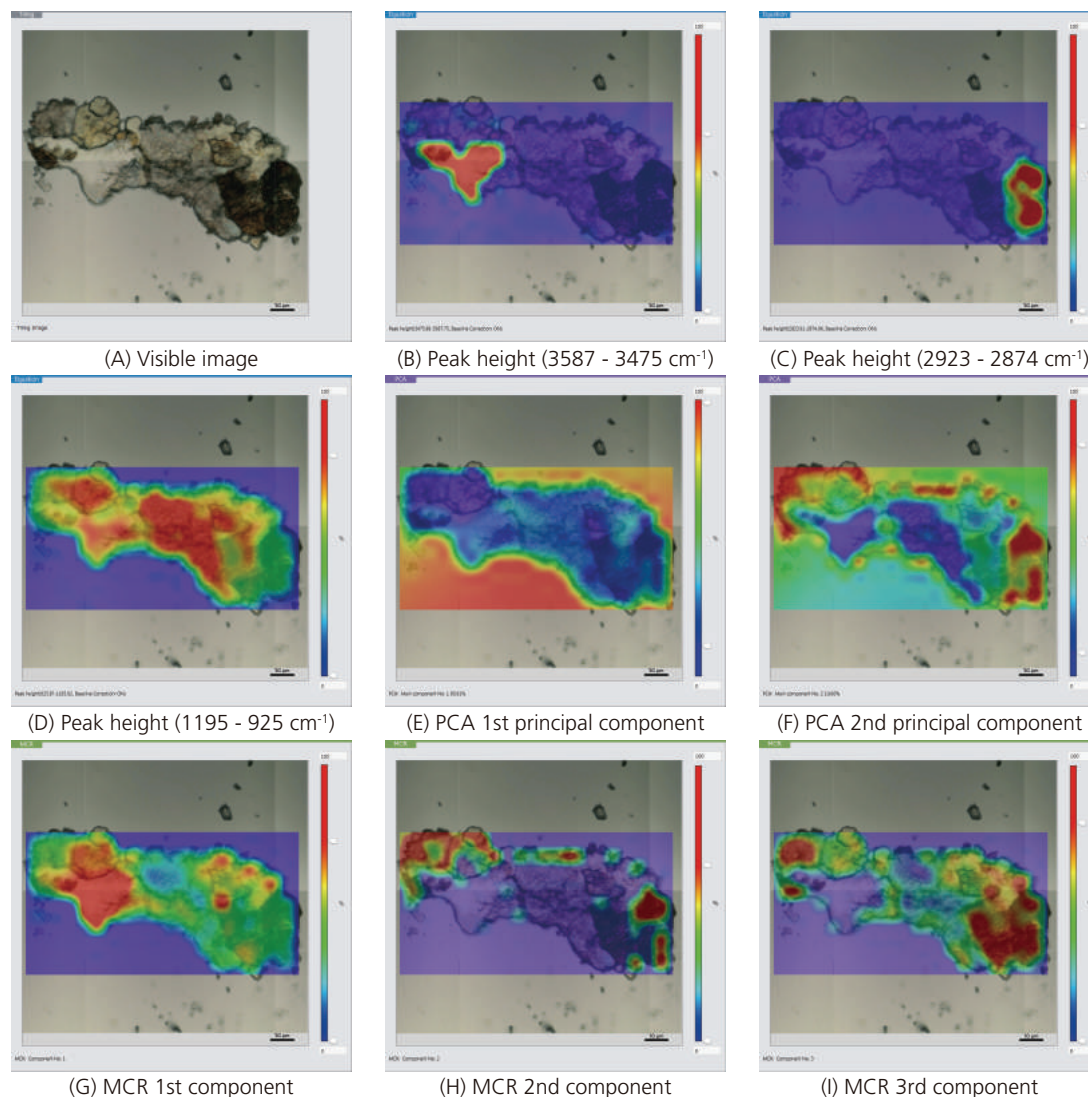

Fig. 6 An Example of Chemical Imaging

(A) Visible image

(B) Peak height (3587 - 3475 cm^{-1})

(C) Peak height (2923 - 2874 cm^{-1})

(D) Peak height (1195 - 925 cm^{-1})

(E) PCA 1st principal component

(F) PCA 2nd principal component

(G) MCR 1st component

(H) MCR 2nd component

(I) MCR 3rd component

Fig. 7 Chemical Imaging of Sample

■ **Results of Data Analysis**

Chemical imaging obtained from the measured sample using several techniques is shown in Fig. 7. From the top left: (A) visible image, (B) peak height at 3587-3475 cm^{-1}, (C) peak height at 2923-2874 cm^{-1}, (D) peak height at 1195-925 cm^{-1}, (E) PCA 1st principal component, (F) PCA 2nd principal component, (G) MCR 1st component, (H) MCR 2nd component, and (I) MCR 3rd component.

The chemical imaging in Fig. 7 displays OH group absorption in (B), CH group absorption in (C), CO group absorption in (D), and difference from the mean of all sample data in (E). While (D) and (G) show different concentration levels in the sample, some components seem to be present throughout the sample. Based on (C), (F), (H), and (I), it is highly likely that a component present on the right end of the sample is different from those in the other portions.

■ **Conclusion**

Performing area measurements with AIMsolution allows for a diverse array of analytical results as images, including the results of multivariate analyses such as PCA and MCR in addition to peak height and peak area.

SHIMADZU

Shimadzu Corporation

www.shimadzu.com/an/

SHIMADZU
Excellence in Science

Application News

No.A515

Spectrophotometric Analysis

Introducing the Automatic Contaminant Recognition System

■ **Introduction**

With the recent growing interest in the safety of many products, including foods, pharmaceuticals, electronic goods, and cars, there is an increasing demand for contaminant analysis. When performing contaminant analysis work, measured positions and aperture sizes (measured area size) can vary between analysts, which introduces variations or errors in the results.

Shimadzu's automatic failure analysis system (IRTracer-100 infrared spectrophotometer and AIM-9000 infrared microscope) comes with an automatic contaminant recognition system as standard, which automatically recognizes contaminants and automatically sets the optimum aperture size and angle in just one second. We describe an example analysis performed using the automatic contaminant recognition system.

■ **Automatic Recognition**

The automatic contaminant recognition system is enabled by clicking the [Automatic Registration] button shown in the red box in Fig. 1.

Then, image processing is performed on the current microscopic image to automatically recognize candidate measurement points, set the optimum aperture size as shown in Fig. 2, and register this information.

The automatic contaminant registration function is available in two types. There is a standard type that generally selects measurement positions of a relatively large size, and a micro type that generally selects measurement positions that are microscopic in size (around 10 μm). Either type can be selected according to the sample to be measured. Up to a maximum of 20 measurement positions can be configured automatically, and positions can be added or removed as needed. After measurement, the image showing measurement positions and aperture information is saved automatically together with the spectra.
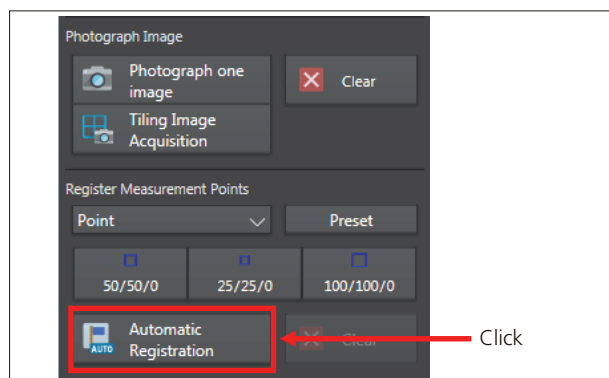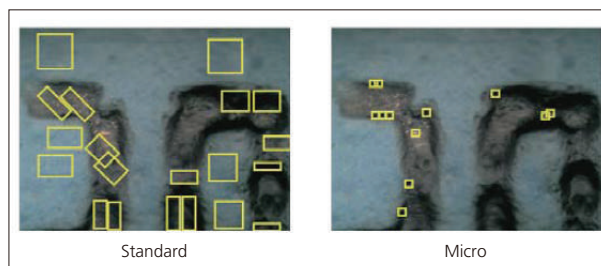

Standard   Micro
Fig. 2 Automatic Recognition

■ **Measurement Procedure**

Fig. 3 shows a flowchart of the measurement sequence. The measurement procedure is very simple, with configuration performed in order of sections A to D of the measurement parameter configuration area. Analysis time is reduced since measurement points and aperture sizes can be configured automatically in Step A.
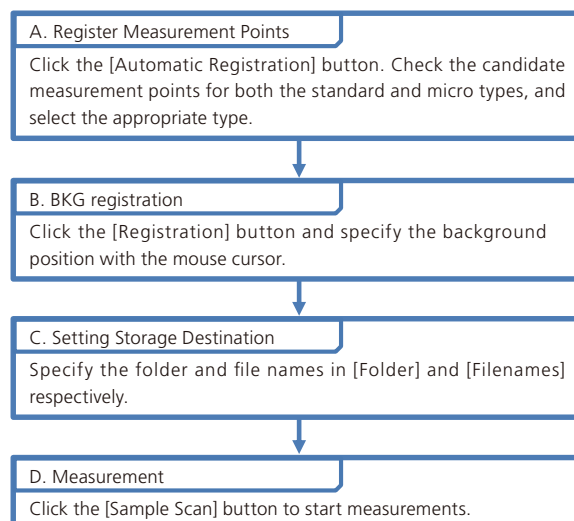

A. Register Measurement Points
Click the [Automatic Registration] button. Check the candidate measurement points for both the standard and micro types, and select the appropriate type.

B. BKG registration
Click the [Registration] button and specify the background position with the mouse cursor.

C. Setting Storage Destination
Specify the folder and file names in [Folder] and [Filenames] respectively.

D. Measurement
Click the [Sample Scan] button to start measurements.

Fig. 3 Measurement Procedure Flowchart

Click
Fig. 1 AIMsolution Window

■ Contaminant Analysis Example

Fig. 4 Contaminants on a Frozen Pizza

We analyzed the black contaminant on the surface of a frozen pizza as shown in Fig. 4. Contaminant was collected, compressed in a diamond cell, and analyzed with an infrared microscope. Fig. 5 is the images shown by the automatic contaminant recognition system after automatic registration. The measurement positions on the left are standard type, and the positions on the right are micro type. For this analysis, standard type measurement positions were chosen.

Looking at Fig. 5, there are black areas and transparent areas in the compressed contaminant. Normal (transparent) parts of the pizza were probably collected together with black contaminant during sample collection. Both the black and transparent areas were analyzed. Fig. 6 shows infrared spectra for representative black areas and transparent areas.
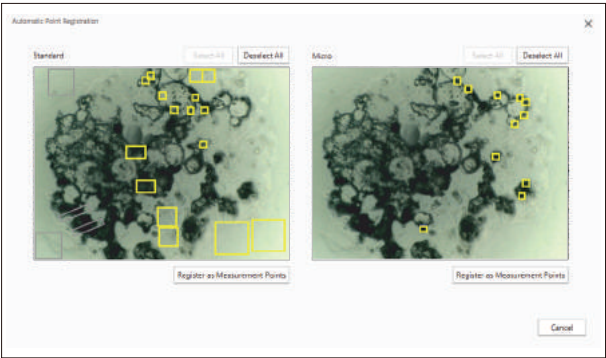
Fig. 5 Automatic Contaminant Recognition System

Table 1 Measurement Conditions

Resolution	: 8 cm^{-1}
Accumulation	: 40
Apodization	: Happ-Genzel
Detector	: MCT
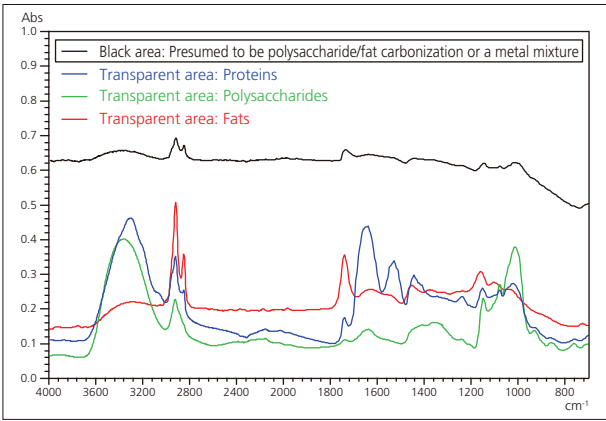
Fig. 6 Infrared Spectra and Qualitative Results

Proteins, polysaccharides, and fats were detected in each position on the collected contaminant that was analyzed, and are all presumed to be normal components of the pizza dough. The baseline of the infrared spectrum of the black area is noticeably elevated, and is presumed to be caused by carbonized fats/polysaccharides or a metal mixture.

X-ray fluorescence spectrometry examination of the black area was performed separately, and Fe, Cr, and Ni were detected, which identifies the black area as stainless steel.

■ Conclusion

There will probably be a demand for quicker and more accurate methods of contaminant analysis in the future. Shimadzu's automatic contaminant recognition system can automatically configure measurement positions and aperture sizes optimized for the sample, and perform highly accurate contaminant analysis in a short period of time.

Fig. 7 IRTracer-100 Infrared Spectrophotometer and AIM-9000 Infrared Microscope

SHIMADZU

Shimadzu Corporation

www.shimadzu.com/an/

SHIMADZU
Excellence in Science

Application News

Spectrophotometric Analysis

Printed Circuit Board Defect Analysis

No.A521

Contaminants and stains on printed circuit boards can cause conduction defects. Identifying these materials is an important part of preventing the same problem occurring again.

We describe a qualitative analysis of contaminants found on a printed circuit board performed using the AIM-9000 Infrared Microscope, which is specially designed for defect analysis.

■ Contaminants/Stains Found on Printed Circuit Board

Contaminants and stains found on the terminal of a microSD[TM 1)] card were analyzed. Fig. 1 shows an image of the microSD[TM] card placed on the sample stage of the AIM-9000, captured with a wide field camera. Almost the entire card is within the field of view. Using a wide field camera allows observation of a wide area around the defect with a field of view of approximately 10 mm × 13 mm. Positional information is shared between the wide field camera and a 15X reflection objective mirror that will be used for analysis. Once a defect is found with the wide field camera, the operator can switch to a 15X reflection objective mirror view of the same location, and only need to adjust image focus. This feature makes it easy to bring a defect within the analytical field of view. An auto-centering function is also included as standard. This function automatically moves a desired position on the sample stage to the middle of the field of view by simply double-clicking a point on the wide field image or microscope image. This can be useful for analyzing electrical products with multiple terminals.
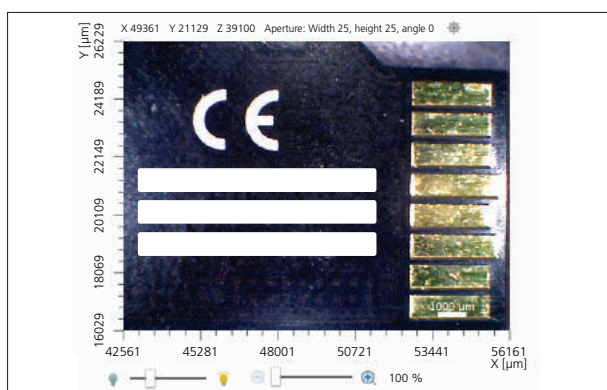

Fig. 1 Wide Field Camera Image of microSD[TM] Card

■ Measurement

Methods of analyzing contaminants on a terminal surface and other parts of a printed circuit board are broadly divided into two types: specular reflection and attenuated total reflection (ATR). For specular reflection microspectroscopy, incident light is absorbed by the sample as it passes through the sample, and light reflected by the circuit board is detected by a detector. This creates similar spectra to those obtained by the transmission spectroscopy, and measurements can be performed without touching the sample. This method is suited to sample thicknesses of around 10 µm. Contamination or staining that is too thick can result in

saturated peak tops, and contamination or staining that is too thin can result in indistinct peaks. For ATR microspectroscopy, peak saturation is not affected by sample thickness, but the sample must be in contact with a prism for measurements to be taken. This contact can cause issues such as losing the sample during measurement, or difficulty involved in achieving contact due to sample shape.

■ Measurement by Specular Reflection Microspectroscopy

Measurements were performed by specular reflection microspectroscopy which requires no contact with the sample. Fig. 2 shows an image of the defect for which a specular reflection spectrum was measured. The blue box shows the location of contamination on the sample. Aperture size was set to 25 µm × 25 µm. Analytical conditions are shown in Table 1, and the spectrum obtained and a library spectra search result are shown in Fig. 3. The contaminant spectrum matched the spectrum for magnesium silicate (talc).
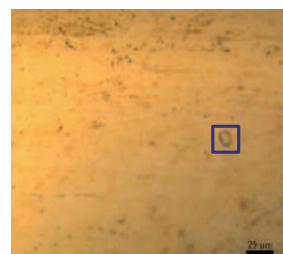

Fig. 2 Microscope Image of Contaminant (blue box size: 25 µm × 25 µm)

Table 1 FTIR Analytical Conditions

Instrument	: IRTracer[TM 2)]-100, AIM-9000
Resolution	: 8 cm^{-1}
Accumulation	: 20
Apodization	: Happ-Genzel
Detector	: MCT

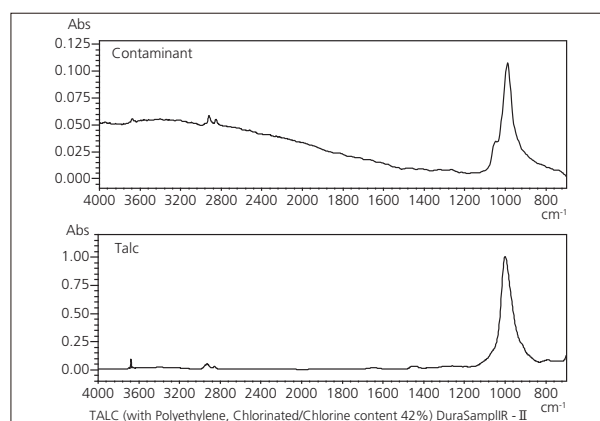TALC (with Polyethylene, Chlorinated/Chlorine content 42%) DuraSamplIR - II

Fig. 3 Library Spectra Search Result (Top: contaminant, bottom: library spectrum for talc)

■ Measurement by Specular Reflection and ATR Microspectroscopy

As mentioned above, when analyzing thick samples, good spectra may be obtained by ATR microspectroscopy but not by specular reflection microspectroscopy. Both specular reflection microspectroscopy and ATR microspectroscopy were used to analyze a thin, stain-like contaminant. A visual field image of the stain is shown in Fig. 4, and analytical conditions are shown in Table 2. Aperture sizes were 25 μm × 25 μm for specular reflection measurements and 50 μm × 50 μm for ATR measurements. The respective spectra obtained are shown on the same graph in Fig. 5.

Table 2 FTIR Analytical Conditions

Instrument	: IRTracer™ -100, AIM-9000
Resolution	: 8cm⁻¹
Accumulation	: 100
Apodization	: Happ-Genzel
Detector	: MCT
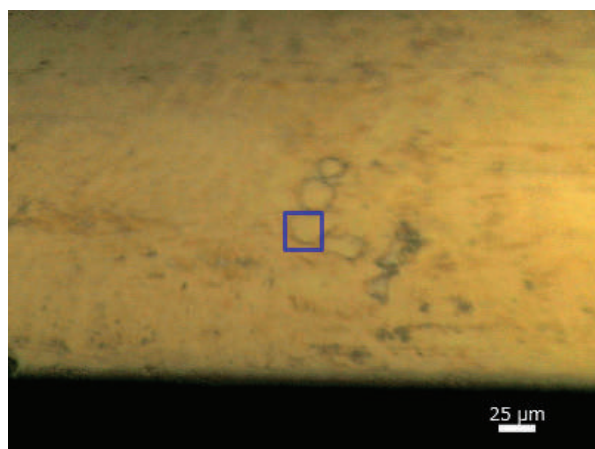
**Fig. 4 Image of Stain on Printed Circuit Board
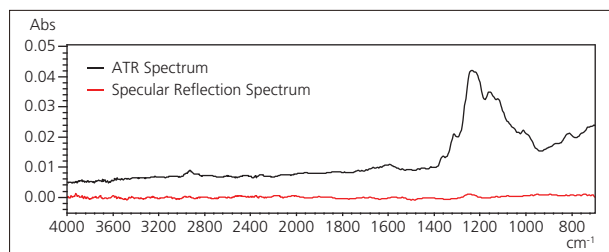(blue box size: 25 μm × 25 μm)**

Fig. 5 Specular Reflection Spectrum and ATR Spectrum of Stain

With specular reflection microspectroscopy the peak intensity is lower overall and shows a very slight peak at around 1250 cm⁻¹, though not distinct enough for qualitative analysis. The same position measured by ATR microspectroscopy resulted in a more distinct spectrum compared to specular reflection microspectroscopy. A library spectrum search for the ATR spectrum gave the results shown in Fig. 6, with a fluorinated lubricant and a fluorine resin appearing at the top of the list. It was presumed that a thin layer of a fluorine-containing lubricant was adhered to the metal substrate.
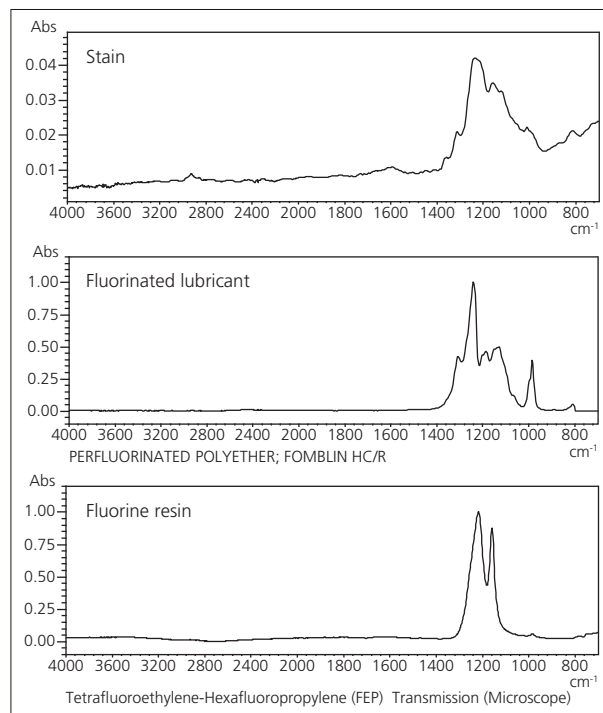

**Fig. 6 Spectrum Search Result
(Top: stain ATR spectrum, middle: fluorinated lubricant library spectrum, bottom: fluorine resin library spectrum)**

■ Conclusion

Qualitative analysis was performed on contaminants found on the terminal of a microSD™ card. The wide field camera of the AIM-9000 was used to examine a wide area of the sample and determine the contaminant position for analysis.

Choosing between using specular reflection microspectroscopy and ATR microspectroscopy of analysis based on contaminant shape allows the operator to obtain better spectra.

1) microSD™ is a trademark or a registered trademark of SD-3C, LLC in the United States, other countries or both.
2) IRTracer™ is a trademark or a registered trademark of Shimadzu Corporation in Japan, other countries or both.

SHIMADZU

Shimadzu Corporation

www.shimadzu.com/an/

![SHIMADZU logo] **SHIMADZU**
Excellence in Science

Application News

No.A523

Spectrophotometric Analysis

Simultaneous Measurement and Visual Observation: Transmittance Measurement of Multilayer Film

By using the AIM-9000 infrared microscope together with AIMsolution Analysis software, measurement points can be visually observed at the same time as a spectrum is measured for the corresponding point.
In this example, a multilayer film sample is analyzed using simultaneous visual observation and spectral measurement.

■ Measurement of Multilayer Film

A microscope image of a 20 µm thick cross-section of multilayer film, sliced using a microtome, is shown in Fig. 1. Fig. 1 shows that the film consists of at least four layers.
The spectrum was measured by the transmission method, with the sliced multilayer film held horizontally. First, the sample and background (BKG) measurement points were specified, as shown in Fig. 2. In this case, a location where there is no film (air) was specified as the BKG position. The aperture sizes were set to 50 × 50 µm for measurement points 1 and 4, and 20 × 50 µm for measurement points 2 and 3.
The aperture size of the BKG point needs to be the same as that of the measurement point. If multiple measurement points with different sizes are selected, BKG is measured with the aperture automatically matched to the respective measurement point size. Measurement conditions are indicated in Table 1.

■ Results

An image of the microscope area and the spectrum from each point are shown in Fig. 3.
After the measurements were finished, the AIMsolution Analysis software launched automatically to make it easy to perform data processing and spectrum searches. A screenshot from the AIMsolution Analysis software is shown in Fig. 4. Measurement points and spectra are color-coded to make them easier to correlate. Furthermore, search results show the acquired spectrum at the top, a spectral hit in the middle, and the hit list at the bottom, as shown in Fig. 5.
That provides powerful support to analysts by providing a smooth process flow from confirming the measurement points, measurements, to analyzing the resulting data.
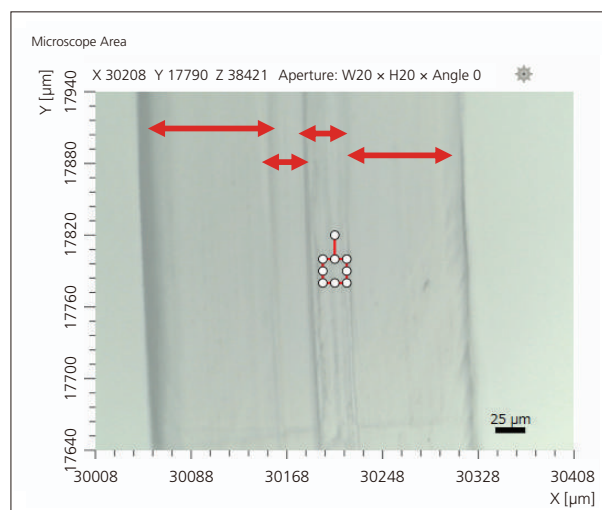

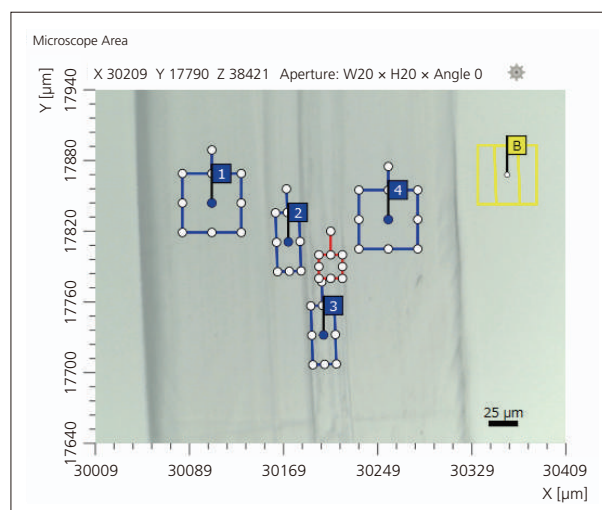**Fig. 1 Microscope Image of Multilayer Film Cross-Section**

Fig. 2 Image Showing Measurement Points

Table 1 FTIR Measurement Conditions

Instrument	: IRTracer-100
	AIM-9000
Resolution	: 8 cm^{-1}
Accumulation	: 10
Apodization	: SqrTriangle
Detector	: MCT
Aperture	: 20 × 50 µm, 50 × 50 µm

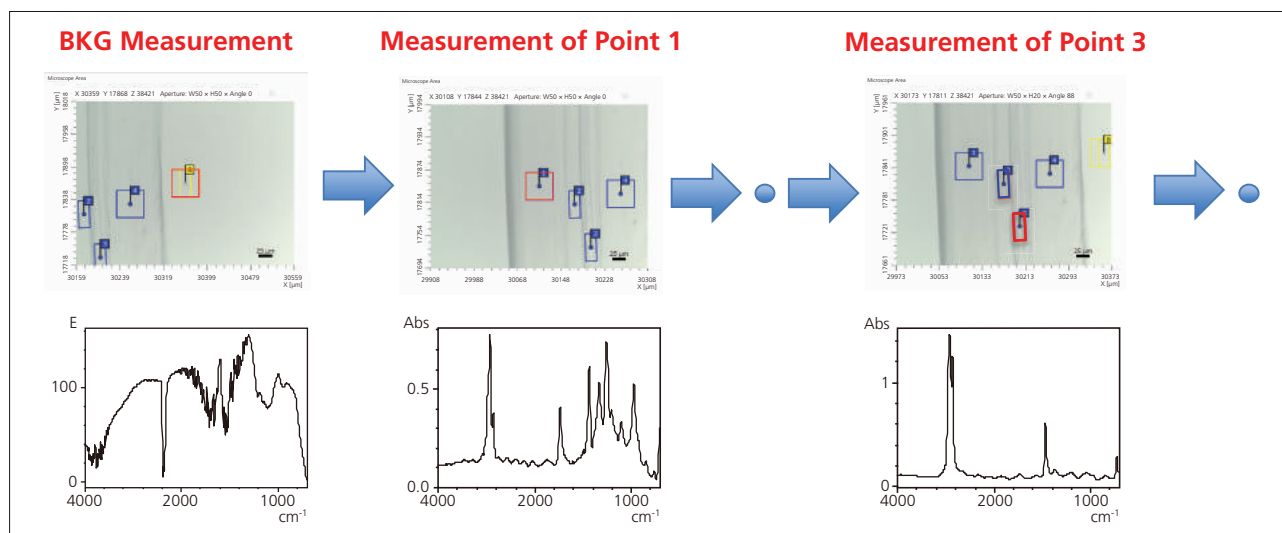**BKG Measurement**   **Measurement of Point 1**   **Measurement of Point 3**

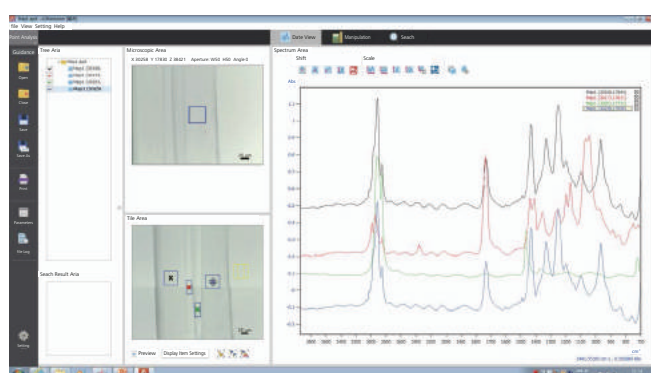**Fig. 3 Microscopic Images During Measurements and Measured Spectra**

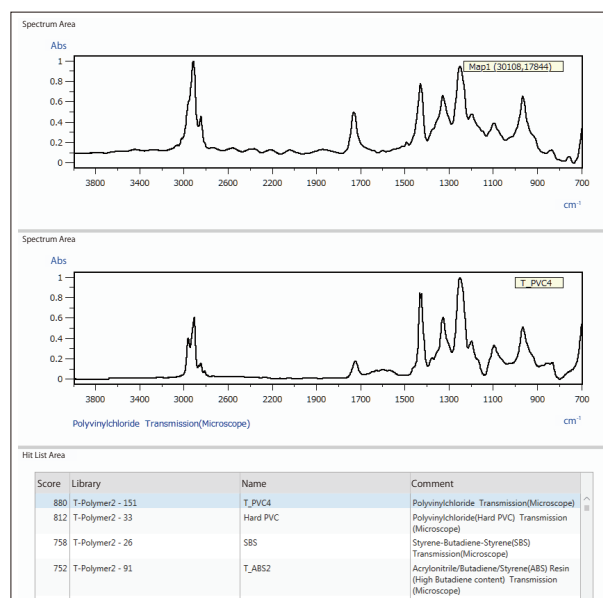**Fig. 4 Screenshot of AIMsolution Analysis Software**

Fig. 5 Search Results

■ **Conclusion**

This simultaneous visual observation and measurement example showed how both images and spectra from measurement points can be viewed simultaneously in real time.

AIMsolution Analysis software displays each measurement point color-coded with the same color as the corresponding spectrum, which makes it visually easier to understand. The software also makes it easy to perform data processing, such as atmospheric correction and searches.

In this way, by using the AIM-9000 microscope with AIMsolution Measurement software for sample analysis and AIMsolution Analysis for data analysis, the system is able to immediately, during any step, provide more reliable information and a stress-free sample analysis workflow.

SHIMADZU

Shimadzu Corporation

www.shimadzu.com/an/

Spectroscopy - FTIR

Analysis of a red Mini BabyBel® using FTIR and EDX technic - Single Reflection ATR method and EDX analysis of cheese and its packaging

To show the effectivity of destroying free analysis techniques one of the most interesting packaging of food is in the focus of this application. The Mini BabyBel® is one example of a famous design - how a little good can be packed. This little cheese offers a wide variety of packaging material. Hard, soft, thin and thick – material from different sources: polymer (printed), wax and cellulose. The ribbon band of the red colored wax casing is a slim and strong white band. The red transparent paper like dress has a print made with red, white, yellow and green color. The cheese itself is source of fat, protein and salt.

The infrared spectroscopy and EDX technology are in their analysis field famous for the aspect to be destroying free.

Figure 1: The striptease of a Mini BabyBel®, the steps to get access to the cheese; 1st remove the red transparent foil, 2nd unstrap, 3rd remove wax, 4th eat it.

What does this mean? There´s no need of an advanced sample preparation, no need of a chemical treatment to separate major components of a good and to identify them afterwards. A direct determination is possible. In case of FTIR a surface measurement technique is used for this specific sample. The technic is called, the attenuated total reflection (ATR). With the ATR it's possible to proof solid materials at the surface as well as creamy or cheesy like substances. Like cheese is.

EDX is by nature a technique penetrating the sample more deeply. The aggregation state from the sample can be solid or liquid.

The mayor differences in the techniques are:

- Infrared is molecular spectroscopy
- X-Ray is elemental spectroscopy.

Both results together gives a good overview from the sample within 5 minutes.

■ Technics

Infrared Spectroscopy uses infrared radiation or in other words heat to cause substances (our sample) to heat up and start with vibration and rotation of molecular groups in a chemical bonding system. These vibrations are unique for the substance and are used for identification. Vibration will occur in molecules or molecular groups and lattices. An analysis of elements only is not possible. For this purpose the EDX or other elemental analysis techniques are recommended. Elemental analysis from solids without treatment can be done in a more comprehensive way with energy dispersive X-Ray fluorescence spectroscopy. X-Ray radiation is used to kick

out electrons from inner atom shells (of sample atoms). Electrons from higher shells fill up this gap by releasing fluorescence radiation. This fluorescence radiation is specific for a certain element and is used for identification. [1]

■ **Sample preparation**

For the infrared measurements the ATR accessory named Quest™ from company Specac was used. The parts of the BabyBel® - the packaging as well as the other parts from the product- were fixed with the anvil of the ATR accessory to the Quest diamond window. ATR is the short for attenuated total reflection.
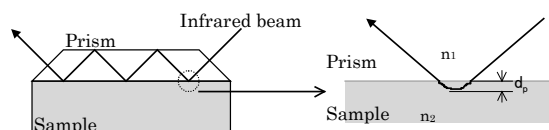
Fig. 2: Principals of ATR technic

This physical phenomenon occurs when the infrared beam coming out of a high refractive index media is reflected at a phase with lower refractive index. A short penetration of the beam into the material is going on, an absorbance happens and the reflected beam contains information about the sample. The penetration distance or called depth is depending on incident angle of the beam and the refractive index of the higher refractive material. Such materials are the crystals: diamond, ZnSe, KRS-5 and more. The Quest is a single reflection ATR accessory with monolithic diamond as high refractive crystal. With a force of about 40 lb a piece from each sample part was pressed against the diamond window. The technique allows a penetration depth of approx. 1 to 2 µm from the IR beam into the surface of the sample. For the EDX less preparation steps are needed - just place the sample in the measurement chamber and close the chamber. The measurement spot was set to 10 mm for all measurements.

■ **Spectral analysis with FTIR**

In the following all measured infrared spectra from the BabyBel ® product are shown. The identifications of the mayor components are explained in the figure annotations 3 to 9.
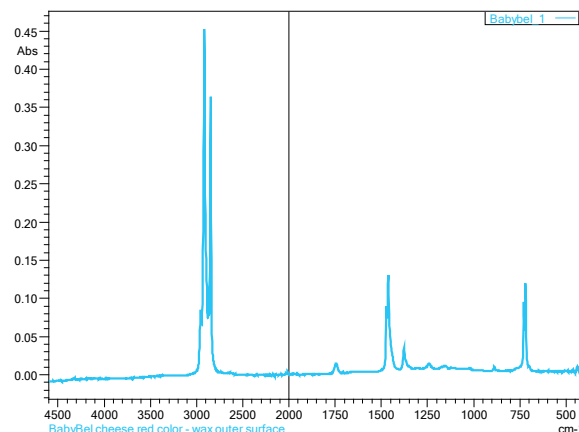
Fig. 3: Infrared spectrum, ATR, from the red colored wax, which is surrounding the cheese, surface (outside) not in contact with cheese
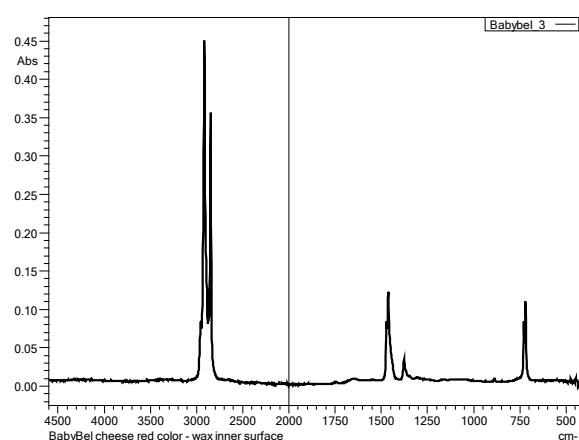
Fig.4; Infrared spectrum, ATR, from the red colored wax which is the cover for the cheese, surface (inside) which is in contact with the cheese

The two surfaces of the wax cover (in- and outside) resulted in two different infrared spectra. The difference is shown in the zoom of the finger print range from their infrared spectra visible in figure 5. Acetate signals were identified in the wax surface which is not in contact with the cheese.
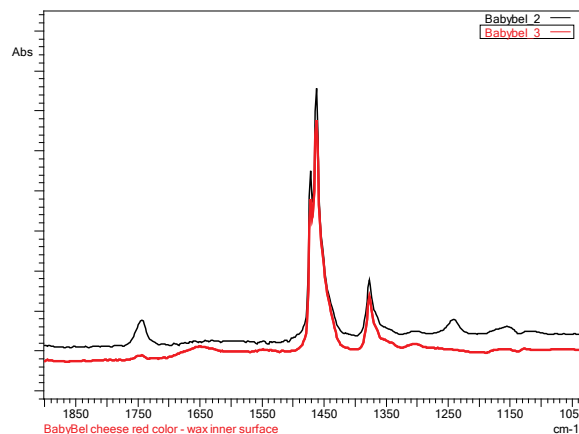
Fig.5: Differences in the two infrared spectra of the red wax surfaces in the range at approx. 1750, 1240 cm^{-1} The changes are related to special treatment of the outer surface with acetate related compounds
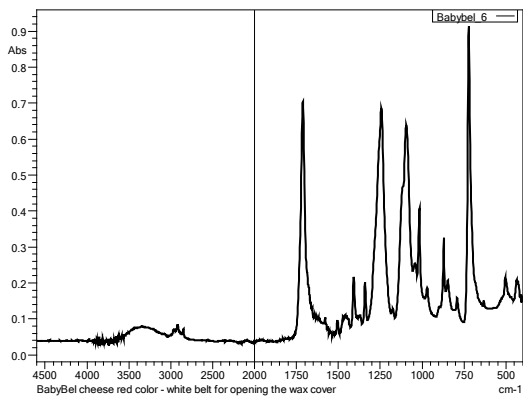
Fig. 6: ATR Infrared spectrum from the white belt for opening of the wax cover from the BabyBel®, it is a PET, with an offset of the signal group into the lower wavenumber region (can be caused by TiO_2 as found with EDX analysis (Table 3, and see Fig. 7 TiO_2 IR spectrum)

Fig.7: The red paper like foil from the BabyBel® is showing a cellulose spectrum (red line), the green print on the paper foil is green and the white print the blue line, the TiO_2 infrared spectrum profile is influencing the baseline of the green and blue spectrum in the region of 750 to 400 cm^{-1} .[2]
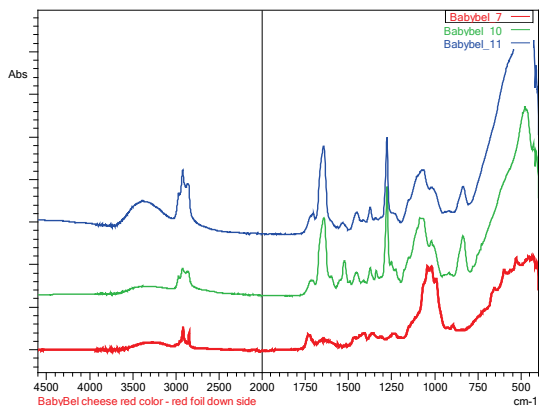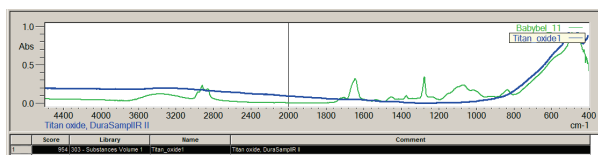

Fig. 8: The comparison of the green colored print from red colored the paper with the TiO_2 IR spectrum from the infrared library "Substances Volume 1". Titanium dioxide is closing the infrared with absorbance starting at 1000cm^{-1}.

The search in libraries could help to analyze the different substances: The search in libraries show effect by TiO_2 (in the baseline growing starting from 750 cm^{-1}), which could be as whitener in the color of the printing. TiO2 was re-found by investigation of EDX energy dispersive equipment on the paper. (EDX-8000).
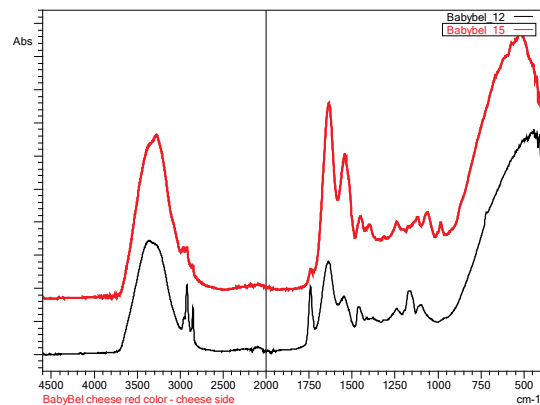

Fig. 9: Infrared spectrum of cheese, dominated by protein, fat and water and inorganic salts which are strongly absorbing the energy throughput of MIR range(red line, from approx. 750 cm^{-1}), the black spectrum shows air dried cheese (red line). Changes at water, the fat and protein region can be observed. The penetration of the IR beam into the surface of the hard cheese is influenced because the hard cheese has less good contact to the ATR accessory. The window area is not filled up properly.

Table 1: Nutritional content of red Mini BabyBel® [3]

Mini BabyBel® red	Nutritional Content (per 100 g)
Fat	24 g
Salt	1.8 g
Calcium	700 mg
Protein	21.5 g

Table 2: listing of the parts and the search result

Red paper (Figure 7)r	matches for micro cristaline cellulose, small amount of PVC, and match to a brown inorganic color
White/green print on red paper (Figure 7)	nitrocellulose filter, TiO_2, polyurethane, PVC matches, and add ons
White belt (figure 6)	PET
Wax with contact to cheese (figure4 and 5)	Wax
Wax without contact to cheese (figure 3 and 5)	Wax with add on (acetate like)
Cheese, fresh, peeled out of wax and dried at air (figure 9)	Mixture of water, fat and more

The destroying free EDX is able to estimate the salt concentration of the sample [1]. With infrared analysis, this can be done only by indirect methods because some salts are almost non MIR active. Their infrared spectrum will start at a lower wavenumber scale. Especially the salt sodium chloride starts at this region with own absorption at 645 cm^{-1}.

■ **EDX analysis of the packaging and the cheese**

Table 3: EDX screening analysis results for Cheese and its packaging

Sample	Al (ppm)	Ti (ppm)	Si (ppm)	S (ppm)	P (ppm)	K (ppm)	Cu (ppm)	Ca (ppm)	Fe (ppm)	Zr (ppm)	Zn (ppm)	Cl (%)	others
Babybel Foil	3746	1471	1456	296		213	47	37	25	16		6.10	Organic
Babybel Wax				5072			52	267	40		27		Organic
Babybel Wax without Cheese				2689				129					Organic
Babybel White Stripe		360		338	732	657	67	1794	60		18		Organic
Babybell Cheese (Fresh)				1861	7354	564	39	8156			42		Organic
Babybell Cheese (Dry)				2470	10110	502	38	14206			70		Organic

All measurements were done using standard-less FP methods. (Higher accuracy can be achieved with advanced FP methods and external calibrations) The higher concentrations for Ca and P for the dried cheese can be explained with the more dense volume of the sample after drying. The wax contains more S in comparison to the cheese. In the foil a high amount of chlorine was found. The foil contains in addition Ti and Si. Ti is most probably TiO_2, a white pigment (E171). The white stripe is maybe slightly contaminated with "cheese" The stripe shows a Ti signal as well, but with a much lower intensity. TiO_2 as white pigment which is not strongly visible in the FTIR spectrum when using the ATR and 2 µm surface penetration of the IR beam.

■ **Conclusion**

The infrared spectroscopy is able to identify the major components in natural and complex systems as samples from the field are, like this cheese sample.
The EDX analysis is simple and the analysis showed inorganics which were not able to be detected by FTIR.

To get a more complete impression from the taste of a cheese - the flavor of a cheese can be determined with GCMS analysis technique (house method from Shimadzu SEG).

■ **Instrumentation**
- Shimadzu IRAffinity-1S with LabSolutions IR software
- Single reflection unit – Quest™
- Shimadzu Libraries
- EDX-8000

■ **Literature**
[1] "White Gold – Salts in food", Shimadzu News 3/2009
[2] Infrarot-Spektroskopie, Günzler, Böck, Taschentext Bd. 43/44
[3] „Produkte", BabyBel, http://www.babybel.de/de-de/produkte

SHIMADZU

Shimadzu Europa GmbH

www.shimadzu.eu
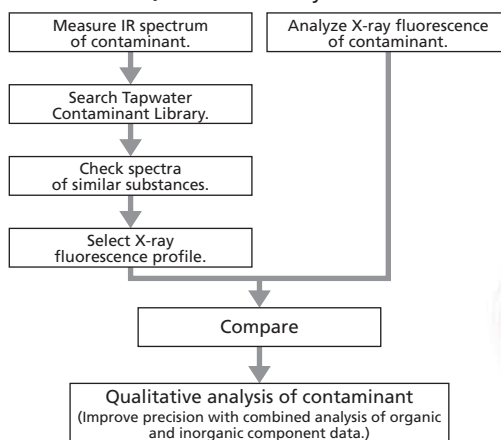
SHIMADZU
Excellence in Science

FTIR/EDX Tapwater Contaminant
Search System for LabSolutions IR/IRsolution

Inquiries from organizations involved in public water supply systems reflect a wide range of issues, such as objectionable mold, chlorine, or other tastes or odors; trihalomethane or other environmental pollutants; and the inclusion of other contaminants. Possible substances causing contamination include the various rubber and metal gaskets, packings, and sealing materials used in public water systems, minerals, and microorganisms.

A major cause of contaminants revolves around the aging, servicing, or installation of the water system infrastructure as well as the fixtures and other equipment involved in delivering the water. While eliminating these causes is difficult, identifying the contaminants as quickly as possible helps to ease the concerns of users.

Infrared spectrometry and X-ray fluorescence spectrometry provide an effective way to identify contaminants. The Tapwater contaminant system is a comprehensive search system that incorporates both techniques.

Procedure for Qualitative Analysis of Contaminants

Measure IR spectrum of contaminant. → Analyze X-ray fluorescence of contaminant.

Measure IR spectrum of contaminant. → Search Tapwater Contaminant Library. → Check spectra of similar substances. → Select X-ray fluorescence profile.

→ Compare ←

Qualitative analysis of contaminant
(Improve precision with combined analysis of organic and inorganic component data.)

Features of Search System

- Shimadzu's proprietary and state-of-the-art contaminant library, compiled specifically for public drinking water, was prepared with cooperation from organizations in the public water supply industry.
- Includes information from actual contaminant samples and commercially-available service parts used in public water systems.
- Includes both an infrared spectral library and X-ray fluorescence profiles (in PDF file format), which significantly improves precision of contaminant searches.

Applicable Fields

- Various organizations involved in water supply systems
- Petroleum and chemistry ● Foods ● Contract analysis

Content of Search System

● Infrared Spectral Library

IRAffinity-1

Instrument used : Shimadzu Fourier Transform Infrared Spectrophotometer
(IRPrestige-21/IRAffinity-1)

Measurement method : Single-reflection ATR (prism: Ge or diamond/ZnSe)

Number of spectra : 217 spectra
(For rubber, spectra are included for both interior and exterior)

Information included : Material names, colors, shapes, hardness, etc.

Prism selection criteria : Ge - Enables measurement of samples with high refractive indices (such as black rubber).
Absorption peak is smaller than diamond/ZnSe.
Diamond/ZnSe - Less prone to scratching and provides larger absorption peaks than Ge.
Cannot measure samples with high refractive indices (such as black rubber).

EDX-800HS

● X-Ray Fluorescence Profile Library

Instrument used : Shimadzu Energy Dispersive X-Ray Fluorescence Spectrometer (EDX-800HS)

Detectable elements : From C to U

Profile count : 217 profiles

Information included : Qualitative results and FP method quantitative results
(Uses FTIR qualitative results for principal components.)

Example of Infrared Spectral Search Results and Corresponding X-Ray Fluorescence Profile for a Contaminant

The following shows an example of infrared spectral search results and qualitative/quantitative EDX information for matching substances in search results. The contaminant was discovered in a public water system. The Tapwater Contaminant Library was utilized to determine the contaminant and corresponding profile.

Infrared Spectral Search Results
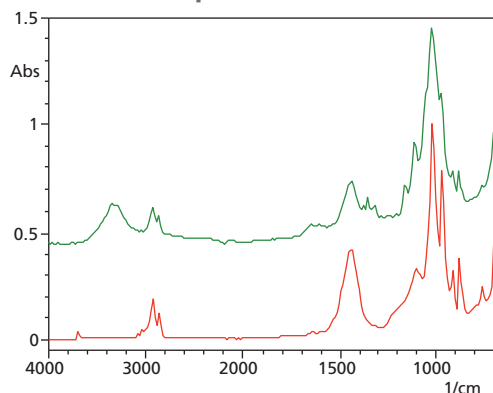
Detailed information:

Green (measured IR spectrum):
Infrared spectrum from contaminant detected in public drinking water

Red (specialized Tapwater Contaminant Database):
Interior residue (gray) on fitting seal for 32 mm diameter water drain pipe

|	
Material	: Styrene butadiene styrene (SBS), calcium carbonate ($CaCO_3$), and magnesium silicate (talc - $3Mg_4SiO_2H_2O$)
Color	: Gray
Shape	: Plastic ring
Hardness	: Pliable
Metal shine	: None
Measurement method	: ATR (Diamond)

Infrared spectral search results indicated the contaminant is identical or similar to the metal fitting seal material from the water drain pipe (principal component: styrene butadiene styrene [SBS]).

X-Ray Fluorescence Profile of Corresponding Substance

Sample Information
Name: 199 Discharge pipe 32 packing Gray_Inside_D
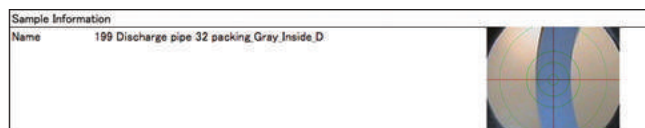
Measurement Condition

Analyte	Voltage	Current	Filter	Acr.(keV)	Anal.(keV)	Collimator 3mm	Time	Atmosphere Vac. DT%
Ti–U	50	41–Auto	——	0 – 40	4.20–37.00		Live– 100	25
S–K	15	1000–Auto	Al	0 – 20	2.42– 2.82		Live– 300	25
C–Sc	15	318–Auto	——	0 – 20	0.10– 4.20		Live– 300	26
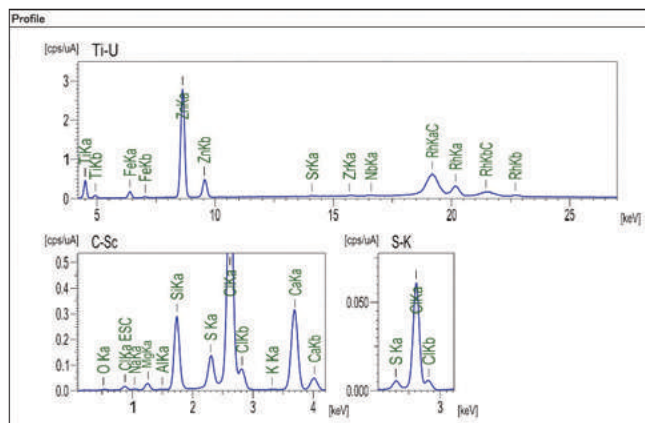
Quantitative Result

Analyte	Result		(Std.Dev.)	Proc.–Calc.	Line	Int.
Cl	9.114	%	(0.020)	Quan-FP	ClKa	0.7206
Ca	5.661	%	(0.009)	Quan-FP	CaKa	4.0402
Si	5.391	%	(0.010)	Quan-FP	SiKa	2.9346
Mg	2.043	%	(0.015)	Quan-FP	MgKa	0.2429
S	1.154	%	(0.003)	Quan-FP	S Ka	1.5087
Zn	1.100	%	(0.003)	Quan-FP	ZnKa	27.2646
Ti	1.054	%	(0.009)	Quan-FP	TiKa	3.2267
Na	0.956	%	(0.025)	Quan-FP	NaKa	0.0398
Fe	0.139	%	(0.002)	Quan-FP	FeKa	1.4017
Al	0.069	%	(0.003)	Quan-FP	AlKa	0.0198
K	0.039	%	(0.002)	Quan-FP	K Ka	0.0202
Sr	0.003	%	(0.000)	Quan-FP	SrKa	0.2143
Nb	0.003	%	(0.000)	Quan-FP	NbKa	0.2288
Zr	0.002	%	(0.000)	Quan-FP	ZrKa	0.1738
C12H14	73.272	%	(———)	Balance	————	————

Note: Quantitative results were calculated based on the principal components (SBS) determined from infrared spectral search results.

Qualitative and quantitative information can be obtained for iron rust, scaling, and other inorganic components, which is difficult to obtain only with infrared spectra.
It also provides an effective means for qualitative analysis or refining results for seals and other substances with the same principal components (organic substances), but different additives.

SHIMADZU

3. Spectrofluorimétrie

Application News

No. SCA-105-006

PicoGreen™ analysis with fluorescence Spectroscopy –double stranded DNA detection

Fluorescence spectroscopy is a highly selective analysis method. Within mixtures it is possible to get a luminescence effect only from a target substance. The application shown here is a special chapter of the bio analysis. The focus lays on double stranded DNA. Whereas other measurement techniques will analyze a sum of diverse DNA as it is done with standard UV transmission measurement [1, 2]. Of interest for this application is the selectivity of the fluorescence active complex which dsDNA forms with PicoGreen™. The dye PicoGreen will bond to double stranded DNA (dsDNA) only. It can be used for following application field: Genomic DNA, Viral dsDNA, PCR products, Plasmid preps, Subcloning fragments, and Genotyping. The PicoGreen is a fluorescence dye with high quantum yield. It is on similar level like fluoresceine. The chemical formula is (2-(n-bis-(3-dimethylaminopropyl)-amino)-4-(2,3-dihydro-3-methyl-(benzo-1,3-thiazol-2-yl)-methylidene)-1-phenyl-quinolinium) and the structure is shown in figure 1.
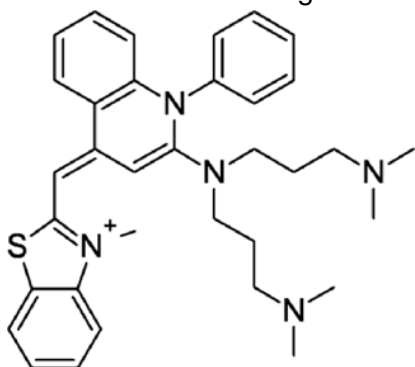

Fig. 1: Chemical structure of PicoGreen [1]

The structure shows three active regions in the PicoGreen which can get in contact to the dsDNA. These are the nitrogens in the dimethylaminopropyl group and the one in the thiazo ring which is with positive charge. The literature explains the interaction with dsDNA as activity of the positive charge with the negative charge from the dsDNA phosphate backbone, and the nitrogen from the amine group as coupling to the minor groves from the double helix. [1, 2, 3] The double stranded DNA (Fig.2) is deoxyribonucleic acid.

Fig. 2: Schematics of dsDNA, **d**ouble-**s**tranded **d**eoxyribo**n**ucleic **a**cid, with phosphate backbone, sugar is deoxyribose, and the bases are Adenine (A), Guanine(G), Cytosine(C) and Thymine(T) which are represented by the colored fragment in the lattice of the helix. Double-stranded DNA consists of two chains (strands) whose nitrogenous bases are connected by hydrogen bonds. Each strand mirrors the other as a result of the anti-parallel orientation of the sugar-phosphate backbones, as well as the complementary nature of the A-T and C-G base pairing [4].

A typical PicoGreen and dsDNA spectrum is shown in figure 3. With excitation wavelength 480nm a wide broad fluorescence appears at 530nm, measurement was done in a range of 490 to 600nm.
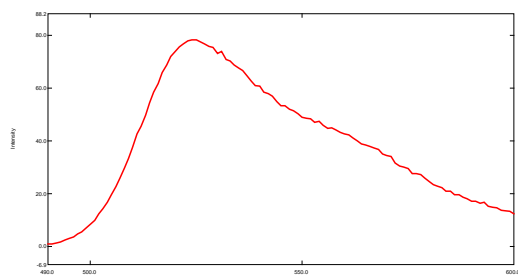
Fig. 3: Fluorescence spectrum from dsDNA treated with PicoGreen color complex

In a quantitative modelling the concentration was checked from 0.05µg DNA/ml and the dilution factor 5 the concentration of 0.025µg DNA/ml.
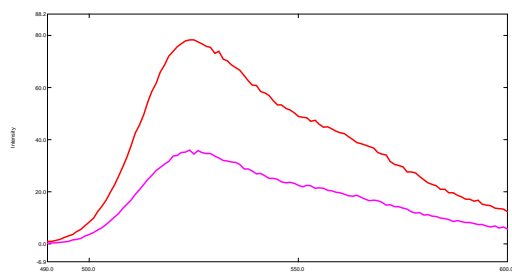
The result is shown in figure 4.

Fig. 4: Fluorescence spectra of two concentrations (0.05 and 0.025 µg/ml) of DNA treated with PicoGreen as fluorescence complex.

From a DNA solution combined with PicoGreen fluorophore is given the relation between PicoGreen and the dsDNA concentration (Table 1). The two solutions observed had a content of 50 and 25ng/ml of dsDNA. The distance of the intensity in the spectra at the maximum 530 nm shows linear development in the intensity. The measurements were done with a small slit to avoid saturation of the detector. By the sensitivity of the instrument even much lower concentrations are detectable.

Volume (µL) of 2 µg/mL DNA Stock	Volume (µL) of TE	Volume (µL) of Diluted PicoGreen Reagent	Final DNA Concentration in PicoGreen Assay
1000	0	1000	1000 ng/mL
500	500	1000	500 ng/mL
100	900	1000	100 ng/mL
10	990	1000	10 ng/mL
1	999	1000	1ng/mL
0	1000	1000	blank

Table 1: Relation between PicoGreen™ and dsDNA concentration

- **Measurement parameters RF-6000**

Parameter	Value
[Measurement]	
Spectrum Type	Emission
EX Wavelength	480.0 nm
EM Wavelength Start	490.0 nm
EM Wavelength End	600.0 nm
Data Interval	1.0 nm
Scan Speed	600 nm/min
[Instrument]	
Light Source	Xenon Arc Lamp
Signal Processing	Analog (Intensity)
EX Bandwidth	3.0 nm
EM Bandwidth	3.0 nm
Sensitivity	Auto

- **Literature**

[1] "Characterization of PicoGreen Interaction with dsDNA and the Origin of Its Fluorescence Enhancement upon Binding", I. Dragan, et al., Biophysical Journal Volume 99 November 2010 3010–3019

[2] "Quantitative assay of total dsDNA with PicoGreen reagent and real-time fluorescent detection", Ida BLOTTA, et all, *Ann Ist Super Sanità* 2005; 41(1):119-123

[3] PicoGreen™ is a product by Molecular Probes and Invitrogen; "Quant-iT™ Assays for high-throughput quantitation of DNA, RNA, and oligos", Invitrogen, Nucleic Acid Determination – catalog

[4] Essentials of Genetics, Unit 1, 1.2 DNA Is a Structure That Encodes Biological Information, ebook, 2014, Nature Education

SHIMADZU

Shimadzu Europa GmbH
www.shimadzu.eu

SHIMADZU
Excellence in Science

Application News

No.A493

Spectrophotometric Analysis

Measuring Peroxyoxalate Chemiluminescence Using a Spectrofluorophotometer

Chemiluminescence is a phenomenon where molecules are excited by a chemical reaction and then emit light energy as they return to ground state. Chemiluminescence based on using oxalate esters features high-emission efficiency and long emission time and provides illumination for long periods without any electricity. Consequently, it is used for recreational, fishing, and many other applications where it is commonly called glow sticks. The following describes the luminescent process of peroxyoxalate chemiluminescence and gives an example of using an RF-6000 spectrofluorophotometer to measure the emission spectra of glow sticks.

■ Luminescent Process of Peroxyoxalate Chemiluminescence

Peroxyoxalate chemiluminescence is caused by a chemical reaction between an oxalate ester and hydrogen peroxide within a fluorescent dye solution. As shown in Fig. 1, the oxalate ester is oxidized by hydrogen peroxide to produce ROH and 1,2-dioxetanedione. The 1,2-dioxetanedione is a high-energy reaction intermediate that exchanges electrons with the fluorescent dye as it breaks down to carbon dioxide. However, when the electrons return to the fluorescent dye, they enter the lowest unoccupied molecular orbital, causing the fluorescent dye to be in an excited state.[1], [2] Then the excited fluorescent dye releases light (hv) when it returns to its ground state, where the wavelength of that light depends on the fluorescent dye.

■ Fluorescent Dyes Used in Glow Sticks

Commercially marketed glow sticks are shown in Fig. 2. The oxalate ester and fluorescent dye solution are placed in a sealed thin-walled glass container and the glass container is placed inside a polyethylene tube together with hydrogen peroxide solution to which a catalyst is added. Bending the polyethylene tube breaks the glass container, which causes both solutions to mix together and emit light.

Examples of the fluorescent dyes used in glow sticks are shown in Fig. 3. Polycyclic aromatic fluorescent dyes are used, which emit different colors based on the wavelength of light emitted when the fluorescent dyes change from excited to ground state.
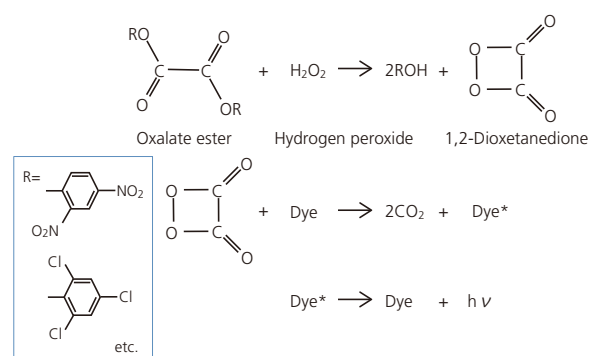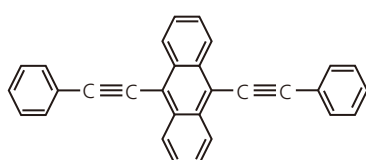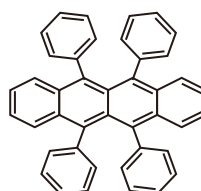

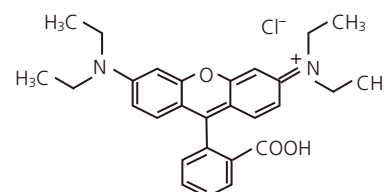**Fig. 1 Luminescent Process of Peroxyoxalate Chemiluminescence**

Fig. 2 Glow Sticks

9,10-Bis (phenylethynyl) anthracene
Green

Rubren (5,6,11,12-Tetraphenylnaphthacene)
Yellow

Rhodamine B
Red

Fig. 3 Fluorescent Dyes Used in Glow Sticks

Measuring the Light Emitted From Glow Sticks

A diagram of the RF-6000 spectrofluorophotometer system and its sample compartment is shown in Fig. 4. A shutter placed in front of the excitation light inlet window was closed to prevent excitation light from entering the sample compartment. A metal mesh filter was placed next to the fluorescent light outlet to reduce the amount of light reaching the detector.

The small lid inside the sample compartment cover was removed to insert the glow sticks into the sample compartment. Additionally, a blackout curtain was placed over the glow stick to prevent external light from entering the sample compartment.

Fig. 5 shows the corresponding emission spectra of yellow-green, yellow, and red glow sticks. Measurement conditions are indicated in Table 1.
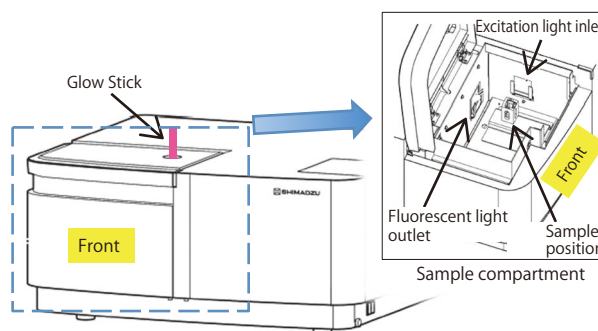

Fig. 4 Diagram of RF-6000 Spectrofluorophotometer and Sample Compartment

Table 1 Instrument and Analytical Conditions

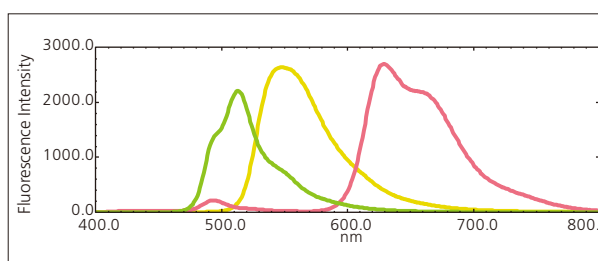|	
Instrument	: RF-6000 spectrofluorophotometer
Fluorescent light measurement wavelength range	: 400 to 800 nm
Scan speed	: 60 nm/min
Sampling interval	: 1 nm
Fluorescent light band width	: 3 nm
Sensitivity	: Low

Fig. 5 Emission Spectra of Glow Sticks
The color of spectrum corresponds to the glow stick color.

Time-Course Measurement of Glow Sticks

The red glow stick was bent, placed in the RF-6000 sample compartment, and its emission spectrum was measured as a function of time for 100 minutes. Measurement results are shown in Fig. 6 and measurement conditions in Table 2. Due to the active chemical reaction and correspondingly high level of fluorescent dye excitation, the brightness was high immediately after bending the glow stick, but the initial brightness quickly diminished. The results show that about 10 minutes later, the reaction slowed and brightness decreased at a roughly constant rate.
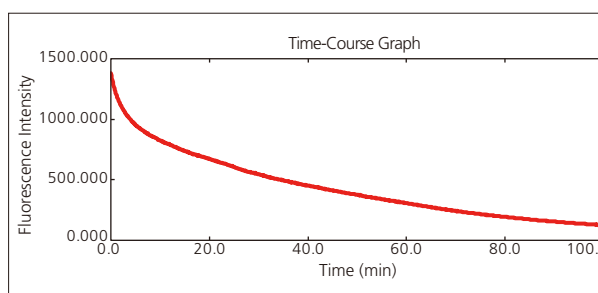

Fig. 6 Time-Course Measurement of Red Glow Stick

Conclusion

An RF-6000 spectrofluorophotometer was used to measure the light emitted from glow sticks based on peroxyoxalate chemiluminescence. The RF-6000 is able to measure wavelengths from 200 nm to 900 nm, which was especially helpful for investigating light emission phenomena over a wide range of wavelengths.

Table 2 Instrument and Analytical Conditions

Instrument	: RF-6000 spectrofluorophotometer
Fluorescence wavelength	: 629 nm
Data interval	: 0.1 min
Fluorescent light band width	: 3 nm
Integration time	: 500 ms
Sensitivity	: Low

[References]
1) C. V. Stevani, S. M. Silva, W. J. Baader, *Eur. J. Org. Chem.*, 4037 (2000)
2) S.Ohba, T. Mukai, Hiyoshi Review of Natural Science Keio University No.49, 1 (2011)

SHIMADZU

Shimadzu Corporation

www.shimadzu.com/an/

![SHIMADZU - Excellence in Science]

Application News

No.A504

Spectrophotometric Analysis

Relative Quantum Yield Measurement of a Sample in Solution

■ Introduction

Quantum yield is the ratio of the number of photons of excitation light adsorbed by a fluorescent material to the number of photons emitted by that material as fluorescent light. Quantum yield is used to evaluate the luminous intensity and luminous efficiency of fluorescent materials used in lighting and displays, and of fluorescent probes used in life sciences.

Quantum yield can be calculated for unknown samples by a relative method that uses a fluorescent material of known quantum yield as a standard sample, or by an absolute method that uses an integrating sphere to calculate quantum yield directly (values calculated by the absolute method are called absolute quantum yield or quantum efficiency).

We describe using the RF-6000 spectrofluorophotometer to measure and calculate quantum yield by the relative method.

■ Formula for Calculating Relative Quantum Yield

By the relative method, the absorbance measured using a UV-VIS spectrophotometer "A", the area of the FWHM of the corrected emission spectrum peak "F", the solvent refractive index "n", and the dilution ratio of the sample during emission spectrum measurement compared to its concentration during UV-VIS spectrum measurement "D" are used to calculate the quantum yield "ϕx" of an unknown sample using formula (1).

$$\phi_x = \phi_{st} \cdot \left(\frac{A_{st}}{A_x}\right) \cdot \left(\frac{F_x}{F_{st}}\right) \cdot \left(\frac{n_x^2}{n_{st}^2}\right) \cdot \left(\frac{D_x}{D_{st}}\right) \quad (1)$$

In formula (1), the suffix "st" represents the standard sample and "x" represents the unknown sample.

■ Matters of Note for Calculating Quantum Yield by the Relative Method

Matters of note for calculating quantum yield by the relative method according to formula (1) are shown below.

(1) Selection of standard sample and excitation wavelength
　・Choose a fluorescent material of known quantum yield with an excitation spectrum in a wavelength range that overlaps the excitation spectrum of the unknown sample, as the standard sample.
　・Choose a wavelength in the wavelength range over which the excitation spectrum of both the standard sample and unknown sample overlaps. The standard sample and the unknown sample should be excited by the same wavelength. If either the standard sample or unknown sample have a peak in the overlapping wavelength range, choose that peak wavelength as the excitation wavelength.

(2) Absorbance measured using a UV-VIS spectrophotometer
　・Place each of the solvents dissolving the standard sample and unknown sample on the reference beam side of the UV-VIS spectrophotometer when obtaining their UV-VIS spectra.
　・Read absorbance at the excitation wavelength on the UV-VIS spectrum of the standard sample and unknown sample.

(3) Sample concentration
　・Using a high-concentration sample without dilution can result in concentration quenching when measuring the emission spectrum. If the absorbance measured in (2) is high, dilute the standard sample and unknown sample so absorbance at the excitation wavelength is ≤ 0.05.[1] Insert the dilution ratio used for this adjustment into formula (1).

The RF-6000 spectrofluorophotometer used for calculating quantum yield by the relative method is shown in Fig. 1, and the UV-2600 UV-VIS spectrophotometer used for measuring absorbance is shown in Fig. 2.

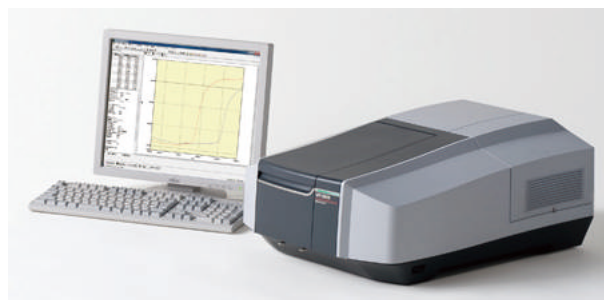**Fig. 1 RF-6000 Spectrofluorophotometer**

Fig. 2 UV-2600 UV-VIS Spectrophotometer

■ **Measuring Relative Quantum Yield of Rhodamine B**

Rhodamine B is fluorescent red pigment used to dye textiles and to color paper and other materials. As shown in Fig. 3, a wavelength region on the excitation spectrum of uranine (sodium fluorescein) in ethanol, a substance of known quantum yield, overlaps with the excitation spectrum of rhodamine B in ethanol. Based on this, uranine in ethanol was chosen as the standard sample for calculating the quantum yield of rhodamine B. The analytical conditions used to obtain the spectra shown in Fig. 3 are shown in Table 1.

Looking at Fig. 3, because uranine has a peak at 498 nm (red arrow) that overlaps with the excitation spectrum of rhodamine B in ethanol, this peak wavelength was chosen as the excitation wavelength. The UV-VIS spectra of rhodamine B and uranine in ethanol are shown in Fig. 4, and the analytical conditions used are shown in Table 2. Based on these spectra, at 498 nm rhodamine B and uranine have an absorbance of 0.0216 and 0.0243, respectively. The absorbance of both samples was ≤ 0.05, so the solutions were used without dilution to obtain emission spectra.

Quantum yield program included as a standard feature of the LabSolutions RF control software for RF-6000 was used to calculate quantum yield according to formula (1). Required parameters for formula (1) relating to uranine in ethanol, including quantum yield and absorbance, were entered into the formula and then the emission spectrum of uranine in ethanol was obtained. Required parameters for formula (1) relating to rhodamine B in ethanol were then entered into the formula and its emission spectrum was obtained. The areas of the FWHM of the peak height in each spectrum, shown in blue in Fig. 5 (I) and (II), were calculated, and finally the quantum yield of the unknown sample rhodamine B in ethanol was calculated automatically and displayed as shown in Fig. 6. The analytical conditions used to obtain Fig. 5 are shown in Table 3. The quantum yield program displays emission spectra with wavelength on the horizontal axis, while the FWHM area is calculated using emission spectra with values proportional to the number of photons on the vertical axis and wavenumber on the horizontal axis.

Taking the quantum yield of the standard sample uranine in ethanol as 0.97,[1] the quantum yield calculated for rhodamine B in ethanol was 0.7149, which is within the 0.69 to 0.97 range seen in literature.[1]

Fig. 3 Excitation Spectra of Rhodamine B (Blue) and Uranine (Red) in Ethanol

Table 1 Analytical Conditions

Measurement Instrument	: RF-6000
Emission Wavelength	: Rhodamine B: 568 nm, Uranine: 520 nm
Scanning Speed	: 200 nm/min
Slit Width	: Ex = 3 nm, Em = 3 nm
Sensitivity	: Low
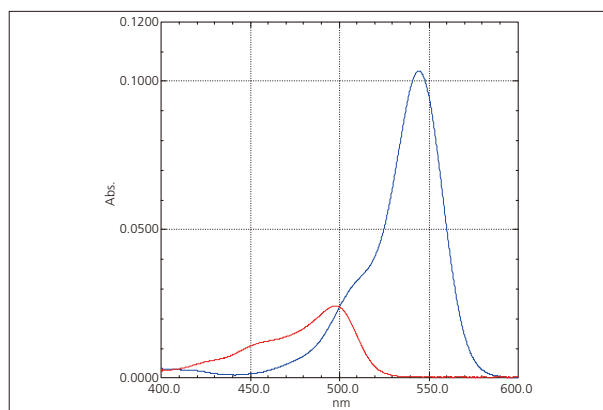
Fig. 4 UV-VIS Spectra of Rhodamine B (Blue) and Uranine (Red) in Ethanol

Table 2 Analytical Conditions

Measurement Instrument	: UV-2600
Spectra Type	: Absorbance
Scanning Speed	: Medium speed
Slit Width	: 2 nm

Table 3 Analytical Conditions

Measurement Instrument	: RF-6000
Excitation Wavelength	: 498 nm
Scanning Speed	: 200 nm/min
Slit Width	: Ex = 3 nm, Em = 3 nm
Sensitivity	: Low

Standard sample table

No.	name	QY	Abs	RI	Memo
0	Uranine	0.9700	0.0243	1.3000	

Unknown sample table

No.		name	QY	Abs	RI	Memo
1	✓	Rhodamine B	0.7149	0.0216	1.3000	

Fig. 6 Quantum Yield of Rhodamine B in Ethanol
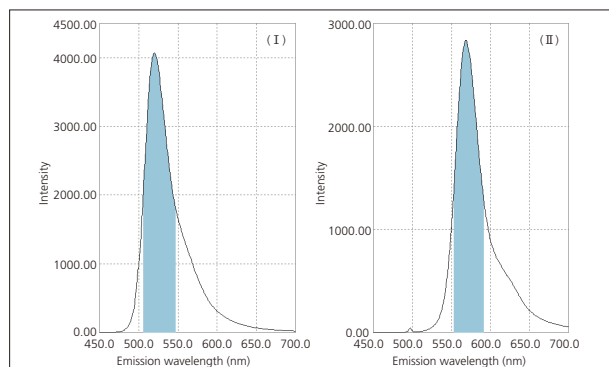**QY: Quantum Yield, Abs: Absorbance, RI: Refractive Index of Solution**

Fig. 5 Emission Spectra of Uranine (I) and Rhodamine B (II) in Ethanol

1) Kinoshita, K. and Mihashi, K., eds. 1983. The Spectroscopical Society of Japan Measurement Method Series 3 "Fluorometry— Applications in Biological Sciences". Japan: Gakkai Shuppan Center.
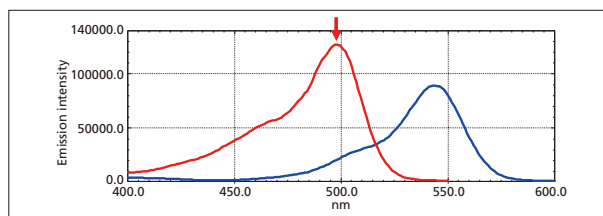
■ **Conclusion**

Because the RF-6000 can obtain corrected emission spectra in real time, using the quantum yield program included as standard in the LabSolutions RF software allows easy calculation of quantum yield for a target substance.

First Edition: Jul. 2016

SHIMADZU

Shimadzu Corporation

www.shimadzu.com/an/

![SHIMADZU Excellence in Science]

Application News

No.A516

Spectrophotometric Analysis

Fluorescence Measurement of Organic Electroluminescent Material

Screens, lighting, and other products that incorporate organic electroluminescent (EL) materials are being developed on a daily basis in the electrical and electronic goods sector. Organic EL material development involves the synthesis of new substances and verification of their optical properties using photoluminescence (PL) technique. Researching the PL allows us to find materials that emit light with high efficiency, and we can elucidate the mechanism of its fluorescence in solution. Organic EL materials are developed through this process to meet specific criteria that can include hue, low energy consumption, or high luminous efficiency.

In order to evaluate organic EL materials, fluorescence must be measured quickly and accurately over a wide range of wavelengths.

Introduced here are the measurements of porphyrin solution (solvent: chloroform), an organic EL material, using an RF-6000 spectrofluorophotometer, with the help of the Institute for Basic Science, Pohang University of Science and Technology (POSTECH), South Korea.

Fig. 1 RF-6000 Spectrofluorophotometer

■ Three-Dimensional (3D) Spectra Measurement

Fig. 1 shows the RF-6000. To first verify which fluorescence wavelength(s) appear at which excitation wavelength(s), the 3D spectra of porphyrin solution were measured using the analytical conditions shown in Table 1.

Fig. 2 shows the 3D spectra obtained, with excitation wavelength (Ex) is shown on the vertical axis, fluorescence wavelength (Em) is shown on the horizontal axis, and fluorescence intensity represented by different colors. The RF-6000 performs spectral correction in real time, allowing for the acquisition of corrected spectra with the factors due to instrument characteristics removed as soon as sample analysis is complete. Intense fluorescence of the analyzed sample was observed at around Em 660 nm and Em 720 nm. This fluorescence appeared at many excitation wavelengths, though results show the strongest fluorescence appeared at Ex 390 nm, followed by Ex 520 nm.
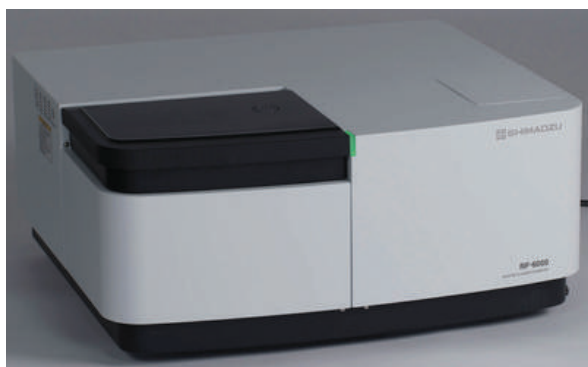
Table 1 Measurement Conditions

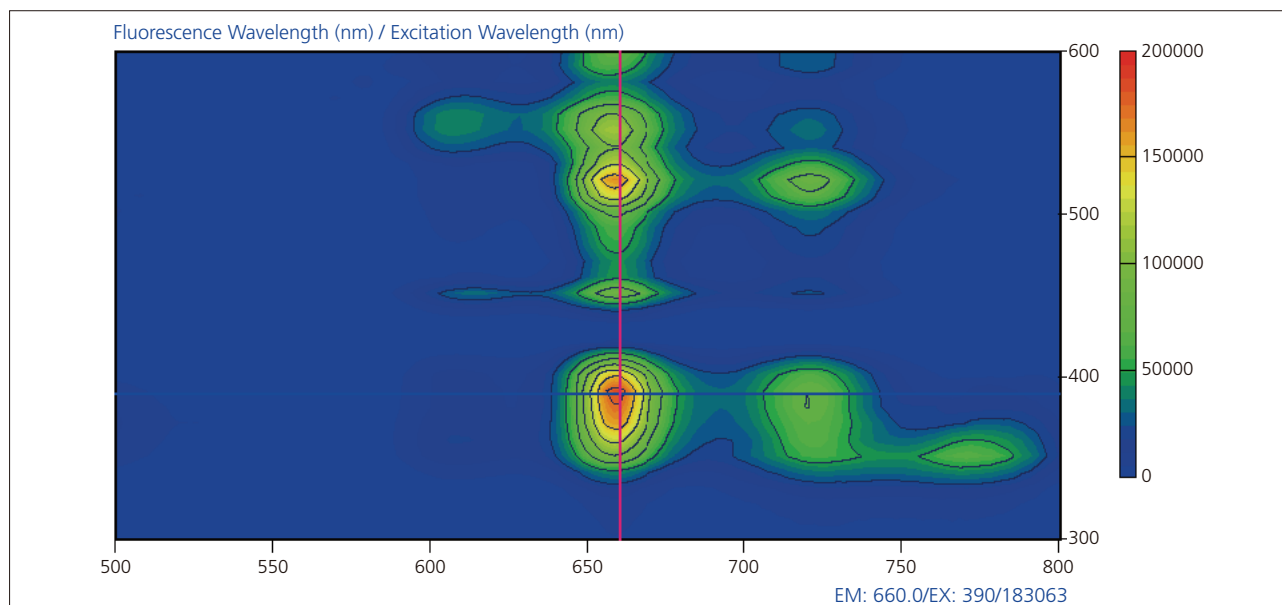|	
Instrument used	: RF-6000
Spectrum Type	: 3D spectrum
Measured Wavelength Range	: Ex 300-600 nm, Em 500-800 nm
Scanning Speed	: 6000 nm/min
Wavelength Interval	: Ex 10.0 nm, Em 2.0 nm
Bandwidth	: Ex 5.0 nm, Em 5.0 nm
Sensitivity	: Low
Measurement Time	: Approximately 2 minutes

EM: 660.0/EX: 390/183063

Fig. 2 Three-Dimensional Spectra of Porphyrin

■ Fluorescence Spectra Measured at Different Excitation Wavelengths

The 3D spectra in Fig. 2 shows fluorescence peaks at multiple excitation wavelengths. To observe fluorescence peaks in more detail, fluorescence spectra measurements were performed using the conditions in Table 2.

Fig. 3 shows fluorescence spectra at various excitation wavelengths, and that fluorescence peaks at 658 nm and 720 nm are present for all excitation wavelengths used. Fig. 3 also shows that the 658 nm fluorescence peak appears strongest at an excitation wavelength of 390 nm, and the 720 nm fluorescence peak appears strongest at an excitation wavelength of 520 nm.

Table 2 Measurement Conditions

Instrument used	: RF-6000
Spectrum Type	: Fluorescence spectrum
Measured Wavelength Range	: 390/420/520 nm for Ex, Ex to 800 nm for Em
Scanning Speed	: 200 nm/min
Wavelength Interval	: 1.0 nm
Bandwidth	: Ex 5.0 nm, Em 5.0 nm
Sensitivity	: Low

■ Conclusion

As the development of various organic EL materials continues, there will be a demand for spectra of higher sensitivity over a broader wavelength range to use in organic EL material evaluation. The RF-6000 is able to acquire 3D spectra quickly and accurately, and simultaneously acquire spectra with high sensitivity up to 900 nm. Using an optional integrating sphere with the RF-6000 also allows the measurement of quantum efficiency (absolute quantum yield).

In this study, using the RF-6000 spectrofluorophotometer, we successfully verified the 3D spectra and fluorescence spectra of an organic EL material.
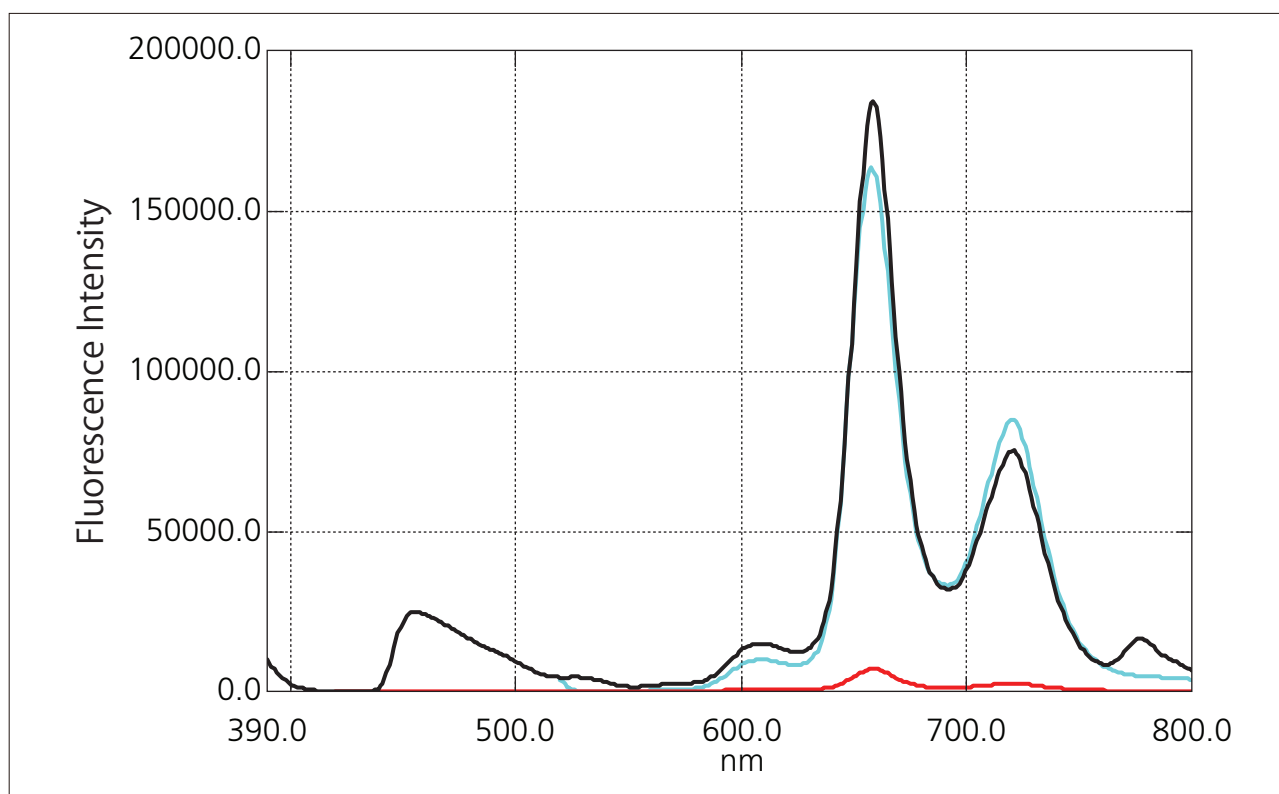
Fig. 3 Fluorescence Spectra of Porphyrin
Black line: Ex 390 nm, Red line: Ex 420 nm, Blue line: Ex 520 nm

SHIMADZU

Shimadzu Corporation

www.shimadzu.com/an/

Fondée en 1875, Shimadzu Corporation, leader dans le développement de technologies avancées possède une histoire unique dans l'innovation. Elle s'est construite avec l'envie de contribuer à l'amélioration de la société à travers la Science et la Technologie. Nous possédons un réseau mondial de vente, de service, de support technique et de centres d'applications sur six continents. Nous avons établi des partenariats à long terme avec de nombreux distributeurs hautement qualifiés localisés dans plus de 100 pays.

Pour plus d'informations ou pour nous contacter, merci de visiter notre site web
www.shimadzu.fr

SHIMADZU
Excellence in Science

Shimadzu France
Le Luzad II – Bât. A
Bd Salvador Allende – Noisiel
77448 Marne-la-Vallée Cedex 02
Tél : +33 (0)1 60 95 10 10
Fax : +33 (0)1 60 06 51 66
Email : shimadzu@shimadzu.fr
URL : www.shimadzu.fr